

Fire Fighting Tactics Under Wind Driven Conditions

Final Report

Prepared by:

National Institute of Standards and Technology

A DHS/Assistance to Firefighter Grants (AFG) Funded Study



THE
FIRE PROTECTION
RESEARCH FOUNDATION

FIRE RESEARCH

The Fire Protection Research Foundation
One Batterymarch Park
Quincy, MA, USA 02169-7471
Email: foundation@nfpa.org
<http://www.nfpa.org/foundation>

© Copyright Fire Protection Research Foundation
January 2009

FOREWORD

Large structures, such as high rise buildings, have additional challenges for fire fighters and building occupant safety such as increased travel distance (exposure time), more complicated egress path, and potentially larger fires. Most notably, changes in the building's ventilation or presence of an external wind, especially in high-rise buildings, can increase the energy release of the fire. This can also increase the spread of fire gases through the building.

What tactics or tools are appropriate for use with a wind driven fire and how should the tactics or tools be implemented? Positive Pressure Ventilation (PPV) is being used by fire departments on smaller structures, and if done correctly, this tactic can remove significant amounts of heat and smoke from the structure. However the question remains as to whether these PPV fans can be used successfully under wind driven fire conditions in large structures? Other tactics incorporating devices, such as fire window blankets or smoke curtains to control the ventilation conditions or the use of a special fire nozzle from the floor below the fire floor have been tried by the fire service under "real fire" conditions with varying levels of success. Unfortunately, there is no data to understand the capabilities and limitations of these fire fighting approaches.

This project provides real-scale data to guide the development of appropriate tactical options for use under wind driven conditions. The goal is to improve the safety of fire fighters and building occupants by enabling a better understanding of wind driven firefighting tactics, including structural ventilation and suppression. The technical information resulting from this study contributes to our understanding of the dynamics of fire phenomena and prediction of fire intensity and growth under wind driven conditions. This data provides a basis to identify methods and promulgate improved Standard Operating Guidelines (SOG) for the fire service to enhance firefighter safety, fire ground operations, and use of equipment.

The Research Foundation expresses gratitude to the report authors Daniel Madrzykowski and Steve Kerber, the Project Technical Panelists, and all others who contributed to this research effort. Special thanks are expressed to the U.S. Department of Homeland Security for providing the funding for this project.

The content, opinions and conclusions contained in this report are solely those of the author.

PROJECT TECHNICAL PANEL

Brett Bowman, Prince William County Fire & Rescue, Fairfax VA (IAFC SHS Section Rep)

John (Skip) Coleman, Toledo FD, Toledo OH

Kevin Courtney, Star FD, Star ID (NVFC Rep)

Rich Duffy, International Association of Fire Fighters

Richard Edgeworth, Chicago FD, Chicago IL

Wei Gao, Director, Science & Technology Division, Ministry of Public Security of P.R. China
and Director of China Fire Protection Association

George Healey, FDNY, New York NY

Mark Huff, Phoenix FD, Phoenix AZ

Carl Matejka, Houston FD, Houston TX

Peter McBride, Ottawa FD, Ottawa ON Canada

Jim Milke, University of Maryland (NFPA TC on Smoke Management)

John Miller, LA City FD, Los Angeles CA (HRB-SAC Rep)

Jack Mooney, FDNY, New York NY

Carl Peterson, NFPA (NFPA 1500 TC Staff Liaison)

Gerald Tracy, FDNY, New York NY

Peter Vandorpe, Chicago FD, Chicago IL

Rick Verlinda, Seattle FD, Seattle WA

Phil Welch, Gaston College, Dallas NC (NFPA Training TC rep)

Michael Wieder, OSU Fire Protection Publications, Stillwater OK (IFSTA Rep)

PROJECT SPONSOR

U.S. Department of Homeland Security
(AFG Fire Prevention & Safety Grants)



NIST Technical Note 1618

Fire Fighting Tactics Under Wind Driven Conditions: Laboratory Experiments

Daniel Madrzykowski
Stephen Kerber

U.S. Department of Commerce
Building and Fire Research Laboratory
National Institute of Standards and Technology
Gaithersburg, MD 20899

January 2009



Homeland
Security



NIST Technical Note 1618

Fire Fighting Tactics Under Wind Driven Conditions: Laboratory Experiments

Daniel Madrzykowski
Stephen Kerber

U.S. Department of Commerce
Building and Fire Research Laboratory
National Institute of Standards and Technology
Gaithersburg, MD 20899

January 2009



THE
FIRE PROTECTION
RESEARCH FOUNDATION



Homeland
Security

Department of Homeland Security

Janet Napolitano, *Secretary*

Federal Emergency Management Association,

Nancy Ward, *Acting Administrator*

United States Fire Administration

Denis Onieal, *Acting Administrator*



U.S. Department of Commerce

Otto J. Wolff, *Acting Secretary*

**National Institute of Standards and
Technology**

Patrick D. Gallagher, *Deputy Director*

Abstract

The National Institute of Standards and Technology, with the support of the Fire Protection Research Foundation and the U.S. Fire Administration conducted eight fire experiments to examine the impact of wind on fire spread through a multi-room structure and examine the capabilities of wind-control devices (WCD) and externally applied water to mitigate the hazard. The measurements used to examine the impact of the WCDs and the external water application tactics were heat release rate, temperature, heat flux, and gas velocity inside the structure. Measurements of oxygen, carbon dioxide, carbon monoxide, total hydrocarbons and differential pressures were also measured. Each of the experiments was recorded with video and thermal imaging cameras.

The experiments were designed to expose a public corridor area to a wind driven, post-flashover apartment fire. The door from the apartment to the corridor was open for each of the experiments. The conditions in the corridor were of critical importance because that is the portion of the building that firefighters would use to approach the fire apartment or that occupants from an adjoining apartment would use to exit the building.

The fires were ignited in the bedroom of the apartment. Prior to the failure or venting of the bedroom window, which was on the upwind side of the experimental apartment, the heat release rate from the fire was on the order of 1 MW. Prior to implementing either of the mitigating tactics, the heat release rates from the post-flashover structure fire were typically between 15 MW and 20 MW. When the door from the apartment to the corridor was open, temperatures in the corridor area near the open doorway, 1.52 m (5.00 ft) below the ceiling, were in excess of 600 °C (1112 °F) for each of the experiments. The heat fluxes measured in the same location, during the same experiments, were in excess of 70 kW/m². These extreme thermal conditions are not teneable, even for a firefighter in fully protective gear. These conditions were attained within 30 s of the window failure.

In these experiments, the WCDs reduced the temperatures in corridor outside the doorway by more than 50 % within 60 s of deployment. The heat fluxes were reduced by at least 70 % during this same time period. The WCDs also mitigated completely any gas velocity due to the external wind.

The externally applied water streams were implemented in three different ways; a fog stream across the face of the window opening, a fog stream into the window opening, and a solid water stream into the window opening. The fog stream across the window was not effective at reducing the thermal conditions in the corridor. The fog stream in the window decreased the corridor temperature by at least 20 % and the corresponding heat flux measures by at least 30 %. The solid streams experiments resulted in corridor temperature and heat flux reductions of at least 40 % within 60 s of application. None of the water applications had a significant impact on reducing the gas velocities in the structure. In some cases the gas velocity increased during water application.

These experiments demonstrated the thermal conditions that can be generated by a “simple room and contents” fire and how these conditions can be extended along a flow path within a structure when a wind condition and an open vent are present. Two potential tactics which could be implemented from either the floor above the fire in the case of a WCD or from the floor below the fire in the case of the external water application were demonstrated to be effective in reducing the thermal hazard in the corridor. Other data and observations, such as the fire pulsing out of the window opening against the wind, can provide valuable information to the fire service for hazard recognition purposes.

Further research in an actual building is required to fully understand the ability of firefighters to implement these tactics, to examine the thermal condition through the structure such as in stairways, and to examine the interaction of these tactics with building ventilation strategies both natural and with positive pressure ventilation. This report also includes a series of heat release rate experiments which were used to characterize the fuel packages for these and future experiments.

Disclaimer

Certain trade names or company products are mentioned in the text to specify adequately the experimental procedure and equipment used. In no case does such identification imply recommendation or endorsement by the National Institute of Standards and Technology, nor does it imply that the equipment is the best available for the purpose.

Regarding Non-Metric Units: The policy of the National Institute of Standards and Technology is to use metric units in all its published materials. To aid the understanding of this report, in most cases, measurements are reported in both metric and U.S. customary units.

Acknowledgements

The authors would like to express their appreciation to the many Building and Fire Research staff members, who provided their technical expertise to make these experiments a success, especially Roy McLane, Jay McElroy, Jonathan Kent, Laurean DeLauter, Anthony Chakalis, Greg Masenheimer, Doris Rinehart, Matt Bundy, Nelson Bryner, J. Randall Lawson, John Wamsley and Luis Luyo. We would also like to thank Anthony Hamins and Rodney Bryant for their thorough review of this document.

NIST would like to thank the Montgomery County Fire and Rescue Service for their support of this project, especially the use of the Yankee Air Boat, from the Cabin John Park Volunteer Fire Department and especially Larry Simmons for his skill and consistency in controlling the motor speed of the air boat to provide a consistent “wind” for the experiments and Donald Simmons for his efforts in co-ordinating the experiment schedules with the availability of staff and equipment. We would also like to thank Rick Merck, Tyler Mosman and Patsy Warnick of the Montgomery County Fire Marshal’s Office for their assistance in mapping the NIST Large Fire Facility.

We would like to thank Casey Grant, Kathleen Almand and Tracy Golinveaux of the Fire Protection Research Foundation and Meredith Lawler of the U.S. Fire Administration and the DHS Assistance to Firefighters Research and Development Grant Program staff for their support of this project.

Finally we would like to thank the members of the project panel for their passion for firefighter safety and expertise especially; Brett Bowman, Prince William County Fire & Rescue, Fairfax VA (IAFC SHS Section Rep); John (Skip) Coleman, Toledo FRD, Toledo, OH; Kevin Courtney, Star FD, Star ID (NVFC Rep); Rich Duffy (IAFF); Richard Edgeworth, Chicago FD, Chicago, IL; Wei Gao (China Fire Protection Association); George Healey, FDNY, New York; Mark Huff, Phoenix FD, Phoenix, AZ; Carl Matejka, Houston FD, Houston TX; Peter McBride, Ottawa FD, Ottawa ON Canada; Jim Milke, University of Maryland (NFPA TC on Smoke Management); John Miller, LA City FD, Los Angeles CA (HRB-SAC Rep); Jack Mooney, FDNY, New York; Carl Peterson, NFPA (NFPA 1500 TC Staff Liaison); Gerald Tracy, FDNY, New York NY; Peter Vandorpe, Chicago FD, Chicago IL; Rick Verlinda, Seattle FD, Seattle WA; Phil Welch, Gaston College, Dallas NC (NFPA Training TC rep); and Michael Wieder, OSU Fire Publications, Stillwater OK, (IFSTA).

Table of Contents

Abstract.....	i
Disclaimer.....	ii
Acknowledgements.....	iii
Table of Contents.....	v
List of Figures.....	viii
List of Tables.....	xxii
1 Introduction.....	1
1.1 Background.....	1
1.1.1 Historical Wind Driven Fires.....	2
1.1.2 Experience of the Fire Department of New York City.....	2
1.1.3 U.S. Wind Driven Fire Experience.....	4
1.1.4 NFPA Wind Driven Analysis.....	4
1.1.5 Wind Driven Tactics Research.....	4
2 Technical Approach.....	6
2.1 Objectives.....	6
2.2 Experiments.....	7
3 Heat Release Rate Experiments.....	7
3.1 Instrumentation and Uncertainty.....	7
3.2 Trash Container Fuel Package.....	9
3.3 Bed Fuel Package.....	14
3.3.1 Bed Fuel Package 1.....	16
3.3.2 Bed Fuel Package 2.....	20
3.4 Upholstered Chair.....	24
3.4.1 Upholstered Chair 1.....	25
3.4.2 Upholstered Chair 2.....	30
3.5 Sleeper Sofa Fuel Package.....	34
3.6 Discussion - Heat Release Rate Experiment Results.....	40
4 Experimental Arrangement.....	41
4.1 Facility.....	41
4.1.1 Structure.....	41
4.1.2 Instrumentation.....	46
4.1.3 Estimated Measurement Uncertainty.....	47
4.2 Fuel Load.....	51
4.3 Wind Source.....	56
4.3.1 Wind Speed and Pressure Experiments.....	56
4.3.2 Wind Control Device Experiments.....	58
4.3.3 Water Spray Distribution Experiments.....	60
5 Structure Fire Experiments.....	64
5.1 Baseline Experiment (WDF1).....	66
5.1.1 Observations.....	66
5.1.2 Heat Release Rate.....	80
5.1.3 Temperatures.....	80
5.1.4 Heat Flux.....	89
5.1.5 Pressure.....	90

5.1.6	Velocities	90
5.1.7	Gas Concentrations	94
5.2	Wind Control Devices WDF 2.....	98
5.2.1	Observations	99
5.2.2	Heat Release Rate	111
5.2.3	Temperatures.....	111
5.2.4	Heat Flux.....	120
5.2.5	Pressure.....	121
5.2.6	Velocities	122
5.2.7	Gas Concentrations.....	126
5.3	Wind Control Devices WDF 3.....	129
5.3.1	Observations	129
5.3.2	Heat Release Rate	144
5.3.3	Temperatures.....	145
5.3.4	Heat Flux.....	153
5.3.5	Pressure.....	154
5.3.6	Velocities	155
5.3.7	Gas Concentrations.....	159
5.4	Wind Control Devices with suppression WDF 4.....	162
5.4.1	Observations	162
5.4.2	Heat Release Rate	177
5.4.3	Temperatures.....	177
5.4.4	Heat Flux.....	186
5.4.5	Pressure.....	186
5.4.6	Velocities	187
5.4.7	Gas Concentrations.....	191
5.5	Wind Control Devices with suppression WDF 5.....	194
5.5.1	Observations	194
5.5.2	Heat Release Rate	210
5.5.3	Temperatures.....	210
5.5.4	Heat Flux.....	218
5.5.5	Pressure.....	219
5.5.6	Velocities	220
5.5.7	Gas Concentrations.....	224
5.6	External Water Application (indirect attack) WDF 6 (fog).....	226
5.6.1	Observations	227
5.6.2	Heat Release Rate	245
5.6.3	Temperatures.....	245
5.6.4	Heat Flux.....	258
5.6.5	Pressure.....	259
5.6.6	Velocities	260
5.6.7	Gas Concentrations.....	265
5.7	External Water Application (indirect attack) WDF 7 (smooth bore).....	270
5.7.1	Observations	271
5.7.2	Heat Release Rate	286
5.7.3	Temperatures.....	286

5.7.4	Heat Flux.....	294
5.7.5	Pressure.....	295
5.7.6	Velocities.....	296
5.7.7	Gas Concentrations.....	300
5.8	External Water Application (indirect attack) WDF 8 (smooth bore).....	303
5.8.1	Observations.....	303
5.8.2	Heat Release Rate.....	320
5.8.3	Temperatures.....	320
5.8.4	Heat Flux.....	327
5.8.5	Pressure.....	327
5.8.6	Velocities.....	328
5.8.7	Gas Concentrations.....	332
6	Discussion.....	335
6.1	Fire Conditions with no external wind.....	335
6.2	Tactics.....	339
6.2.1	Wind Control Devices.....	339
6.2.2	External Water Application.....	345
6.2.3	Door Control.....	351
7	Future Research.....	352
7.1.1	Full-scale experiments.....	353
7.1.2	Pilot Programs.....	353
7.1.3	Standard Test Methods for equipment.....	353
8	Summary.....	353
9	References.....	356

Appendix A: Summary of Fire Events Where Wind Did or Could Have Impact Fire Fighting Tactics
Appendix B: FPRF Project Technical Panel Roster

List of Figures

Figure 3.1-1. Typical heat release rate experimental arrangement, using the bed fuel package, with the heat flux positions labeled. This arrangement was used for all chair, bed, and sofa heat release rate experiments.....	8
Figure 3.2-1. Trash container 1, ignition	11
Figure 3.2-2. Trash container 1, 100 s after ignition	11
Figure 3.2-3. Trash container 1, 200 s after ignition	11
Figure 3.2-4. Trash container 1, 300 s after ignition	11
Figure 3.2-5. Trash container 1, 400 s after ignition	11
Figure 3.2-6. Trash container 1, at peak heat release rate, 406 s after ignition	11
Figure 3.2-7. Trash container 1, 500 s after ignition	11
Figure 3.2-8. Trash container 1, 600 s after ignition	11
Figure 3.2-9. Trash container 2, ignition	12
Figure 3.2-10. Trash container 2, 100 s after ignition	12
Figure 3.2-11. Trash container 2, 200 s after ignition	12
Figure 3.2-12. Trash container 2, 300 s after ignition	12
Figure 3.2-13. Trash container 2, at peak heat release rate, 363 s after ignition	12
Figure 3.2-14. Trash container 2, 400 s after ignition	12
Figure 3.2-15. Trash container 2, 500 s after ignition	12
Figure 3.2-16. Trash container 2, 600 s after ignition	12
Figure 3.2-17. Heat release rate versus time for Trash Container 1 and 2.	13
Figure 3.2-18. Heat flux versus time for Trash Container 1 and 2.....	13
Figure 3.2-19. Mass loss versus time for Trash Containers 1 and 2.....	14
Figure 3.3-1. Top side of box spring.....	15
Figure 3.3-2. Bottom side of box spring.....	15
Figure 3.3-3. Electric match ignition of bed fuel package.....	16
Figure 3.3-4. Trash container ignition of bed fuel package.....	16
Figure 3.3.1-1. Bed 1, ignition.....	17
Figure 3.3.1-2. Bed 1, 100 s after ignition.....	17
Figure 3.3.1-3. Bed 1, 200 s after ignition.....	17
Figure 3.3.1-4. Bed 1, 300 s after ignition.....	17
Figure 3.3.1-5. Bed 1, 400 s after ignition.....	17
Figure 3.3.1-6. Bed 1, at peak heat release rate, 484 s after ignition.....	17
Figure 3.3.1-7. Bed 1, 500 s after ignition.....	17
Figure 3.3.1-8. Bed 1, 600 s after ignition.....	17
Figure 3.3.1-9. Bed 1, 700 s after ignition.....	17
Figure 3.3.1-10. Bed 1, 800 s after ignition.....	17
Figure 3.3.1-11. Heat release rate versus time for bed fuel package 1.	18
Figure 3.3.1-12. Heat flux versus time for the bed fuel package 1.....	19
Figure 3.3.1-13. Mass loss versus time for bed fuel package 1.....	20
Figure 3.3.2-1. Bed 2, ignition.....	21
Figure 3.3.2-2. Bed 2, 100 s after ignition.....	21
Figure 3.3.2-3. Bed 2, 200 s after ignition.....	21
Figure 3.3.2-4. Bed 2, 300 s after ignition.....	21
Figure 3.3.2-5. Bed 2, at peak heat release rate, 380 s after ignition.....	21

Figure 3.3.2-6. Bed 2, 400 s after ignition	21
Figure 3.3.2-7. Bed 2, 500 s after ignition	21
Figure 3.3.2-8. Bed 2, 600 s after ignition	21
Figure 3.3.2-9. Heat release rate versus time for bed fuel package 2	22
Figure 3.3.2-10. Heat flux versus time for bed fuel package 2	23
Figure 3.3.2-11. Mass loss versus time for bed fuel package 2	24
Figure 3.4-1. Upholstered chair, front view	25
Figure 3.4-2. Upholstered chair, side view	25
Figure 3.4-3. Seat cushion, showing layers of upholstery fabric, polyester batting and polyurethane foam.	25
Figure 3.4-4. Back cushion, showing the upholstery fabric, inner liner, and polyurethane foam.	25
Figure 3.4.1-1. Chair 1, ignition	27
Figure 3.4.1-2. Chair 1, 100 s after ignition	27
Figure 3.4.1-3. Chair 1, 200 s after ignition	27
Figure 3.4.1-4. Chair 1, 300 s after ignition	27
Figure 3.4.1-5. Chair 1, 400 s after ignition	27
Figure 3.4.1-6. Chair 1, at peak heat release rate, 417 s after ignition	27
Figure 3.4.1-7. Chair 1, 500 s after ignition	27
Figure 3.4.1-8. Chair 1, 600 s after ignition	27
Figure 3.4.1-9. Chair 1, 700 s after ignition	27
Figure 3.4.1-10. Chair 1, 800 s after ignition	27
Figure 3.4.1-11. Heat release rate versus time for chair 1.	28
Figure 3.4.1-12. Heat flux versus time for chair 1	29
Figure 3.4.1-13. Mass loss versus time for chair 1.	30
Figure 3.4.2-1. Chair 2, ignition	31
Figure 3.4.2-2. Chair 2, 100 s after ignition	31
Figure 3.4.2-3. Chair 2, 200 s after ignition	31
Figure 3.4.2-4. Chair 2, 300 s after ignition	31
Figure 3.4.2-5. Chair 2, 400 s after ignition	31
Figure 3.4.2-6. Chair 2, at peak heat release rate, 437 s after ignition	31
Figure 3.4.2-7. Chair 2, 500 s after ignition	31
Figure 3.4.2-8. Chair 2, 600 s after ignition	31
Figure 3.4.2-9. Chair 2, 700 s after ignition	31
Figure 3.4.2-10. Chair 2, 800 s after ignition	31
Figure 3.4.2-11. Heat release rate versus time for chair 2.	32
Figure 3.4.2-12. Heat flux versus time for chair 2	33
Figure 3.4.2-13. Mass loss versus time for chair 2.	33
Figure 3.5-1. Sofa 1, ignition	35
Figure 3.5-2. Sofa 1, 100 s after ignition	35
Figure 3.5-3. Sofa 1, 200 s after ignition	35
Figure 3.5-4. Sofa 1, 300 s after ignition	35
Figure 3.5-5. Sofa 1, 400 s after ignition	35
Figure 3.5-6. Sofa 1, at peak heat release rate, 455 s after ignition	35
Figure 3.5-7. Sofa 1, 500 s after ignition	35
Figure 3.5-8. Sofa 1, 600 s after ignition	35
Figure 3.5-9. Sofa 1, 700 s after ignition	35

Figure 3.5-10. Sofa 1, 800 s after ignition	35
Figure 3.5-11. Sofa 2, ignition	36
Figure 3.5-12. Sofa 2, 100 s after ignition	36
Figure 3.5-13. Sofa 2, 200 s after ignition	36
Figure 3.5-14. Sofa 2, 300 s after ignition	36
Figure 3.5-15. Sofa 2, at peak heat release rate, 389 s after ignition	36
Figure 3.5-16. Sofa 2, 400 s after ignition	36
Figure 3.5-17. Sofa 2, 500 s after ignition	36
Figure 3.5-18. Sofa 2, 600 s after ignition	36
Figure 3.5-19. Sofa 2, 700 s after ignition	36
Figure 3.5-20. Sofa 2, 800 s after ignition	36
Figure 3.5-21. Heat release rate versus time for sofas 1 and 2.	37
Figure 3.5-22. Heat flux versus time for sofa 1.	38
Figure 3.5-23. Heat flux versus time for sofa 2.	38
Figure 3.5-24. Mass loss versus time for sofa 1.	39
Figure 3.5-25. Mass loss versus time for sofa 2.	40
Figure 4.1.1-1. Schematic plan view of the experimental structure.	42
Figure 4.1.1-2. Steel framing for walls of experimental structure inside the NIST Large Fire Facility.	43
Figure 4.1.1-3. Ceiling supports for experimental structure.	44
Figure 4.1.1-4. Dimensioned floor plan of experimental structure.	45
Figure 4.1.3-1. Schematic floor plan of instrumentation types and locations.	49
Figure 4.1.3-2. Thermocouple arrays along center line of structure looking from east to west.	50
Figure 4.1.3-3. Bi-directional probe array in west window.	50
Figure 4.1.3-4. Wall mounted thermocouples, heat flux sensor, and differential pressure sampling port.	50
Figure 4.1.3-5. Gas sampling probe installation on south wall of living room.	50
Figure 4.2-1. Schematic floor plan of bedroom with furniture locations.	52
Figure 4.2-2. Bedroom furnishings, looking north.	52
Figure 4.2-3. Bedroom furnishings, looking south.	52
Figure 4.2-4. Schematic floor plan of living room with furniture locations.	54
Figure 4.2-5. Living room furniture, looking north.	54
Figure 4.2-6. Living room furnishings, looking east.	54
Figure 4.3-1. Air boat from inside of fire lab looking west.	56
Figure 4.3-2. Air boat from outside of the fire lab looking east.	56
Figure 4.3.2-1. Small WCD deployed over window opening.	58
Figure 4.3.2-2. Large WCD deployed over window opening.	58
Figure 4.3.3-1. Water spray distribution experiment arrangement.	62
Figure 4.3.3-2. Fog stream discharged across window opening.	62
Figure 4.3.3-3. Fog stream discharged into window opening.	62
Figure 4.3.3-4. Solid stream discharged into window opening.	62
Figure 4.3.3-5. Water distribution results for fog stream discharged across window opening (kg), the gray area does not contain a measurable amount of water.	63
Figure 4.3.3-6. Water distribution results for fog stream discharged into window opening (kg) , the gray area does not contain a measurable amount of water.	63

Figure 4.3.3-7. Water distribution results for solid stream discharged into window opening (kg), the gray area does not contain a measurable amount of water.	64
Figure 5-1. Photograph of the placement of the trash container fuel package ignition source.....	65
Figure 5.1.1-1. Experiment 1, ignition.....	69
Figure 5.1.1-2. Experiment 1, 60 s after ignition.....	70
Figure 5.1.1-3. Experiment 1, 120 s after ignition.....	71
Figure 5.1.1-4. Experiment 1, 180 s after ignition.....	72
Figure 5.1.1-5. Experiment 1, 240 s after ignition.....	73
Figure 5.1.1-6. Experiment 1, window fully vented, 260 s after ignition.....	74
Figure 5.1.1-7. Experiment 1, 300 s after ignition.....	75
Figure 5.1.1-8. Experiment 1, 360 s after ignition.....	76
Figure 5.1.1-9. Experiment 1, 420 s after ignition.....	77
Figure 5.1.1-10. Experiment 1, 480 s after ignition.....	78
Figure 5.1.1-11. Experiment 1, 540 s after ignition.....	79
Figure 5.1.2-1. Heat release rate versus time, Experiment 1.....	80
Figure 5.1.3-1. Temperature versus time from the bedroom window (BRW) thermocouple array, Experiment 1.....	83
Figure 5.1.3-2. Temperature versus time from the bedroom (BR) thermocouple array, Experiment 1.....	84
Figure 5.1.3-3. Temperature versus time from the hall thermocouple array, Experiment 1.....	84
Figure 5.1.3-4. Temperature versus time from the living room corner (LRC) thermocouple array, Experiment 1.....	85
Figure 5.1.3-5. Temperature versus time from the living room (LR) thermocouple array, Experiment 1.....	85
Figure 5.1.3-6. Temperature versus time from the corridor center (CC) thermocouple array, Experiment 1.....	86
Figure 5.1.3-7. Temperature versus time from the corridor south (CS) thermocouple array, Experiment 1.....	86
Figure 5.1.3-8. Temperature versus time from the corridor southwest (CSW) thermocouple array, Experiment 1.....	87
Figure 5.1.3-9. Temperature versus time from the corridor north (CN) thermocouple array, Experiment 1.....	87
Figure 5.1.3-10. Temperature versus time from the ceiling vent thermocouple array, Experiment 1.....	88
Figure 5.1.3-11. Temperature versus time from the target room (TR) door knobs, Experiment 1.....	88
Figure 5.1.4-1. Heat flux versus time at five locations, Experiment 1.....	89
Figure 5.1.5-1. Pressure versus time at five locations, Experiment 1.....	90
Figure 5.1.6-1. Velocity versus time from the bedroom window (BRW) bi-directional probe array, Experiment 1.....	92
Figure 5.1.6-2. Velocity versus time from the hall bi-directional probe array, Experiment 1.....	92
Figure 5.1.6-3. Velocity versus time from the corridor south (CS) bi-directional probe array, Experiment 1.....	93
Figure 5.1.6-4. Velocity versus time from the corridor north (CN) bi-directional probe array, Experiment 1.....	93
Figure 5.1.6-5. Velocity versus time from the ceiling vent (V) bi-directional probe array, Experiment 1.....	94

Figure 5.1.7-1. Oxygen, carbon dioxide, carbon monoxide, and total hydrocarbon percent volume versus time from the upper bedroom (BR) sampling location, Experiment 1.....	96
Figure 5.1.7-2. Oxygen, carbon dioxide, and carbon monoxide percent volume versus time from the lower bedroom (BR) sampling location, Experiment 1.....	96
Figure 5.1.7-3. Oxygen, carbon dioxide, carbon monoxide, and total hydrocarbon percent volume versus time from the upper living (LR) room sampling location, Experiment 1.....	97
Figure 5.1.7-4. Oxygen, carbon dioxide, and carbon monoxide percent volume versus time from the lower living room (LR) sampling location, Experiment 1.....	97
Figure 5.1.7-5. Total hydrocarbon percent volumes versus time from the upper bedroom (BR) and living room (LR) sampling locations, Experiment 1.....	98
Figure 5.2.1-1. Experiment 2 ignition.....	101
Figure 5.2.1-2. Experiment 2, 60 s after ignition.....	102
Figure 5.2.1-3. Experiment 2, 120 s after ignition.....	103
Figure 5.2.1-4. Experiment 2, 180 s after ignition.....	104
Figure 5.2.1-5. Experiment 2, corridor flames, 189 s after ignition.....	105
Figure 5.2.1-6. Experiment 2, WCD deployed, 200 s after ignition.....	106
Figure 5.2.1-7. Experiment 2, WCD in place, 205 s after ignition.....	107
Figure 5.2.1-8. Experiment 2, 240 s after ignition.....	108
Figure 5.2.1-9. Experiment 2, WCD removed, 270 s after ignition.....	109
Figure 5.2.1-10. Experiment 2, 300 s after ignition.....	110
Figure 5.2.2-1. Heat release rate versus time, Experiment 2.....	111
Figure 5.2.3-1. Temperature versus time from the bedroom window (BRW) thermocouple array, Experiment 2.....	114
Figure 5.2.3-2. Temperature versus time from the bedroom (BR) thermocouple array, Experiment 2.....	115
Figure 5.2.3-3. Temperature versus time from the hall thermocouple array, Experiment 2.....	115
Figure 5.2.3-4. Temperature versus time from the living room corner (LRC) thermocouple array, Experiment 2.....	116
Figure 5.2.3-5. Temperature versus time from the living room (LR) thermocouple array, Experiment 2.....	116
Figure 5.2.3-6. Temperature versus time from the corridor center (CC) thermocouple array, Experiment 2.....	117
Figure 5.2.3-7. Temperature versus time from the corridor south (CS) thermocouple array, Experiment 2.....	117
Figure 5.2.3-8. Temperature versus time from the corridor southwest (CSW) thermocouple array, Experiment 2.....	118
Figure 5.2.3-9. Temperature versus time from the corridor north (CN) thermocouple array, Experiment 2.....	118
Figure 5.2.3-10. Temperature versus time from the ceiling vent thermocouple array, Experiment 2.....	119
Figure 5.2.3-11. Temperature versus time from the target room (TR) door knobs, Experiment 2.....	119
Figure 5.2.3-12. Temperature versus time from the target room (TR) thermocouple array, Experiment 2.....	120
Figure 5.2.4-1. Heat flux versus time at five locations, Experiment 2.....	121
Figure 5.2.5-1. Pressure versus time at five locations, Experiment 2.....	122

Figure 5.2.6-1. Velocity versus time from the bedroom window (BRW) bi-directional probe array, Experiment 2.....	123
Figure 5.2.6-2. Velocity versus time from the hall bi-directional probe array, Experiment 2.	124
Figure 5.2.6-3. Velocity versus time from the corridor south (CS) bi-directional probe array, Experiment 2.....	124
Figure 5.2.6-4. Velocity versus time from the corridor north (CN) bi-directional probe array, Experiment 2.....	125
Figure 5.2.6-5. Velocity versus time from the ceiling vent (V) bi-directional probe array, Experiment 2.....	125
Figure 5.2.7-1. Oxygen, carbon dioxide, carbon monoxide, and total hydrocarbon percent volume versus time from the upper bedroom (BR) sampling location, Experiment 2.....	127
Figure 5.2.7-2. Oxygen, carbon dioxide, and carbon monoxide percent volume versus time from the lower bedroom (BR) sampling location, Experiment 2.....	127
Figure 5.2.7-3. Oxygen, carbon dioxide, carbon monoxide, and total hydrocarbon percent volume versus time from the upper living (LR) room sampling location, Experiment 2.....	128
Figure 5.2.7-4. Oxygen, carbon dioxide, and carbon monoxide percent volume versus time from the lower living room (LR) sampling location, Experiment 2.....	128
Figure 5.3.1-1. Experiment 3, ignition.....	132
Figure 5.3.1-2. Experiment 3, 60 s after ignition.....	133
Figure 5.3.1-3. Experiment 3, 120 s after ignition.....	134
Figure 5.3.1-4. Experiment 3, 180 s after ignition.....	135
Figure 5.3.1-5. Experiment 3, window fully vented, 208 s after ignition.....	136
Figure 5.3.1-6. Experiment 3, corridor flames, 222 s after ignition.....	137
Figure 5.3.1-7. Experiment 3, 240 s after ignition.....	138
Figure 5.3.1-8. Experiment 3, WCD deployed, 266 s after ignition.....	139
Figure 5.3.1-9. Experiment 3, WCD in place, 270 s after ignition.....	140
Figure 5.3.1-10. Experiment 3, 300 s after ignition.....	141
Figure 5.3.1-11. Experiment 3, WCD removed, 330 s after ignition.....	142
Figure 5.3.1-12. Experiment 3, 360 s after ignition.....	143
Figure 5.3.2-1. Heat release rate versus time, Experiment 3.....	144
Figure 5.3.3-1. Temperature versus time from the bedroom window (BRW) thermocouple array, Experiment 3.....	147
Figure 5.3.3-2. Temperature versus time from the bedroom (BR) thermocouple array, Experiment 3.....	148
Figure 5.3.3-3. Temperature versus time from the hall thermocouple array, Experiment 3.....	148
Figure 5.3.3-4. Temperature versus time from the living room corner (LRC) thermocouple array, Experiment 3.....	149
Figure 5.3.3-5. Temperature versus time from the living room (LR) thermocouple array, Experiment 3.....	149
Figure 5.3.3-6. Temperature versus time from the corridor center (CC) thermocouple array, Experiment 3.....	150
Figure 5.3.3-7. Temperature versus time from the corridor south (CS) thermocouple array, Experiment 3.....	150
Figure 5.3.3-8. Temperature versus time from the corridor southwest (CSW) thermocouple array, Experiment 3.....	151

Figure 5.3.3-9. Temperature versus time from the corridor north (CN) thermocouple array, Experiment 3.....	151
Figure 5.3.3-10. Temperature versus time from the ceiling vent thermocouple array, Experiment 3.....	152
Figure 5.3.3-11. Temperature versus time from the target room (TR) door knobs, Experiment 3.....	152
Figure 5.3.3-12. Temperature versus time from the target room (TR) thermocouple array, Experiment 3.....	153
Figure 5.3.4-1. Heat flux versus time at five locations, Experiment 3.....	154
Figure 5.3.5-1. Pressure versus time at five locations, Experiment 3.....	155
Figure 5.3.6-1. Velocity versus time from the bedroom window (BRW) bi-directional probe array, Experiment 3.....	156
Figure 5.3.6-2. Velocity versus time from the hall bi-directional probe array, Experiment 3.....	157
Figure 5.3.6-3. Velocity versus time from the corridor south (CS) bi-directional probe array, Experiment 3.....	157
Figure 5.3.6-4. Velocity versus time from the corridor north (CN) bi-directional probe array, Experiment 3.....	158
Figure 5.3.6-5. Velocity versus time from the ceiling vent (V) bi-directional probe array, Experiment 3.....	158
Figure 5.3.7-1. Oxygen, carbon dioxide, carbon monoxide, and total hydrocarbon percent volume versus time from the upper bedroom (BR) sampling location, Experiment 3.....	160
Figure 5.3.7-2. Oxygen, carbon dioxide, and carbon monoxide percent volume versus time from the lower bedroom (BR) sampling location, Experiment 3.....	160
Figure 5.3.7-3. Oxygen, carbon dioxide, carbon monoxide, and total hydrocarbon percent volume versus time from the upper living (LR) room sampling location, Experiment 3.....	161
Figure 5.3.7-4. Oxygen, carbon dioxide, and carbon monoxide percent volume versus time from the lower living room (LR) sampling location, Experiment 3.....	161
Figure 5.4.1-1. Experiment 4, ignition.....	165
Figure 5.4.1-2. Experiment 4, 60 s after ignition.....	166
Figure 5.4.1-3. Experiment 4, 120 s after ignition.....	167
Figure 5.4.1-4. Experiment 4, 180 s after ignition.....	168
Figure 5.4.1-5. Experiment 4, window fully vented, 218 s after ignition.....	169
Figure 5.4.1-6. Experiment 4, corridor flames, 234 s after ignition.....	170
Figure 5.4.1-7. Experiment 4, 240 s after ignition.....	171
Figure 5.4.1-8. Experiment 4, 268 s after ignition, just prior to WCD deployment.....	172
Figure 5.4.1-9. Experiment 4, WCD in place, 275 s after ignition.....	173
Figure 5.4.1-10. Experiment 4, 300 s after ignition.....	174
Figure 5.4.1-11. Experiment 4, 360 s after ignition.....	175
Figure 5.4.1-12. Experiment 4, 420 s after ignition.....	176
Figure 5.4.2-1. Heat release rate versus time, Experiment 4.....	177
Figure 5.4.3-1. Temperature versus time from the bedroom window (BRW) thermocouple array, Experiment 4.....	180
Figure 5.4.3-2. Temperature versus time from the bedroom (BR) thermocouple array, Experiment 4.....	181
Figure 5.4.3-3. Temperature versus time from the hall thermocouple array, Experiment 4.....	181
Figure 5.4.3-4. Temperature versus time from the living room corner (LRC) thermocouple array, Experiment 4.....	182

Figure 5.4.3-5. Temperature versus time from the living room (LR) thermocouple array, Experiment 4.....	182
Figure 5.4.3-6. Temperature versus time from the corridor center (CC) thermocouple array, Experiment 4.....	183
Figure 5.4.3-7. Temperature versus time from the corridor south (CS) thermocouple array, Experiment 4.....	183
Figure 5.4.3-8. Temperature versus time from the corridor southwest (CSW) thermocouple array, Experiment 4.....	184
Figure 5.4.3-9. Temperature versus time from the corridor north (CN) thermocouple array, Experiment 4.....	184
Figure 5.4.3-10. Temperature versus time from the ceiling vent thermocouple array, Experiment 4.....	185
Figure 5.4.3-11. Temperature versus time from the target room (TR) thermocouple array, Experiment 4.....	185
Figure 5.4.4-1. Heat flux versus time at five locations, Experiment 4.....	186
Figure 5.4.5-1. Pressure versus time at five locations, Experiment 4.....	187
Figure 5.4.6-1. Velocity versus time from the bedroom window (BRW) bi-directional probe array, Experiment 4.....	189
Figure 5.4.6-2. Velocity versus time from the hall bi-directional probe array, Experiment 4.....	189
Figure 5.4.6-3. Velocity versus time from the corridor south (CS) bi-directional probe array, Experiment 4.....	190
Figure 5.4.6-4. Velocity versus time from the corridor north (CN) bi-directional probe array, Experiment 4.....	190
Figure 5.4.6-5. Velocity versus time from the ceiling vent (V) bi-directional probe array, Experiment 4.....	191
Figure 5.4.7-1. Oxygen, carbon dioxide, and carbon monoxide percent volume versus time from the lower bedroom (BR) sampling location, Experiment 4.....	192
Figure 5.4.7-2. Oxygen, carbon dioxide, carbon monoxide, and total hydrocarbon percent volume versus time from the upper living (LR) room sampling location, Experiment 4.....	193
Figure 5.4.7-3. Oxygen, carbon dioxide, and carbon monoxide percent volume versus time from the lower living room (LR) sampling location, Experiment 4.....	193
Figure 5.5.1-1. Experiment 5, ignition.....	197
Figure 5.5.1-2. Experiment 5, 60 s after ignition.....	198
Figure 5.5.1-3. Experiment 5, 120 s after ignition.....	199
Figure 5.5.1-4. Experiment 5, 180 s after ignition.....	200
Figure 5.5.1-5. Experiment 5, 240 s after ignition.....	201
Figure 5.5.1-6. Experiment 5, corridor flames, 257 s after ignition.....	202
Figure 5.5.1-7. Experiment 5, 300 s after ignition.....	203
Figure 5.5.1-8. Experiment 5, WCD deployed, 327 s after ignition.....	204
Figure 5.5.1-9. Experiment 5, WCD in place, 335 s after ignition.....	205
Figure 5.5.1-10. Experiment 5, 360 s after ignition.....	206
Figure 5.5.1-11. Experiment 5, 420 s after ignition.....	207
Figure 5.5.1-12. Experiment 5, 480 s after ignition.....	208
Figure 5.5.1-13. Experiment 5, WCD removed, 515 s after ignition.....	209
Figure 5.5.2-1. Heat release rate versus time, Experiment 5.....	210

Figure 5.5.3-1. Temperature versus time from the bedroom window (BRW) thermocouple array, Experiment 5.....	213
Figure 5.5.3-2. Temperature versus time from the bedroom (BR) thermocouple array, Experiment 5.....	213
Figure 5.5.3-3. Temperature versus time from the hall thermocouple array, Experiment 5.....	214
Figure 5.5.3-4. Temperature versus time from the living room corner (LRC) thermocouple array, Experiment 5.....	214
Figure 5.5.3-5. Temperature versus time from the living room (LR) thermocouple array, Experiment 5.....	215
Figure 5.5.3-6. Temperature versus time from the corridor center (CC) thermocouple array, Experiment 5.....	215
Figure 5.5.3-7. Temperature versus time from the corridor south (CS) thermocouple array, Experiment 5.....	216
Figure 5.5.3-8. Temperature versus time from the corridor southwest (CSW) thermocouple array, Experiment 5.....	216
Figure 5.5.3-9. Temperature versus time from the corridor north (CN) thermocouple array, Experiment 5.....	217
Figure 5.5.3-10. Temperature versus time from the ceiling vent thermocouple array, Experiment 5.....	217
Figure 5.5.3-11. Temperature versus time from the target room (TR) thermocouple array, Experiment 5.....	218
Figure 5.5.4-1. Heat flux versus time at five locations, Experiment 5.....	219
Figure 5.5.5-1. Pressure versus time at five locations, Experiment 5.....	220
Figure 5.5.6-1. Velocity versus time from the bedroom window (BRW) bi-directional probe array, Experiment 5.....	221
Figure 5.5.6-2. Velocity versus time from the hall bi-directional probe array, Experiment 5.....	222
Figure 5.5.6-3. Velocity versus time from the corridor south (CS) bi-directional probe array, Experiment 5.....	222
Figure 5.5.6-4. Velocity versus time from the corridor north (CN) bi-directional probe array, Experiment 5.....	223
Figure 5.5.6-5. Velocity versus time from the ceiling vent (V) bi-directional probe array, Experiment 5.....	223
Figure 5.5.7-1. Oxygen, carbon dioxide, and carbon monoxide percent volume versus time from the lower bedroom (BR) sampling location, Experiment 5.....	225
Figure 5.5.7-2. Oxygen, carbon dioxide, carbon monoxide, and total hydrocarbon percent volume versus time from the upper living (LR) room sampling location, Experiment 5.....	225
Figure 5.5.7-3. Oxygen, carbon dioxide, and carbon monoxide percent volume versus time from the lower living room (LR) sampling location, Experiment 5.....	226
Figure 5.6.1-1. Experiment 6, ignition.....	230
Figure 5.6.1-2. Experiment 6, 60 s after ignition.....	231
Figure 5.6.1-3. Experiment 6, 120 s after ignition.....	232
Figure 5.6.1-4. Experiment 6, window fully vented, 174 s after ignition.....	233
Figure 5.6.1-5. Experiment 6, 180 s after ignition.....	234
Figure 5.6.1-6. Experiment 6, corridor flames, 192 s after ignition.....	235
Figure 5.6.1-7. Experiment 6, 240 s after ignition.....	236
Figure 5.6.1-8. Experiment 6, 265 s after ignition.....	237

Figure 5.6.1-9. Experiment 6, 287 s after ignition, 20 s after window sprinkler activation.	238
Figure 5.6.1-10. Experiment 6, 300 s after ignition.	239
Figure 5.6.1-11. Experiment 6, fog stream across window off, 330 s after ignition.	240
Figure 5.6.1-12. Experiment 6, direct fog stream on, 345 s after ignition.	241
Figure 5.6.1-13. Experiment 6, 360 s after ignition.	242
Figure 5.6.1-14. Experiment 6, 400 s after ignition.	243
Figure 5.6.1-15. Experiment 6, 420 s after ignition.	244
Figure 5.6.2-1. Heat release rate versus time, Experiment 6.	245
Figure 5.6.3-1. Temperature versus time from the bedroom window (BRW) thermocouple array, Experiment 6.	248
Figure 5.6.3-2. Temperature versus time from the bedroom (BR) thermocouple array, Experiment 6.	249
Figure 5.6.3-3. Temperature versus time from the hall thermocouple array, Experiment 6.	250
Figure 5.6.3-4. Temperature versus time from the living room corner (LRC) thermocouple array, Experiment 6.	251
Figure 5.6.3-5. Temperature versus time from the living room (LR) thermocouple array, Experiment 6.	252
Figure 5.6.3-6. Temperature versus time from the corridor center (CC) thermocouple array, Experiment 6.	253
Figure 5.6.3-7. Temperature versus time from the corridor south (CS) thermocouple array, Experiment 6.	254
Figure 5.6.3-8. Temperature versus time from the corridor southwest (CSW) thermocouple array, Experiment 6.	255
Figure 5.6.3-9. Temperature versus time from the corridor north (CN) thermocouple array, Experiment 6.	256
Figure 5.6.3-10. Temperature versus time from the ceiling vent thermocouple array, Experiment 6.	257
Figure 5.6.3-11. Temperature versus time from the target room (TR) thermocouple array, Experiment 6.	258
Figure 5.6.4-1. Heat flux versus time at five locations, Experiment 6.	259
Figure 5.6.5-1. Pressure versus time at five locations, Experiment 6.	260
Figure 5.6.6-1. Velocity versus time from the bedroom window (BRW) bi-directional probe array, Experiment 6.	261
Figure 5.6.6-2. Velocity versus time from the hall bi-directional probe array, Experiment 6.	262
Figure 5.6.6-3. Velocity versus time from the corridor south (CS) bi-directional probe array, Experiment 6.	263
Figure 5.6.6-4. Velocity versus time from the corridor north (CN) bi-directional probe array, Experiment 6.	264
Figure 5.6.6-5. Velocity versus time from the ceiling vent (V) bi-directional probe array, Experiment 6.	265
Figure 5.6.7-1. Oxygen, carbon dioxide, carbon monoxide, and total hydrocarbon percent volume versus time from the upper bedroom (BR) sampling location, Experiment 6.	267
Figure 5.6.7-2. Oxygen, carbon dioxide, and carbon monoxide percent volume versus time from the lower bedroom (BR) sampling location, Experiment 6.	268
Figure 5.6.7-3. Oxygen, carbon dioxide, carbon monoxide, and total hydrocarbon percent volume versus time from the upper living (LR) room sampling location, Experiment 6.	269

Figure 5.6.7-4. Oxygen, carbon dioxide, and carbon monoxide percent volume versus time from the lower living room (LR) sampling location, Experiment 6.....	270
Figure 5.7.1-1. Experiment 7, ignition.....	273
Figure 5.7.1-2. Experiment 7, 60 s after ignition.....	274
Figure 5.7.1-3. Experiment 7, 120 s after ignition.....	275
Figure 5.7.1-4. Experiment 7, 180 s after ignition.....	276
Figure 5.7.1-5. Experiment 7, 240 s after ignition.....	277
Figure 5.7.1-6. Experiment 7, 300 s after ignition.....	278
Figure 5.7.1-7. Experiment 7, window fully vented, 312 s after ignition.....	279
Figure 5.7.1-8. Experiment 7, 360 s after ignition.....	280
Figure 5.7.1-9. Experiment 7, 420 s after ignition.....	281
Figure 5.7.1-10. Experiment 7, indirect suppression started, 438 s after ignition.....	282
Figure 5.7.1-11. Experiment 7, 480 s after ignition.....	283
Figure 5.7.1-12. Experiment 7, 540 s after ignition.....	284
Figure 5.7.1-13. Experiment 7, direct suppression, 550 s after ignition.....	285
Figure 5.7.2-1. Heat release rate versus time, Experiment 7.....	286
Figure 5.7.3-1. Temperature versus time from the bedroom window (BRW) thermocouple array, Experiment 7.....	289
Figure 5.7.3-2. Temperature versus time from the bedroom (BR) thermocouple array, Experiment 7.....	289
Figure 5.7.3-3. Temperature versus time from the hall thermocouple array, Experiment 7.....	290
Figure 5.7.3-4. Temperature versus time from the living room corner (LRC) thermocouple array, Experiment 7.....	290
Figure 5.7.3-5. Temperature versus time from the living room (LR) thermocouple array, Experiment 7.....	291
Figure 5.7.3-6. Temperature versus time from the corridor center (CC) thermocouple array, Experiment 7.....	291
Figure 5.7.3-7. Temperature versus time from the corridor south (CS) thermocouple array, Experiment 7.....	292
Figure 5.7.3-8. Temperature versus time from the corridor southwest (CSW) thermocouple array, Experiment 7.....	292
Figure 5.7.3-9. Temperature versus time from the corridor north (CN) thermocouple array, Experiment 7.....	293
Figure 5.7.3-10. Temperature versus time from the ceiling vent thermocouple array, Experiment 7.....	293
Figure 5.7.3-11. Temperature versus time from the target room (TR) thermocouple array, Experiment 7.....	294
Figure 5.7.4-1. Heat flux versus time at five locations, Experiment 7.....	295
Figure 5.7.5-1. Pressure versus time at five locations, Experiment 7.....	296
Figure 5.7.6-1. Velocity versus time from the bedroom window (BRW) bi-directional probe array, Experiment 7.....	297
Figure 5.7.6-2. Velocity versus time from the hall bi-directional probe array, Experiment 7.....	298
Figure 5.7.6-3. Velocity versus time from the corridor south (CS) bi-directional probe array, Experiment 7.....	298
Figure 5.7.6-4. Velocity versus time from the corridor north (CN) bi-directional probe array, Experiment 7.....	299

Figure 5.7.6-5. Velocity versus time from the ceiling vent (V) bi-directional probe array, Experiment 7.....	299
Figure 5.7.7-1. Oxygen, carbon dioxide, carbon monoxide, and total hydrocarbon percent volume versus time from the upper bedroom (BR) sampling location, Experiment 7.....	301
Figure 5.7.7-2. Oxygen, carbon dioxide, and carbon monoxide percent volume versus time from the lower bedroom (BR) sampling location, Experiment 7.....	301
Figure 5.7.7-3. Oxygen, carbon dioxide, carbon monoxide, and total hydrocarbon percent volume versus time from the upper living (LR) room sampling location, Experiment 7.....	302
Figure 5.7.7-4. Oxygen, carbon dioxide, carbon monoxide, and total hydrocarbon percent volume versus time from the upper living (LR) room sampling location, Experiment 7.....	302
Figure 5.8.1-1. Experiment 8, ignition.....	306
Figure 5.8.1-2. Experiment 8, 60 s after ignition.....	307
Figure 5.8.1-3. Experiment 8, 120 s after ignition.....	308
Figure 5.8.1-4. Experiment 8, window fully vented, 150 s after ignition.....	309
Figure 5.8.1-5. Experiment 8, 180 s after ignition.....	310
Figure 5.8.1-6. Experiment 8, corridor flames, 185 s after ignition.....	311
Figure 5.8.1-7. Experiment 8, 240 s after ignition.....	312
Figure 5.8.1-8. Experiment 8, 300 s after ignition.....	313
Figure 5.8.1-9. Experiment 8, indirect suppression started, 310 s after ignition.....	314
Figure 5.8.1-10. Experiment 8, flames withdraw from vent, 315 s after ignition.....	315
Figure 5.8.1-11. Experiment 8, 360 s after ignition.....	316
Figure 5.8.1-12. Experiment 8, 420 s after ignition.....	317
Figure 5.8.1-13. Experiment 8, indirect suppression stopped, 468 s after ignition.....	318
Figure 5.8.1-14. Experiment 8, 480 s after ignition.....	319
Figure 5.8.2-1. Heat release rate versus time, Experiment 8.....	320
Figure 5.8.3-1. Temperature versus time from the bedroom window (BRW) thermocouple array, Experiment 8.....	322
Figure 5.8.3-2. Temperature versus time from the bedroom (BR) thermocouple array, Experiment 8.....	322
Figure 5.8.3-3. Temperature versus time from the hall thermocouple array, Experiment 8.....	323
Figure 5.8.3-4. Temperature versus time from the living room corner (LRC) thermocouple array, Experiment 8.....	323
Figure 5.8.3-5. Temperature versus time from the living room (LR) thermocouple array, Experiment 8.....	324
Figure 5.8.3-6. Temperature versus time from the corridor center (CC) thermocouple array, Experiment 8.....	324
Figure 5.8.3-7. Temperature versus time from the corridor south (CS) thermocouple array, Experiment 8.....	325
Figure 5.8.3-8. Temperature versus time from the corridor southwest (CSW) thermocouple array, Experiment 8.....	325
Figure 5.8.3-9. Temperature versus time from the corridor north (CN) thermocouple array, Experiment 8.....	326
Figure 5.8.3-10. Temperature versus time from the ceiling vent thermocouple array, Experiment 8.....	326
Figure 5.8.4-1. Heat flux versus time at five locations, Experiment 8.....	327
Figure 5.8.5-1. Pressure versus time at five locations, Experiment 8.....	328

Figure 5.8.6-1. Velocity versus time from the bedroom window (BRW) bi-directional probe array, Experiment 8.....	329
Figure 5.8.6-2. Velocity versus time from the hall bi-directional probe array, Experiment 8.	330
Figure 5.8.6-3. Velocity versus time from the corridor south (CS) bi-directional probe array, Experiment 8.....	330
Figure 5.8.6-4. Velocity versus time from the corridor north (CN) bi-directional probe array, Experiment 8.....	331
Figure 5.8.6-5. Velocity versus time from the ceiling vent (V) bi-directional probe array, Experiment 8.....	331
Figure 5.8.7-1. Oxygen, carbon dioxide, carbon monoxide, and total hydrocarbon percent volume versus time from the upper bedroom (BR) sampling location, Experiment 8.....	333
Figure 5.8.7-2. Oxygen, carbon dioxide, and carbon monoxide percent volume versus time from the lower bedroom (BR) sampling location, Experiment 8.....	333
Figure 5.8.7-3. Oxygen, carbon dioxide, carbon monoxide, and total hydrocarbon percent volume versus time from the upper living (LR) room sampling location, Experiment 8.....	334
Figure 5.8.7-4. Oxygen, carbon dioxide, carbon monoxide, and total hydrocarbon percent volume versus time from the lower living (LR) room sampling location, Experiment 8.....	334
Figure 6.1-1. Heat release rate versus time, Experiment 1, no imposed wind. T = 0 is the time of window failure.....	336
Figure 6.1-2. Temperature versus time, Experiment 1, no imposed wind. T = 0 is the time of window failure.....	337
Figure 6.1-3. Heat flux versus time, Experiment 1, no imposed wind. T = 0 is the time of window failure.....	337
Figure 6.1-4. Velocity versus time, Experiment 1, no imposed wind. T = 0 is the time of window failure.....	338
Figure 6.2.1-1. Heat release rate versus time, Experiments 2 through 5. T = 0 is the time of WCD deployment.....	340
Figure 6.2.1-2. Temperature versus time from the Corridor North array, 1.52 m (5.00 ft) below the ceiling, Experiments 2 through 5. T = 0 is the time of WCD deployment.....	341
Figure 6.2.1-3. Temperature versus time from the Corridor South array, 1.52 m (5.00 ft) below the ceiling, Experiments 2 through 5. T = 0 is the time of WCD deployment.....	341
Figure 6.2.1-4. Temperature versus time from the Corridor Southwest array, 1.52 m (5.00 ft) below the ceiling, Experiments 2 through 5. T = 0 is the time of WCD deployment.....	342
Figure 6.2.1-5. Heat flux versus time from the Corridor North position, 1.52 m (5.00 ft) below the ceiling, Experiments 2 through 5. T = 0 is the time of WCD deployment.....	343
Figure 6.2.1-6. Temperature versus time from the Corridor South position, 1.52 m (5.00 ft) below the ceiling, Experiments 2 through 5. T = 0 is the time of WCD deployment.....	343
Figure 6.2.1-7. Velocity versus time, from the Corridor North position, 1.22 m (4.00 ft) below the ceiling, Experiments 2 through 5. T = 0 is the time of WCD deployment.....	344
Figure 6.2.1-8. Velocity versus time, from the Corridor South position, 1.22 m (4.00 ft) below the ceiling, Experiments 2 through 5. T = 0 is the time of WCD deployment.....	344
Figure 6.2.2-1. Heat release rate versus time, Experiments 6 through 8. T = 0 is the time of water application.....	346
Figure 6.2.2-2. Temperature versus time from the Corridor North position, 1.52 m (5.00 ft) below the ceiling, Experiments 6 through 8. T = 0 is the time of water application.....	347

Figure 6.2.2-3. Temperature versus time from the Corridor South position, 1.52 m (5.00 ft) below the ceiling, Experiments 6 through 8. T = 0 is the time of water application.....	347
Figure 6.2.2-4. Temperature versus time from the Corridor Southwest position, 1.52 m (5.00 ft) below the ceiling, Experiments 6 through 8. T = 0 is the time of water application.....	348
Figure 6.2.2-5. Heat flux versus time from the Corridor North position, 1.52 m (5.00 ft) below the ceiling, Experiments 6 through 8. T = 0 is the time of water application.....	349
Figure 6.2.2-6. Heat flux versus time from the Corridor South position, 1.52 m (5.00 ft) below the ceiling, Experiments 6 through 8. T = 0 is the time of water application.....	349
Figure 6.2.2-7. Velocity versus time, from the Corridor North position, 1.22 m (4.00 ft) below the ceiling, Experiments 6 through 8. T = 0 is the time of water application.....	350
Figure 6.2.2-8. Velocity versus time, from the Corridor South position, 1.22 m (4.00 ft) below the ceiling, Experiments 6 through 8. T = 0 is the time of water application.....	351
Figure 6.2.3-1. Temperature versus time, Experiment 7. T = 0 is the time that the door between the living room and the corridor was opened.	352

List of Tables

Table 1.1-1. FDNY Wind driven fire incidents.....	3
Table 4.2-1. Bedroom fuel load description.....	53
Table 4.2-2. Living room fuel load description.....	55
Table 4.2-3. Hallway fuel load description.....	55
Table 4.3-1. Summary of average wind speeds with respect to fan speeds, (m/s \pm 15 %)......	57
Table 4.3-2. Summary of average baseline differential pressures with respect to fan speed, (Pa \pm 15 %)......	57
Table 4.3-3. Change of wind speed in the hall and vent based on the deployment of a WCD or closing the door to the corridor at two fan speeds, (m/s \pm 15 %).	59
Table 4.3-4. Change of pressures in the apartment due to the deployment of a WCD or closing a door to the corridor at two fan speeds, (Pa \pm 15 %).	60
Table 4.3-1. Table of Structure Fire Experiments	65
Table 5.1-1. Experiment 1 Timeline	66
Table 5.2-1. Experiment 2 Timeline	99
Table 5.3-1. Experiment 3 Timeline	129
Table 5.4-1. Experiment 4 Timeline	162
Table 5.5-1. Experiment 5 Timeline	194
Table 5.6-1. Experiment 6 Timeline	226
Table 5.7-1. Experiment 7 Timeline	271
Table 5.8-1. Experiment 8 Timeline	303

1 Introduction

The National Institute of Standards and Technology (NIST) and the Fire Protection Research Foundation (FPRF) with the support of the Department of Homeland Security (DHS)/ Federal Emergency Management Agency (FEMA) Assistance to Firefighters Research and Development Grant Program and the United States Fire Administration (USFA) have conducted a series of wind driven fire experiments in a laboratory structure. The experiments were conducted in the NIST Large Fire Facility in Gaithersburg, Maryland from November 2007 to January 2008.

The objective of this study was to improve the safety of firefighters and building occupants by enabling a better understanding of wind driven firefighting tactics, including structural ventilation and suppression. This was achieved by investigating technical issues that address the teaching of the dynamics of fire phenomena and prediction of fire intensity and growth under wind driven conditions. The data from this research will also help to identify methods and promulgation of improved standard operating guidelines (SOG) for the fire service to enhance firefighter safety, fire ground operations, and use of equipment.

The experiments were conducted in NIST's Large Fire Facility in order to provide the best levels of control on the experiments and have the capability of making heat release rate and high quality gas concentration measurements which would be difficult and cost prohibitive to make in an acquired structure. As implied by the title, the laboratory experiments documented in this report are only one portion of the research needed to analyze the impact of wind on a fire resistive structure fire and demonstrate potential methods (tactics) for improving firefighter safety and effectiveness. These experiments were conducted in advance of a series of fire experiments that were performed in a 7 story building on Governors Island in New York City in February 2008. The New York City experiments conducted by NIST in partnership with the Fire Department of New York City and Polytechnic University were also done with the support of a DHS/ FEMA Assistance to Firefighters Research and Development Grant Program and the USFA.

1.1 Background

Fires in high-rise buildings create unique safety challenges for building occupants and firefighters. Smoke and heat spreading through the corridors and the stairs of a building during a fire can limit building occupants' ability to escape and can limit firefighters' ability to rescue them. In 2002, there were 7,300 reported fires in high rise structures (structures 7 stories or more). The majority of these high rise fires occurred in residential occupancies, such as apartment buildings. In fires that originate in apartments, 92 % of the civilian fatalities have occurred in incidents where the fire spreads beyond the room of origin [1].

Changes in the building's ventilation, such as the opening of doors or windows can increase the growth of the fire and allow it to spread beyond the room of fire origin. This can also increase the spread of fire gases through the building. In some cases, such as the Cook County Administration Building fire in October 2003, the fire flow into the corridors and the stairway prevented firefighters from suppressing

the fire from inside the structure. This fire resulted in 6 building occupant fatalities and several firefighter injuries in the stairway [2].

The failure of a window in the fire apartment in the presence of an external wind can create significant and rapid increases in the heat production of a fire. Combined with open doors to corridors, stairs, or downwind apartments, many wind driven fire incidents have resulted in firefighter fatalities and injuries [3,4].

1.1.1 Historical Wind Driven Fires

Recognition of wind driven fire conditions has been taken into account in forest fires and large area conflagrations for more than 100 years. This is due in part to the fact that some of the most destructive and deadly conflagrations in the United States such as the Great Pestigo, WI fire and the Great Chicago fire were wind driven events. Both of these fires started on the same day, October 8, 1871. The Pestigo fire resulted in 1,152 fatalities and more than 1.2 million acres burned. The Chicago fire resulted in more than 250 fatalities, and 17,400 structures destroyed over a 2,000 acre area [5]. The magnitude of these fires were, in part, the result of strong south winds combined with “tinder dry” conditions [6].

While wildland fire managers and officers training includes weather conditions in their evaluation of incident conditions (size-up), typically structural firefighters and fire officers do not receive this type of training [7, 8, 9, 10]. Wildland firefighter training manuals dedicate almost half of their fire behavior chapter to weather with significant sections on wind [11]. Structural firefighter training manuals, which are approximately 1000 pages in length, dedicate a page or less to the interaction of wind and structural fire behavior [12, 13, 14]. As a result, structure fires that may have been affected by wind conditions have typically not been recognized as such or well documented, with some notable exceptions. A few such exceptions are presented in the following sections.

1.1.2 Experience of the Fire Department of New York City

The Fire Department of New York City (FDNY) began to recognize that wind driven fires, particularly those in multiple-story, residential occupancies of fire resistive construction (Class I) were challenging their resources, their tactics, and their safety. Norman and Tracy and others in the department began to look at the challenges and results of wind driven fires, with the goal of changing the tactics in order to improve the safety and effectiveness of their members [15, 16, 17]. A listing of notable FDNY wind driven fire incidents is given in Table 1.1-1 [15, 18]. While it might appear that the frequency of occurrence has increased, the reality may be that the recognition of wind driven fires has increased in the department. In fact, the FDNY has developed a training DVD, *Fighting Wind Driven Fires in High Rise Multiple Dwellings*, which was written in November of 2007 with the objective of developing an awareness for wind effects in a structure, and identifying how to control the hazard or find shelter from the hazard by controlling doors and preparing areas of refuge [19].

Another factor Norman [15] identifies is that the fire does not have to be 20 stories or more above ground for wind to be a factor. Table 1.1-1 demonstrates that these FDNY wind driven fire incidents have occurred as low as the 3rd story above ground. NFPA data shows that the majority of fires in high rise buildings occur below the 7th floor [1].

Table 1.1-1. FDNY Wind driven fire incidents.

Date	Location	Victims	Stories	Fire Floor
1/23/80	30 Montrose Avenue, Brooklyn	1 civilian fatality	16	11 th
2/11/89	23 Horace Harding Expressway, Queens	3 civilian fatalities	16	14 th
11/2/94	Park Ave, Bronx	2 civilian fatalities	20	18 th
1/5/96	40-20 Beach Channel Drive, Queens	1 firefighter fatality	13	3 rd
1/7/97	1 Lincoln Place, Manhattan	18 firefighters injured	42	28 th
12/18/98	77 Vandalia Avenue, Brooklyn	3 firefighter fatalities	10	10 th
12/23/98	124 West 60 th St, Manhattan	4 civilian fatalities, 9 firefighters injured	51	19 th
4/23/01	Waterside Plaza, Manhattan	30 firefighters injured, 4 civilians injured	37	24 th
9/9/04	20 Confucious Place, Manhattan	12 firefighters burned	44	37 th
1/26/06	40-20 Beach Channel Drive, Queens	3 firefighters burned	13	6 th
2/26/06	20 Moshulu Parkway, Bronx	3 firefighters burned	41	24 th & 25 th
1/03/08	1700 Bedford Avenue, Brooklyn	1 firefighter fatality 4 firefighters burned, 4 civilians injured	25	14 th
3/28/08	Grand Avenue, Manhattan	1 civilian fatality, 45 injured	26	4 th
4/2/08	Sutter Ave, Brooklyn	3 firefighters injured	22	5 th

Other wind related firefighter line of duty deaths have occurred in New York City in smaller buildings of ordinary construction (Type III) such as the “Black Sunday Fire.” This fire started on the third story of a four story apartment building. The average wind speed was 12 mph with gusts up to 45 mph. Firefighters searching for victims on the floor above the fire reported that, “fire was blowing into the hallway.” The rapid spread of fire to the 4th floor left 6 firefighters trapped. Their only option was to deploy out of the windows to ground, resulting in the death of two of the firefighters and serious injuries to the other four [20].

Buildings and topographical features alone or in combination deflect wind and as a result cause changes in wind speed and direction or localized wind effects around a building. In cities, this may be referred to as “building-spawned” wind. All buildings, regardless of size, can block wind, which may cause “local areas of amplified winds around corners and enhanced turbulence in building wakes” [21]. When wind

hits the face of a structure it will seek the path of least resistance to move around it. For a multi-story building with a flat face on the upwind side, it has been demonstrated that some of the wind will go over the building, a portion of the wind will go around the building and a portion of the wind will be deflected downward, and develop a vortex near the ground. The vortex results in a flow which is in the opposite direction (away from the building) of the source wind [22].

1.1.3 U.S. Wind Driven Fire Experience

These wind driven fire incidents are not limited to New York City. Houston, TX., St. Louis, MO., and Prince William County, VA. are just a few of the other localities in the United States that have experienced losses to wind driven fires [4, 23, 24, 25]. These incidents ranged from a fire that started on the 5th floor of a 41 story, fire resistive building to a fire that started on the wood deck outside a two story, wood frame, single family home.

Recently a near miss was documented in a wood frame Cape Cod-type house in Long Island, NY. Firefighters working to extinguish the fire, making entry from the front of the house, had flames pushed over them by the wind entering the structure from the rear [26].

A search of the National Firefighter Near-Miss Reporting System database also shows a variety of fire incidents and structures where wind caused a significant change in fire conditions resulting in rapid increases in thermal hazard to the firefighters [27, 28, 29, 30, 31, 32, 33].

1.1.4 NFPA Wind Driven Analysis

Given that the impact of wind on structure fires is not typically documented, the NFPA and Fire Protection Research Foundation has conducted an analysis of fatal high rise fires to examine how many may have been affected by wind conditions. The methodology and spread sheets from the analysis are provided in Appendix A of this report.

A database of 565 fires was compiled. Data on each fire included the date of the incident, the location, the type of occupancy, the floor of fire origin, the total number of floors in the building, number of fatalities and a reported dollar loss. This data was correlated with wind speed data for the city on the day of the incident. While this information may not be representative of conditions local to the building involved or representative of the exact wind at the time of the fire, given that there are hundreds of incidents a trend may present itself. The analysis included an “event status” for each fire ranging from 1 to 5. A 1 rating indicates that the wind may have impacted the fire conditions but it is “unlikely” and a 5 rating indicates that wind impact on the fire was “confirmed and relevant”. Of the 565 fire incidents only 30 fires had a rating of 5 (confirmed and relevant) and 55 had a rating of 4 (probable but unconfirmed with documentation). Out of the total 565 fire incidents, there were 342 incidents that had a rating of 3 or higher, these incidents resulted in 1110 fatalities.

1.1.5 Wind Driven Tactics Research

What tactics or tools are appropriate for use with a wind driven fire and how should the tactics or tools be implemented? In order to answer this question, the problem has to be fully defined. The wind driven

fire hazard that has been examined occurs in a high rise building of fire resistive construction with internal corridors and interior stairs. The Vandalia fire incident in which three FDNY firefighters died exemplifies scenarios which result in untenable conditions in a public corridor. The door to the fire apartment was left open. As a result, there was nothing to keep the fire or the smoke contained to the apartment of fire origin. A door to a stair was opened and the stair was vented to the outside or an apartment on the downwind side of the building is opened. If the fire apartment was on the upwind side of the building and the window failed, a ventilation path would be in place for flames to sweep through the apartment of origin and out into the corridor, making it impossible and untenable for firefighters to approach the fire apartment.

Norman summarizes tactics that FDNY has researched to address this condition, 1) breaching, 2) suppressing the fire with an exterior water stream, and 3) controlling the flow of wind into the fire apartment with a window fire blanket or curtain [15]. Breaching involves making a hole from a protected stair and continuing to breach walls until a hole for a hoseline can be made in the wall of the fire apartment or the fire could be attacked from an adjoining balcony. Exterior hose streams have been used when the fire apartment is in reach of an aerial apparatus stream. For apartments on higher floors, an applicator pipe or Navy fog applicator may be used to apply water into the window of a fire apartment on the floor above. The use of a wind control device deployed from the floor above the fire floor to block an open window to a fire apartment on the upwind side of the building has been researched by FDNY. In fact, the department issued wind control devices to Special Operations Units [15].

Positive Pressure Ventilation (PPV) is being used by fire departments on smaller structures, such as single family homes, to control the fire flow by introducing pressure from the front door and venting the house through a strategic exit opening. If done correctly, this tactic can remove significant amounts of heat and smoke from the structure, thus improving the firefighters' working environment and improving the chances of survival for the building occupants. NIST has completed several studies which have a two-fold impact: 1) providing guidance on the safe use of PPV and 2) characterizing and validating the modeling of PPV with a computational fluid dynamics (CFD) model, so that the model can be used as a training tool for the fire service [34, 35, 36, 37].

In 2006, NIST research then turned to examine the use of PPV in high-rise firefighting. To accomplish this task NIST partnered with the Chicago Fire Department (CFD), FDNY and the Toledo Fire and Rescue Department. In a vacant 30 story high-rise in Toledo the capability of PPV to pressurize the stair was demonstrated in an extensive series of pressure experiments [38]. This study was followed with a series of fire experiments conducted in a 16 story high-rise in Chicago [39]. The results of the fire experiments demonstrated the ability of properly sized and placed PPV fans to pressurize stairways in a high rise building and clear them of heat and smoke even with post-flashover fires open to the corridor on the fire floor. Near the end of the test series in Chicago, experiments were conducted to examine the impact of wind on an apartment fire and the potential for a wind control device and/or a large PPV fan to control the hazard and protect the corridor. The experiments conducted on the 3rd floor demonstrated that introducing a wind to a post flashover room fire can result in "blow torch" flames through the apartment and into the corridor in less than 30 s. The experiments also showed that a wind control device could in fact negate the impact of the wind and that PPV fans may have a role in mitigating the hazard from wind driven fires.

Given the limited data on wind driven fires, these experiments were proposed. While the use of wind control devices to control the ventilation conditions or the use of a special fire nozzle from the floor below the fire floor have been tried by the fire service under “real fire” conditions with varying levels of success, there is no fire data to understand the capabilities and limitations of these fire fighting approaches. This study addresses this need to collect real-scale data, in order to guide the development of appropriate tactical options for use under wind driven conditions.

2 Technical Approach

FPRF assembled a panel of experienced fire chiefs and other experts of the fire community to review the proposed experiments and offer their insight to ensure that the resulting data is useful to the fire service. The list of experts is provided in Appendix B. NIST staff presented a draft approach for discussion with the FPRF panel. The experimental geometry was selected to be representative of an apartment and public corridor arrangement with a flow path from the room of fire origin through another furnished room and into the corridor. The corridor was designed to have an open end and a closed end to provide a comparison of flow and non-flow conditions in the corridor. A full description of the experimental arrangement is provided in Section 4.

2.1 Objectives

The objectives of this study were threefold:

- 1) to understand the impact of wind on a structure fire fueled with residential furnishings in terms of temperature, heat flux, heat release rate and gas concentration,
- 2) to quantify the impact of several novel fire fighting tactics on a wind driven structure fire,
- 3) improve firefighter safety.

A series of experiments were designed to accomplish these objectives, and to provide data and documentation for further study. The experiments were to be conducted in NIST’s Large Fire Facility in order to provide the best levels of control on the experiments and have the capability of making heat release rate and high quality gas concentration measurements which would be difficult and cost prohibitive to make in an acquired structure.

A fire resistant structure was constructed and instrumented to measure temperature, heat flux, pressure, gas concentrations, and gas velocity from a well characterized fuel load. Recording of the experiments were made with video and thermal imaging cameras. Experiments were conducted without a fire to establish a baseline for air flows. In addition to the immediate value of characterizing the impact of wind on a structure fire, this data will also be used to assess CFD model results of a wind driven fire in future phases of this project.

These experiments were conducted with mechanically induced wind conditions. Eight fire experiments were conducted to examine the impact of wind on fire spread through the multi-room structure and examine the capabilities of a wind control device and externally applied water.

2.2 Experiments

A series of separate experiments were conducted to develop baseline or benchmark conditions. Full-scale heat release rate experiments were conducted on the waste container, the bed, upholstered chair and sofa. The furnishings were also characterized in terms of material, size and mass.

The next series of tests conducted examined the wind source used for the structure tests. The wind source was characterized based on the engine speed and wind velocity. Differential pressure sensors and pressure probes were used to examine the pressures and flow through the structure with no fire present. Wind tests were also conducted with the wind control devices to examine the changes to the pressures and flow in the structure after deployment.

Water distribution experiments, under wind driven conditions, were also conducted in the structure. These experiments measured the mass of water collected in pans placed on the floor of the structure. The water spray from several different application nozzles was measured. These water distribution experiments provide a map of areas that might be impacted directly by the water during the suppression phase of the wind driven fire experiments.

Eight wind driven fire experiments were conducted in a fire resistant, three room structure with a corridor. In order to understand the impact of the wind and mitigation tactics on the fire conditions within the structure, measurements of heat release rate, temperature, heat flux, pressure, gas concentrations, and gas velocity were made. The constants in each of the fire experiments included fuel load, wind direction, and ignition location and source. Variables included wind speed, wind mitigation technique, and suppression method used.

3 Heat Release Rate Experiments

One of the key measurements for quantifying fire hazard and growth is heat release rate. These experiments were conducted on components of the fuel load used in the structure fire to provide benchmarks for the amount of energy available from the furnishings. In the following heat release rate experiments, the fuel load components were burned under a calorimeter in a “free burn” or “fuel limited” condition. There were no compartmentation effects, or wind driven effects on the burning rates.

3.1 Instrumentation and Uncertainty

The heat release rate experiments were conducted in the NIST Large Fire Laboratory utilizing the 3 m by 3 m and 6 m by 6 m oxygen depletion calorimeters. The estimated expanded uncertainty is $\pm 11\%$ on the measured heat release rate. Details on the operation and uncertainty in measurements associated with the oxygen depletion calorimeter can be found in [40]. The data was recorded at intervals of 1 s on a computer based data acquisition system.

Schmidt-Boelter total heat flux gauges were used to measure the heat flux. Results from an international study on total heat flux gauge calibration and response demonstrated that the uncertainty of a Schmidt-Boelter gauge is typically $\pm 8\%$ [41].

The mass loss was measured by four load cells which supported a non-combustible platform. Each load cell had a range of 0 kg (0 lbs) to 227 kg (500 lbs) with a resolution of a 0.05 kg (0.11 lb) and a calibration uncertainty within 1% [42]. The expanded uncertainty is estimated to be $\pm 5\%$. One of the fuel packages, the trash container was burned on a single load cell with a resolution of a 0.001 kg (0.002 lbs) [42]. The expanded uncertainty is estimated to be $\pm 5\%$.

The experimental arrangement for the heat release rate experiments is shown in the photograph of the bed fuel package in Figure 3.1-1. An error bar representative of the estimated uncertainty for each measurement is given on every data graph.

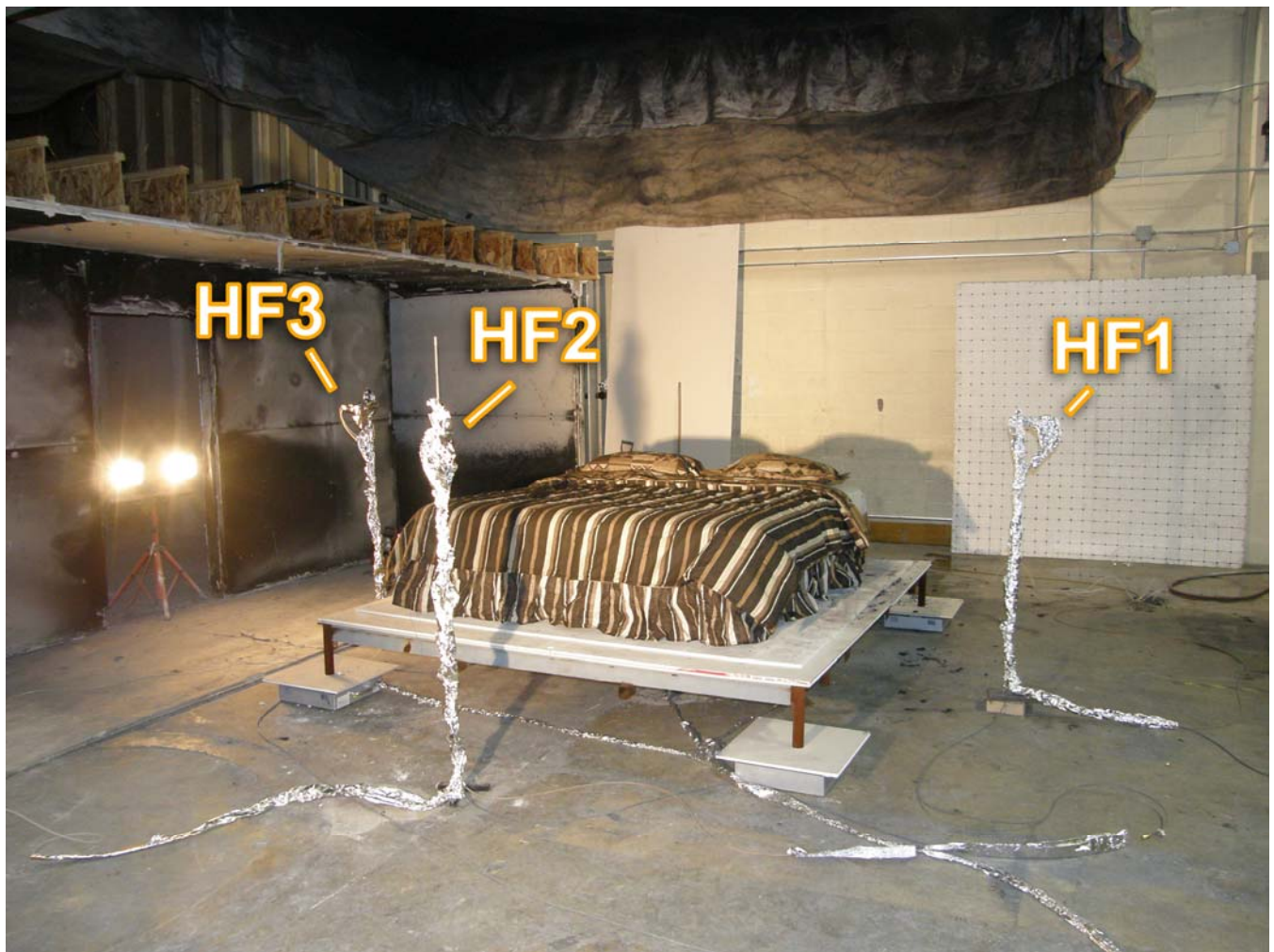


Figure 3.1-1. Typical heat release rate experimental arrangement, using the bed fuel package, with the heat flux positions labeled. This arrangement was used for all chair, bed, and sofa heat release rate experiments.

3.2 Trash Container Fuel Package

The ignition source consisted of a cardboard book of 20 matches that was ignited by an electrically heated wire. This device will be referred to as an electric match in this report. The electric match was placed near the bottom of a 8.5 l (9.0 qt) polypropylene waste container with a mass of 0.315 kg (0.695 lbs) (Figure 3.2-1). The height of the waste container was 270 mm (10.5 in) with interior dimensions at the top opening of 222 mm (8.75 in) by 196 mm (7.75 in). Approximately 0.3 kg (0.7 lbs) of dry newspaper was added to the waste container. The majority of the newspaper was folded flat, and placed on edge along the sides of the waste container. Four sheets of newspaper, 559 mm (22 in) by 635 mm (25 in) were crumpled into “balls” approximately 100 mm in diameter and placed on top of the electric match in the center of the waste container.

Heat release rate experiments were conducted for this fuel package under the 3 m by 3 m oxygen depletion calorimeter at NIST. A single Schmidt-Boelter total heat flux gauge was positioned 0.46 m (1.5 ft) above the base of the load cell and 1.00 m away from the edge of the trash container.

Two replicate experiments were conducted, identified as trash container 1 and 2. A series of photographs is presented for each trash container, Figure 3.2-1 through Figure 3.2-8 for trash container 1 and Figure 3.2-9 through Figure 3.2-16 for trash container 2. Photographs are taken at intervals of 100 s throughout the heat release rate experiment during the period from ignition to 600 s. The measurements continued beyond 600 s as the debris continued to burn. However the visual changes in the fuel after 600 s were minor. Each series also includes a photograph taken at the time of the peak heat release rate measurement.

The heat release rate time histories are shown in Figure 3.2-17. The average peak heat release of the waste container and the newspaper was approximately 32 kW for the two heat release rate experiments conducted. The difference in the heat release rate time histories is attributable to slight variations in the paper loading (position) and the subsequent burning of the paper and plastic container which enable differences in exposed fuel surface area and ventilation paths. The total energy released for each trash container was 15.5 MJ and 16.7 MJ respectively.

The total heat flux time histories are given in Figure 3.2-18. Again small variations in the burning of the paper and plastic led to collapse conditions that in turn led to time differences in the peak heat flux. In both cases, the measured peak heat flux at 1 m from the edge of the fuel was approximately 1 kW/m².

The mass loss time histories are shown in Figure 3.2-19. The initial mass of the plastic container with the paper for each trash container was 0.68 kg (1.50 lbs) and 0.69 kg (1.52 lbs) respectively. Addition of the electric match and electric wire brought the total load to approximately 0.72 kg (1.59 lbs) for each experiment. The mass loss for both experiments is nearly linear for the first 300 s. The discontinuity at approximately 350 s in each experiment is the result of the removal the wire used for the electric match from the load cell. In each experiment, more than 95 % of fuel was consumed within 1200 s after ignition.

The effective heat of combustion was calculated for two different values; an average heat of combustion and a peak heat of combustion. In the first method, the total energy released was divided by the total

mass loss to provide an average heat of combustion for the fuel package. This yielded effective heats of combustion of 23.2 MJ/kg and 24.3 MJ/kg. For the peak heat of combustion value, the peak heat release rate was divided by the mass loss rate occurring at the time. This value was slightly higher for each trash container at 26.9 MJ/kg and 24.3 MJ/kg.



Figure 3.2-1. Trash container 1, ignition



Figure 3.2-2. Trash container 1, 100 s after ignition



Figure 3.2-3. Trash container 1, 200 s after ignition



Figure 3.2-4. Trash container 1, 300 s after ignition



Figure 3.2-5. Trash container 1, 400 s after ignition



Figure 3.2-6. Trash container 1, at peak heat release rate, 406 s after ignition



Figure 3.2-7. Trash container 1, 500 s after ignition



Figure 3.2-8. Trash container 1, 600 s after ignition

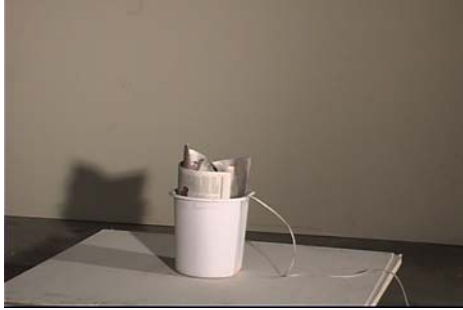


Figure 3.2-9. Trash container 2, ignition



Figure 3.2-10. Trash container 2, 100 s after ignition



Figure 3.2-11. Trash container 2, 200 s after ignition



Figure 3.2-12. Trash container 2, 300 s after ignition



Figure 3.2-13. Trash container 2, at peak heat release rate, 363 s after ignition



Figure 3.2-14. Trash container 2, 400 s after ignition



Figure 3.2-15. Trash container 2, 500 s after ignition



Figure 3.2-16. Trash container 2, 600 s after ignition

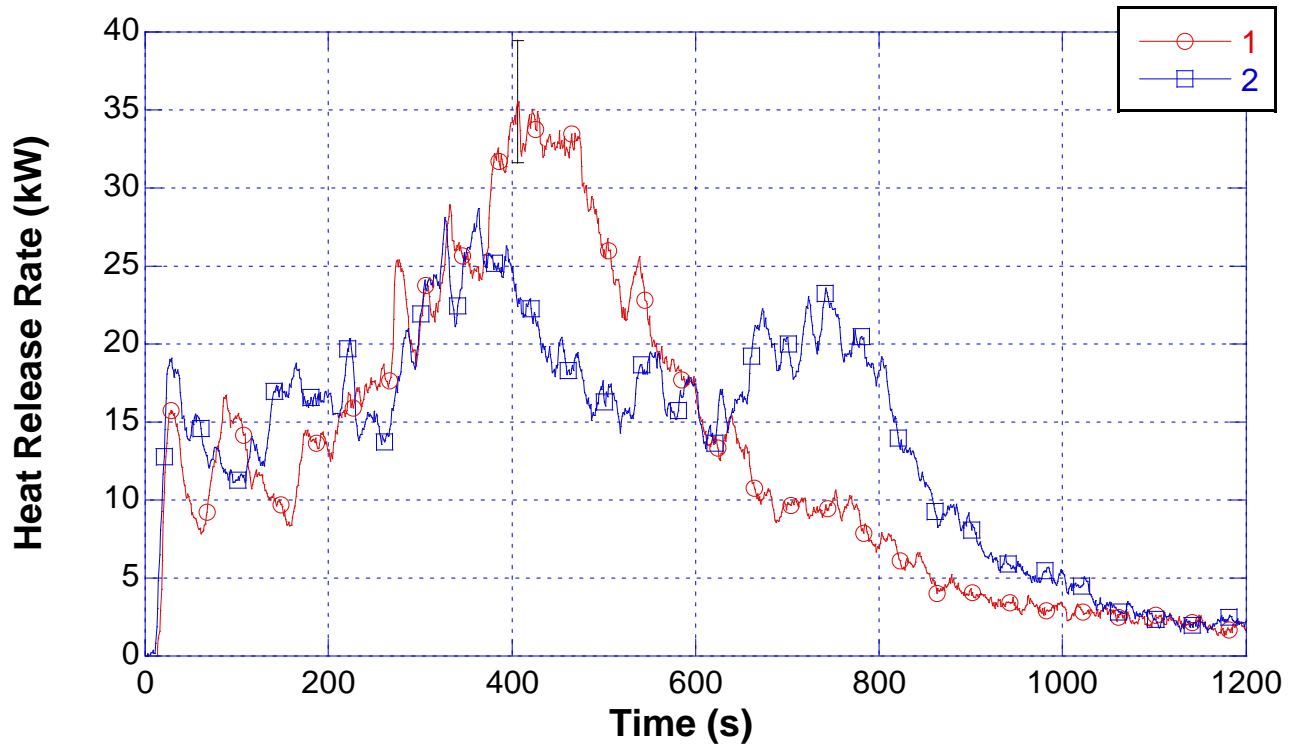


Figure 3.2-17. Heat release rate versus time for Trash Container 1 and 2.

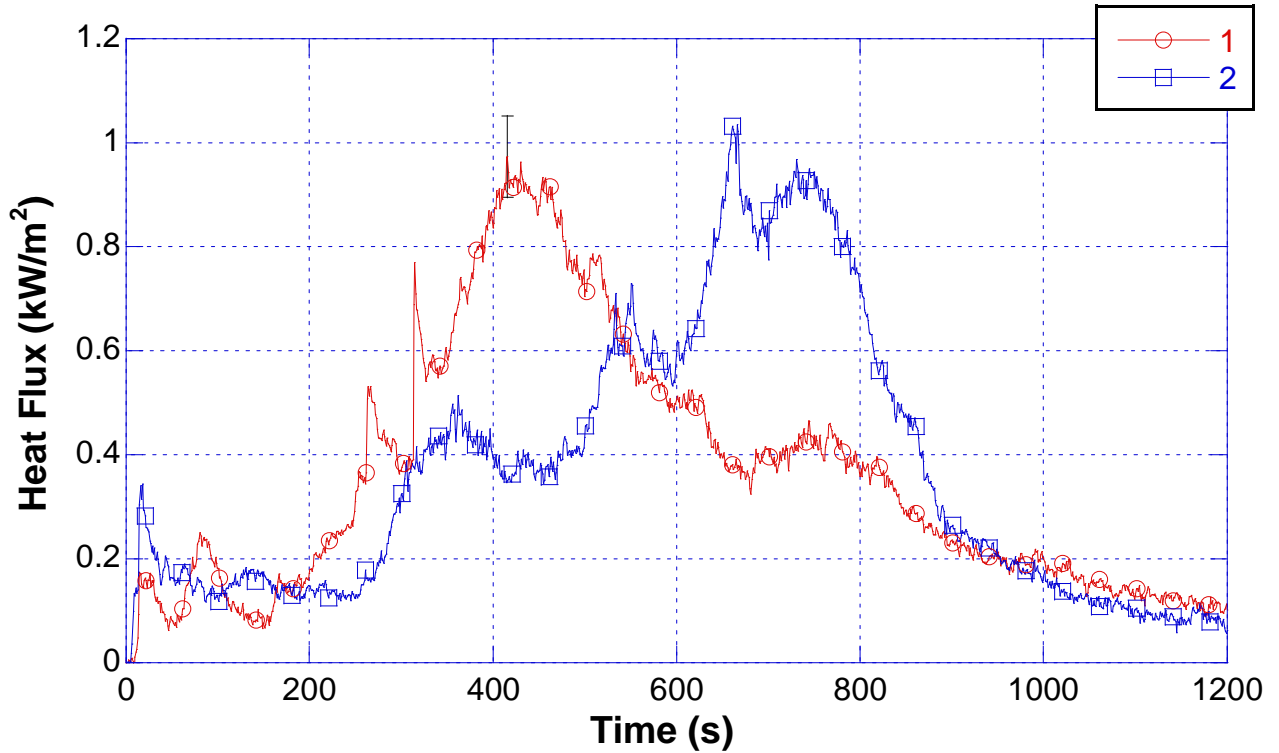


Figure 3.2-18. Heat flux versus time for Trash Container 1 and 2.

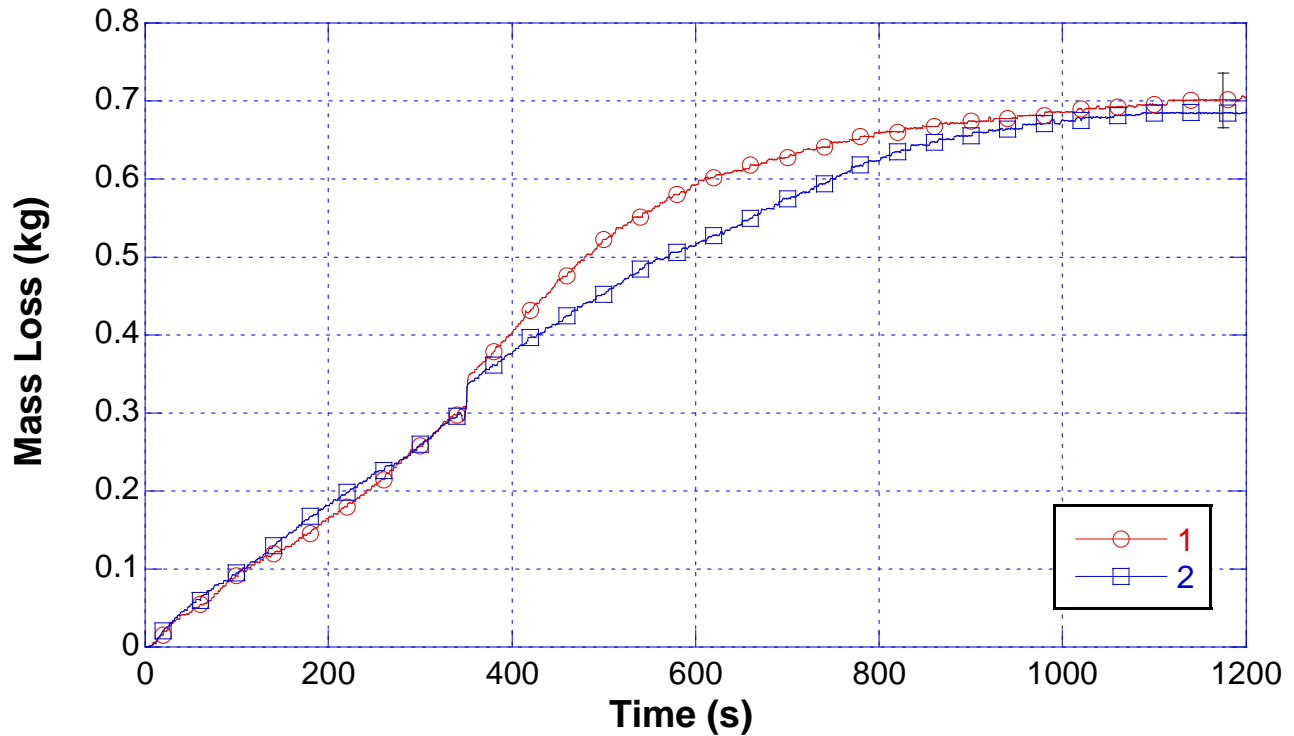


Figure 3.2-19. Mass loss versus time for Trash Containers 1 and 2.

3.3 Bed Fuel Package

The bed used in each of the experiments was a “king size” innerspring mattress with a wood framed, box spring foundation. The box springs were 2.03 m (6.67 ft) long, 0.97 m (3.17 ft) wide and 0.19 m (0.625 ft) thick. The box springs were placed side by side and supported with stacked bricks that kept them 0.15 m (0.5 ft) above the floor. The box spring segments ranged from 17.7 kg (39 lbs) to 18.8 kg (41 lbs) in mass. Photographs of a representative box spring are shown in Figure 3.3-1 and Figure 3.3-2.

The mattress was 2.03 m (6.67 ft) long, 2.01 m (6.58 ft) wide and 0.23 m (0.75 ft) thick. The mattress was positioned on top of the box springs. The mattress weights ranged from 42.0 kg (92 lbs) to 43.5 kg (96 lbs). The mattress was composed of a steel inner spring assembly covered with fabric and foam. Based on the manufacturers tag on the mattress the combustible materials consist of 49 % blended cotton felt and 51 % polyurethane foam.

Each bed was dressed with a king size fitted sheet, flat sheet, bed skirt, two “standard” pillows with pillow cases and a comforter. The pillows were “standard” size, 0.66 m (2.2 ft) x 0.51 m (1.7 ft) x 0.20 m (0.7 ft). The pillow shell was made from 45 % cotton and 55 % polyester. The pillows were filled with 100 % polyester fiber fill. The pillows had a combined mass of 1.1 kg (2.4 lbs). The rest of the bedding set components were made of fabrics that were composed of 60 % cotton and 40 % polyester. The comforter had 100 % polyester filling. The bedding set components, not counting the pillows had a total mass of 5.9 kg (13 lbs). The total mass of the bed fuel package ranged from 84.5 kg (186 lbs) to 87.0 kg (191 lbs).



Figure 3.3-1. Top side of box spring.



Figure 3.3-2. Bottom side of box spring.

Two heat release rate experiments were conducted. In the first experiment, a bed fuel package was ignited by an electric match positioned on the top surface of the mattress, in a fold formed by the comforter and underside of the covered pillow as shown in Figure 3.3-3. The second experiment was ignited with a trash container fuel package positioned next to the bed as shown in Figure 3.3-4.

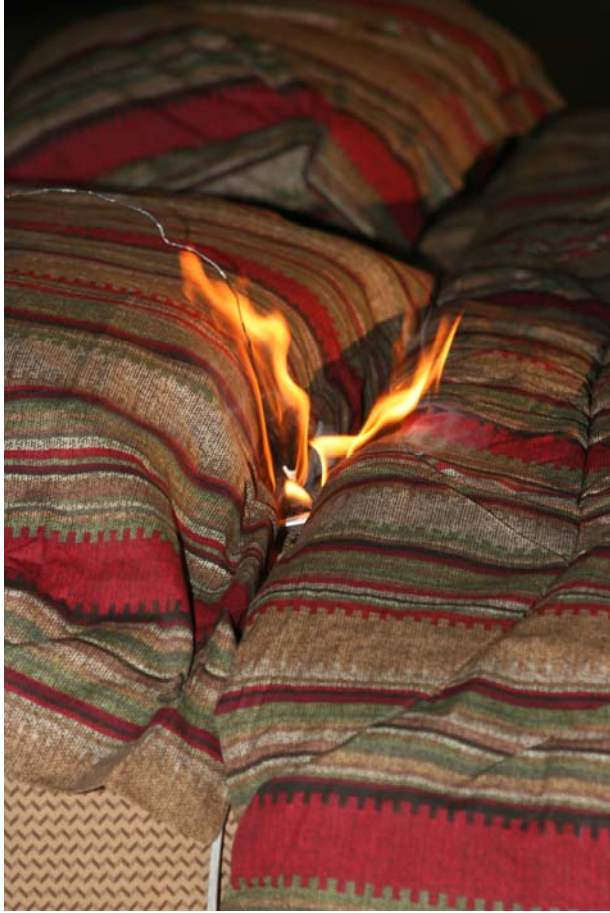


Figure 3.3-3. Electric match ignition of bed fuel package.

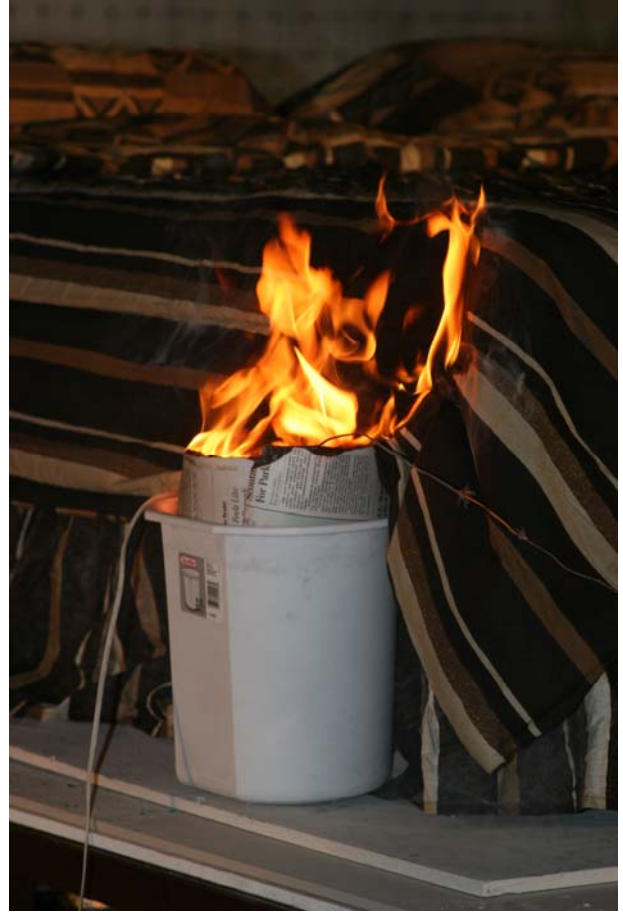


Figure 3.3-4. Trash container ignition of bed fuel package.

3.3.1 Bed Fuel Package 1

Bed fuel package 1 was ignited with an electric match as shown in Figure 3.3-3. Figure 3.3.2-1 through Figure 3.3.1-10 are a series of photographs showing the fire development in the first bed fuel package. The photographs document the period from ignition to 800 s after ignition at which point the fuel package has been reduced to burning debris in and under the springs of the mattress. The photographs are at intervals of 100 s with the exception of Figure 3.3.2-5, which shows the bed fuel package at the time of peak heat release rate, 484 s.



Figure 3.3.1-1. Bed 1, ignition



Figure 3.3.1-2. Bed 1, 100 s after ignition



Figure 3.3.1-3. Bed 1, 200 s after ignition



Figure 3.3.1-4. Bed 1, 300 s after ignition



Figure 3.3.1-5. Bed 1, 400 s after ignition



Figure 3.3.1-6. Bed 1, at peak heat release rate, 484 s after ignition



Figure 3.3.1-7. Bed 1, 500 s after ignition



Figure 3.3.1-8. Bed 1, 600 s after ignition



Figure 3.3.1-9. Bed 1, 700 s after ignition



Figure 3.3.1-10. Bed 1, 800 s after ignition

The heat release rate of the bed fuel package ignited with an electric match is shown in Figure 3.3.1-11. The heat release rate increased slowly with the fire spread being limited to a portion of the ignited pillow for the first 180 s. At 186 s, a portion of the burning comforter falls and spreads the fire to the side of the bed. The fire continued to spread to other components and areas of the bedding and then into the mattress itself. This caused the heat release rate to increase at a faster rate. The peak heat release of nearly 3.5 MW was reached as the bed was fully involved in fire at 484 s. The total energy released was 1001 MJ.

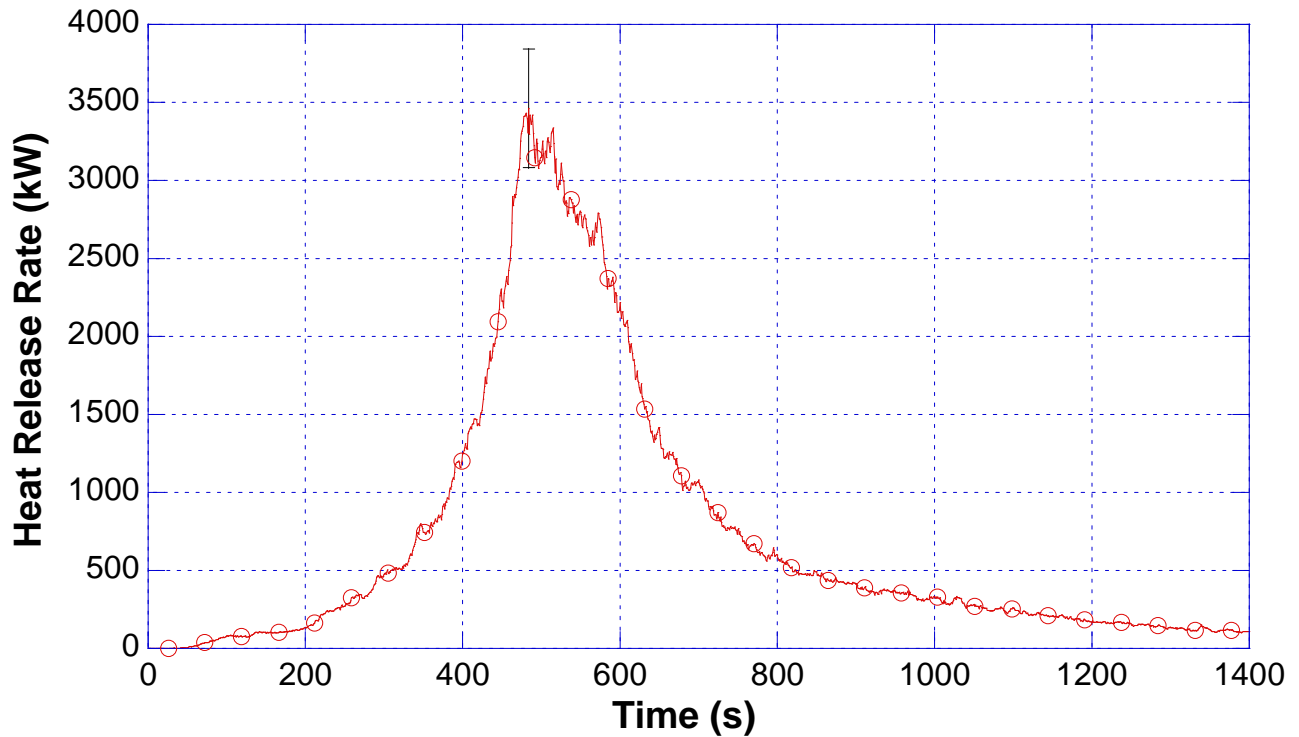


Figure 3.3.1-11. Heat release rate versus time for bed fuel package 1.

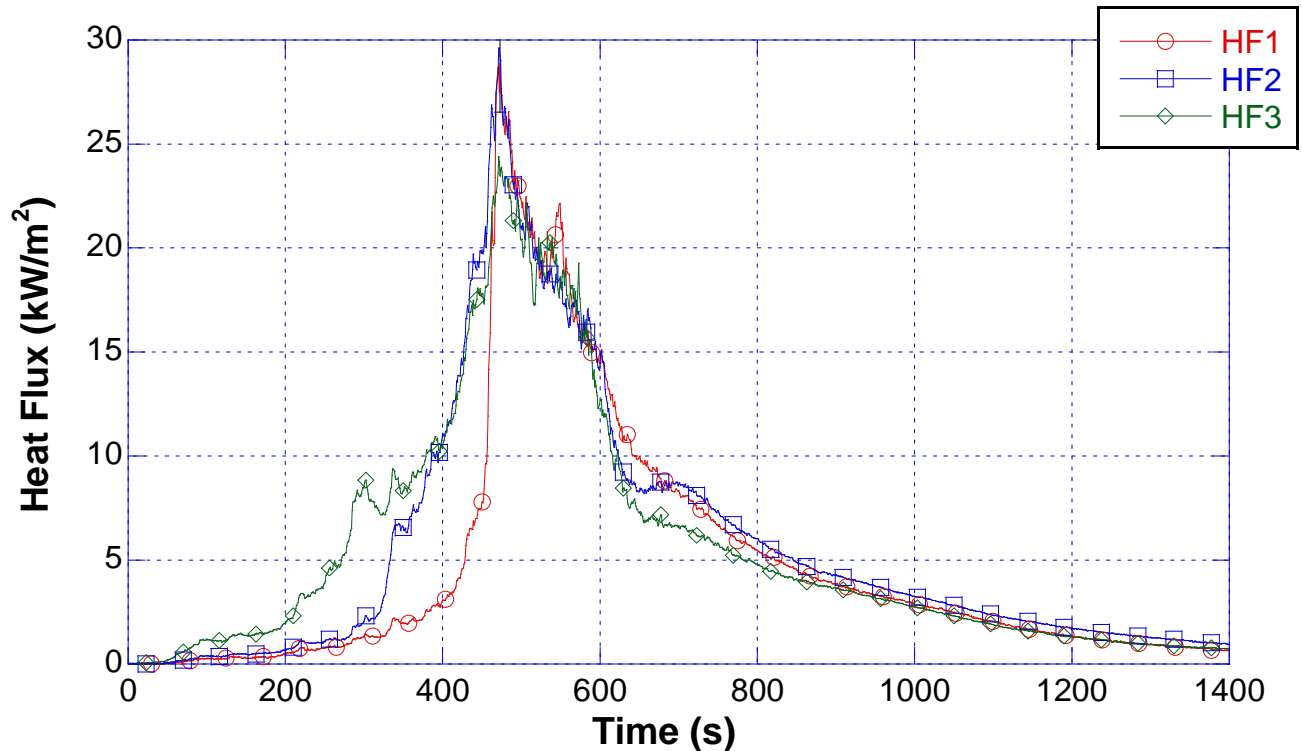


Figure 3.3.1-12. Heat flux versus time for the bed fuel package 1.

The heat flux time histories are presented in Figure 3.3.1-12. The positions of the heat flux gauges as they were arranged in this test are labeled in Figure 3.1-1. The three heat flux sensors were positioned equidistant, at 1.00 m from the edge of the bed. HF1 was positioned on centerline of the east side of the bed (opposite the ignition side), HF2 was located on the center line of the bed, on the south side of the bed, and HF3 was located on the centerline of the west side (ignition side) of the bed. As a result HF 3 began to increase first and was followed by heat flux increases at HF2 and finally at HF1. Near the time of peak heat release rate, all three heat flux sensors were at their peak, reading between 24 kW/m² and 29 kW/m².

The mass loss of the electric match ignited bed fuel package is given in Figure 3.3.1-13. The initial mass of this fuel package was 87.0 kg (191 lbs). The total mass loss at 1400 s was 36.5 kg (80.3). The metal from the inner spring mattress and the box springs, post experiment, weighed 36.0 kg (79.2 lbs). Therefore more than 95 % of the combustible mass was consumed during the experiment. The peak mass loss rate was 0.166 kg/s.

The average effective heat of combustion was calculated to be 19.8 MJ/kg. Based on the peak heat release rate and the mass loss rate, at the time of peak heat release rate, yields an effective heat of combustion of 20.9 MJ/kg.

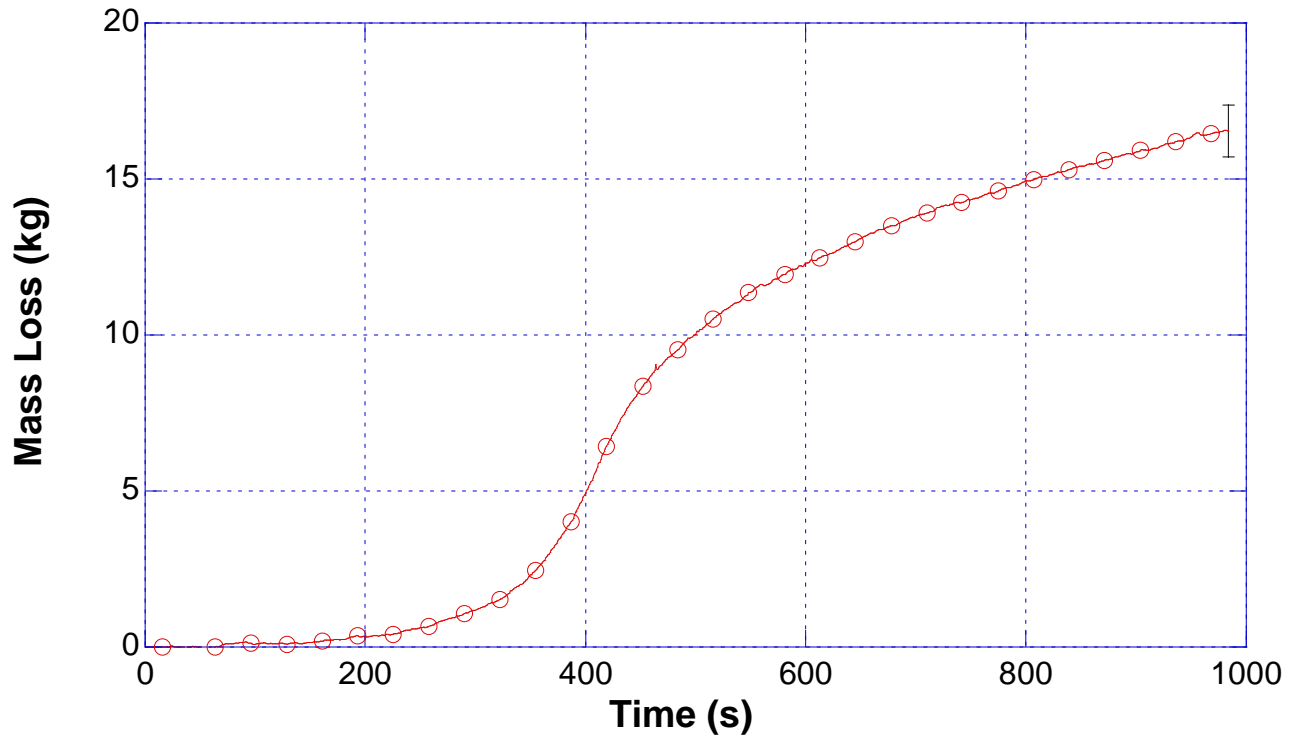


Figure 3.3.1-13. Mass loss versus time for bed fuel package 1.

3.3.2 Bed Fuel Package 2

Bed fuel package 2 was ignited with a trash container fuel package as shown in Figure 3.3-3. Figure 3.3.2-1 through Figure 3.3.2-8 are a series of photographs showing the fire development in bed fuel package 2. The photographs document the period from ignition to 600 s after ignition at which point the fuel package had been reduced to burning debris in and under the springs of the mattress. The photographs are at intervals of 100 s with the exception of Figure 3.3.2-5, which shows the bed fuel package near the time of peak heat release rate, 380 s. Given the larger ignition source, and ignition placement that involved the mattress sooner, the total burn time was reduced by more than 6 minutes.



Figure 3.3.2-1. Bed 2, ignition



Figure 3.3.2-2. Bed 2, 100 s after ignition



Figure 3.3.2-3. Bed 2, 200 s after ignition



Figure 3.3.2-4. Bed 2, 300 s after ignition



Figure 3.3.2-5. Bed 2, at peak heat release rate, 380 s after ignition



Figure 3.3.2-6. Bed 2, 400 s after ignition



Figure 3.3.2-7. Bed 2, 500 s after ignition



Figure 3.3.2-8. Bed 2, 600 s after ignition

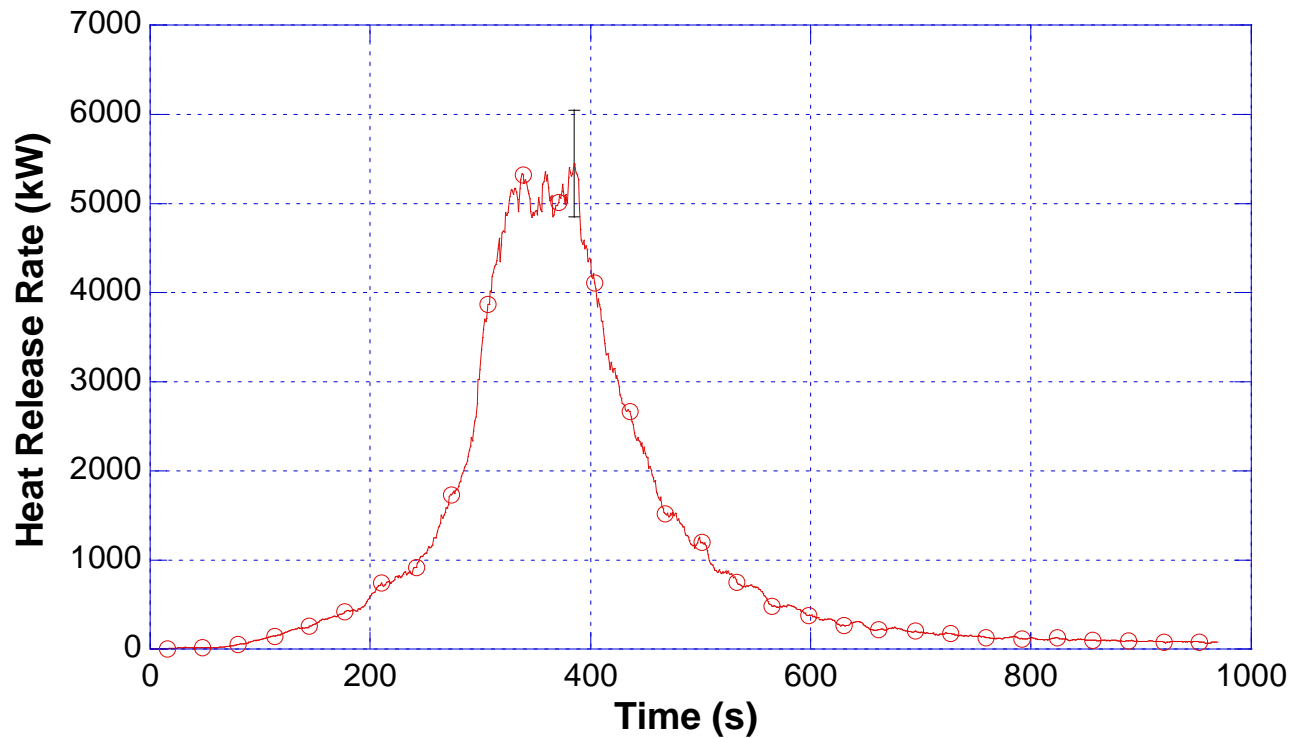


Figure 3.3.2-9. Heat release rate versus time for bed fuel package 2.

The heat release rate for the bed fuel package ignited with the trash container fuel package is shown in Figure 3.3.2-9. Given the larger heat release rate of the trash container, the fire in the bed fuel package developed faster. This led to a larger peak heat release rate. The peak heat release rate reached a quasi-steady plateau from 320 s to 380 s which averaged approximately 5.1 MW. Total energy released was 999 MJ. This value is within the range of uncertainty of the total energy released from the previous bed fuel package.

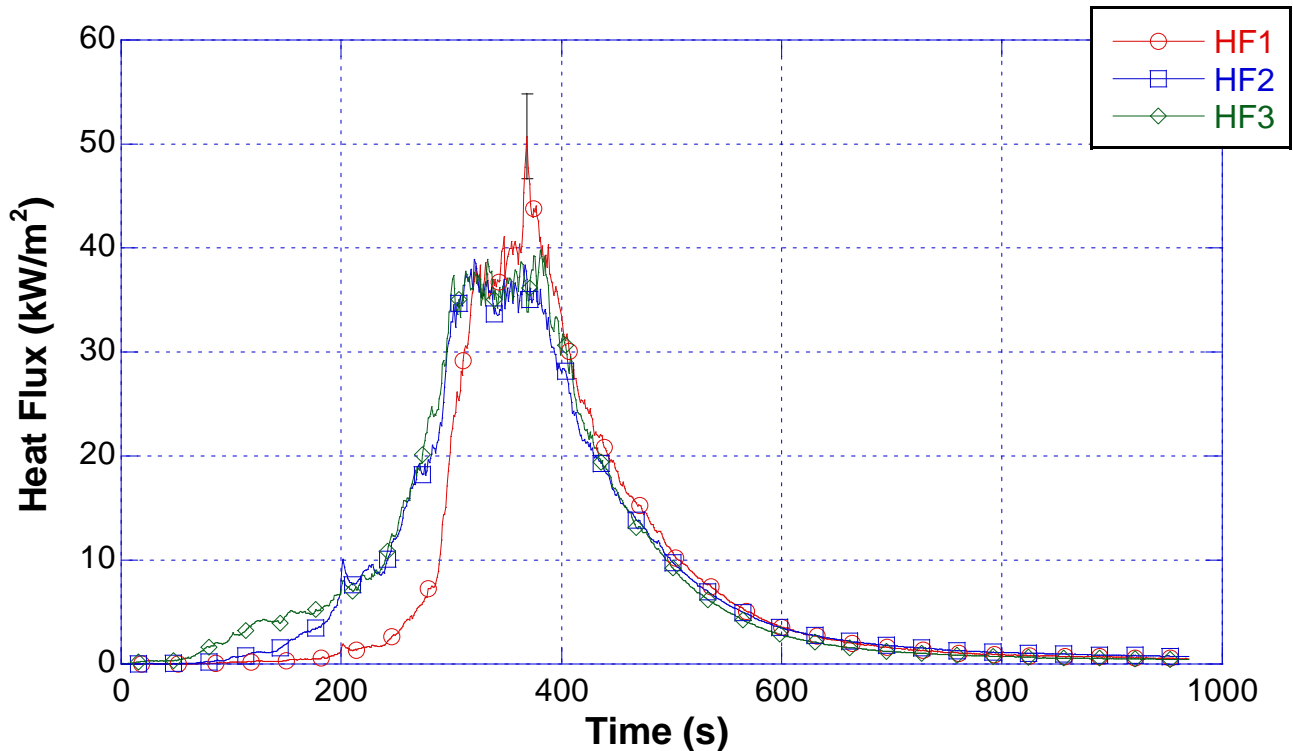


Figure 3.3.2-10. Heat flux versus time for bed fuel package 2.

The heat flux measurements are given in Figure 3.3.2-10. The heat flux sensors were in the same positions as in the previous bed fuel package experiment, as shown in Figure 3.1-1. Heat flux sensor HF3 was located on the ignition side of the bed. Therefore the heat flux increased at HF3 first, followed by HF2 and HF 1. Both of the bed fuel packages had similar heat flux development trends. However the peak heat fluxes of the bed fuel package with the trash container ignition had a greater magnitude and a greater range of approximately 35 kW/m² to 50 kW/m² than the previous experiment. This was consistent with the higher peak heat release rate.

The mass loss is given in Figure 3.3.2-11. The initial mass of this bed fuel package was 84.5 kg (186 lbs). Approximately 45 kg (99 lbs) of mass was consumed during the fire. The metal that was collected and weighed post fire was 38.5 kg (85 lbs). Very similar to the previous experiment and again more than 95 % of the combustible mass was burned away. Given the higher peak heat release rate, it should follow that the mass loss rate was higher as well. Again, the mass loss was nearly linear during the time of peak heat release rate.

The average heat of combustion for the bed fuel package with trash container ignition was 22 MJ/kg. Given the broad profile of the peak heat release rate, the heat release rate and the mass loss rate were averaged from 320 s to 380 s after ignition. The average peak heat release rate of 5.1 MW divided by the average peak mass loss rate of 0.221 kg/s, yields an effective peak heat of combustion of 22 MJ/kg.

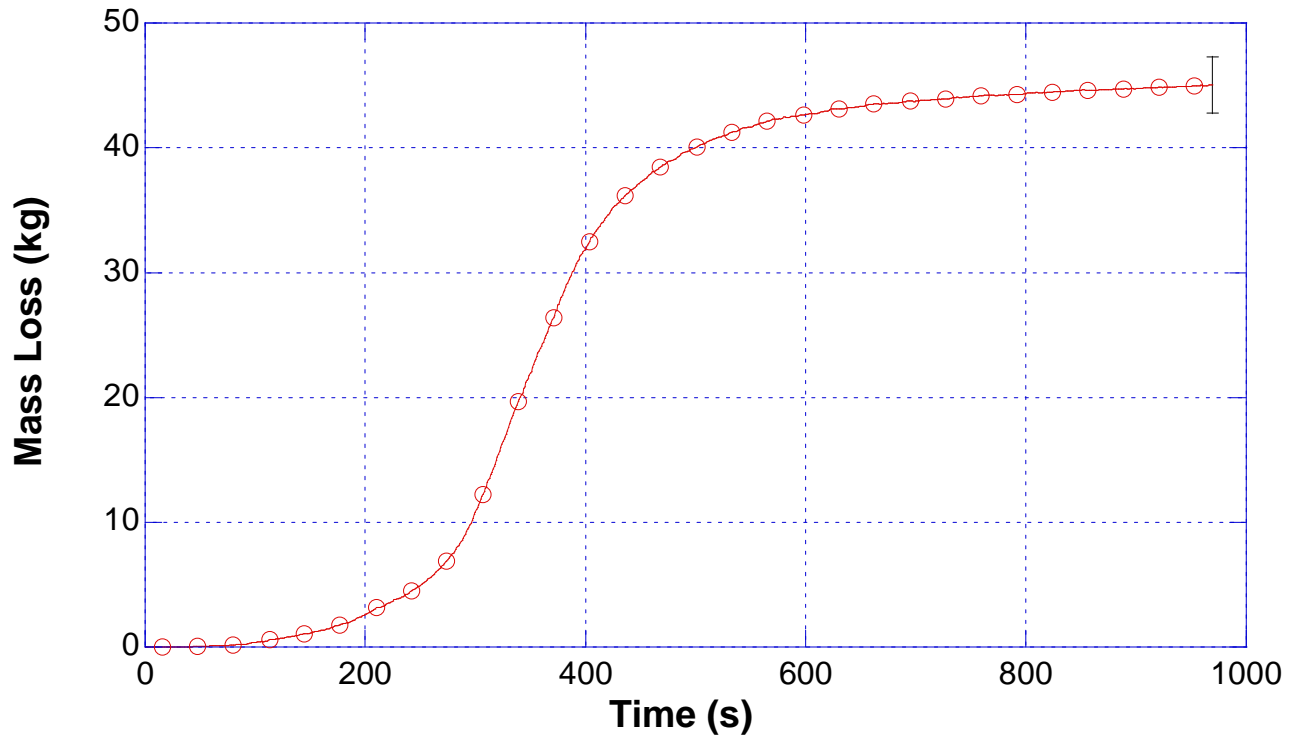


Figure 3.3.2-11. Mass loss versus time for bed fuel package 2.

3.4 Upholstered Chair

The upholstered chair was 0.72 m (2.4 ft) wide, 0.76 m (2.5 ft) deep and 0.73 m (2.4 ft) high. Based on the manufacturer’s information, the chairs had a hard wood frame which was wrapped in the arms and back portions with 10 % blended cotton and 90 % polyurethane foam. The seat cushion, which measured 0.53 m (1.75 ft) wide, 0.66 m (2.2 ft) deep and 0.15 m (0.5 ft) thick, was composed of 90 % polyurethane foam and 10 % polyester fiber. The back pillow measured approximately 0.48 m (1.6 ft) wide, 0.37 m (1.2 ft) high and 0.15 m (0.5 ft) thick. It was made up of polyester fiber 90 % and polyurethane foam 10 %. Six upholstered chairs and sets of cushions were weighed. The chairs had an average mass of 23.7 kg (52 lbs) with a range from 23.3 kg (51.4 lbs) to 24.0 kg (52.9 lbs). The seat cushion had an average mass of 2.12 kg (4.7 lbs) with a range from 2.05 kg (4.52 lbs) to 2.25 kg (4.96 lbs). The back cushions had an average mass of 1.18 kg (2.6 lbs) with a range of 1.17 kg (2.58 lbs) to 1.19 kg (2.62 lbs). Photographs of the chair and cushions are shown in Figure 3.4-1 through Figure 3.4-4.

Two heat release rate experiments were conducted. The first chair was ignited with an electric match located between the seat cushion and the arm of the chair and the second was ignited with a trash container fuel package as documented above.



Figure 3.4-1. Upholstered chair, front view.



Figure 3.4-2. Upholstered chair, side view.



Figure 3.4-3. Seat cushion, showing layers of upholstery fabric, polyester batting and polyurethane foam.



Figure 3.4-4. Back cushion, showing the upholstery fabric, inner liner, and polyurethane foam.

3.4.1 Upholstered Chair 1

The first upholstered chair was ignited with the electric match positioned at the intersection of the rear corner of the seat cushion, a lower corner of the back cushion and an arm of the chair. Figure 3.4.1-1 through Figure 3.4.1-10 make up a series of photographs starting at the time of ignition through 800 s after ignition. The photographs are shown at intervals of 100 s, with the exception of Figure 3.4.1-6.

Figure 3.4.1-6 shows the chair fire at the time of peak heat release rate, 417 s after ignition. As shown in the Figures Figure 3.4.1-2 through Figure 3.4.1-4, the fire spread from a small ignition area to an area that involved a portion of both cushions and both interior surfaces of the arms of the chair. Shortly after this, the fire began to spread through the body of the chair as shown in Figure 3.4.1-5. This was due to flame contact and burning foam from the seat cushion dropping fire down to lower sections of the chair and the floor below the chair.



Figure 3.4.1-1. Chair 1, ignition



Figure 3.4.1-2. Chair 1, 100 s after ignition



Figure 3.4.1-3. Chair 1, 200 s after ignition



Figure 3.4.1-4. Chair 1, 300 s after ignition



Figure 3.4.1-5. Chair 1, 400 s after ignition



Figure 3.4.1-6. Chair 1, at peak heat release rate, 417 s after ignition



Figure 3.4.1-7. Chair 1, 500 s after ignition



Figure 3.4.1-8. Chair 1, 600 s after ignition



Figure 3.4.1-9. Chair 1, 700 s after ignition



Figure 3.4.1-10. Chair 1, 800 s after ignition

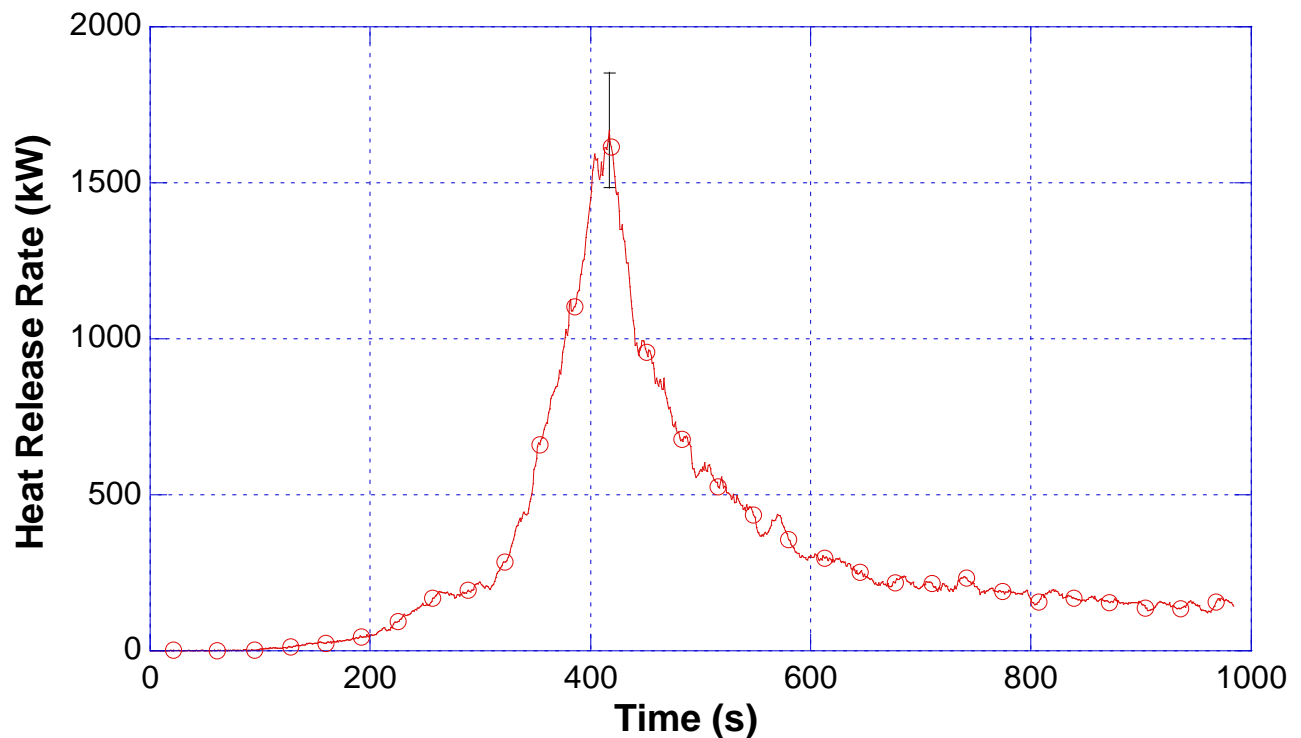


Figure 3.4.1-11. Heat release rate versus time for chair 1.

Figure 3.4.1-11 shows the heat release rate curve for the upholstered chair with the electric match ignition. The peak heat release rate of approximately 1.67 MW was reached at 417 s after ignition. The heat release rate decreased to a steady level of approximately 150 kW, 900 s after ignition. The total heat released over this period was 305 MJ.

The heat flux sensor arrangement was similar to the bed fuel package experiments in section 3.3, with the layout demonstrated in Figure 3.1-1. The heat flux time histories from the three heat flux sensors are shown in Figure 3.4.1-12. Given the similar lengths of the width and depth of the chair and the relatively small footprint of the chair resulted in similar heat flux curves from each of the sensors within the range of uncertainty. The average peak heat flux of the three sensors was 25 kW/m² at approximately 415 s.

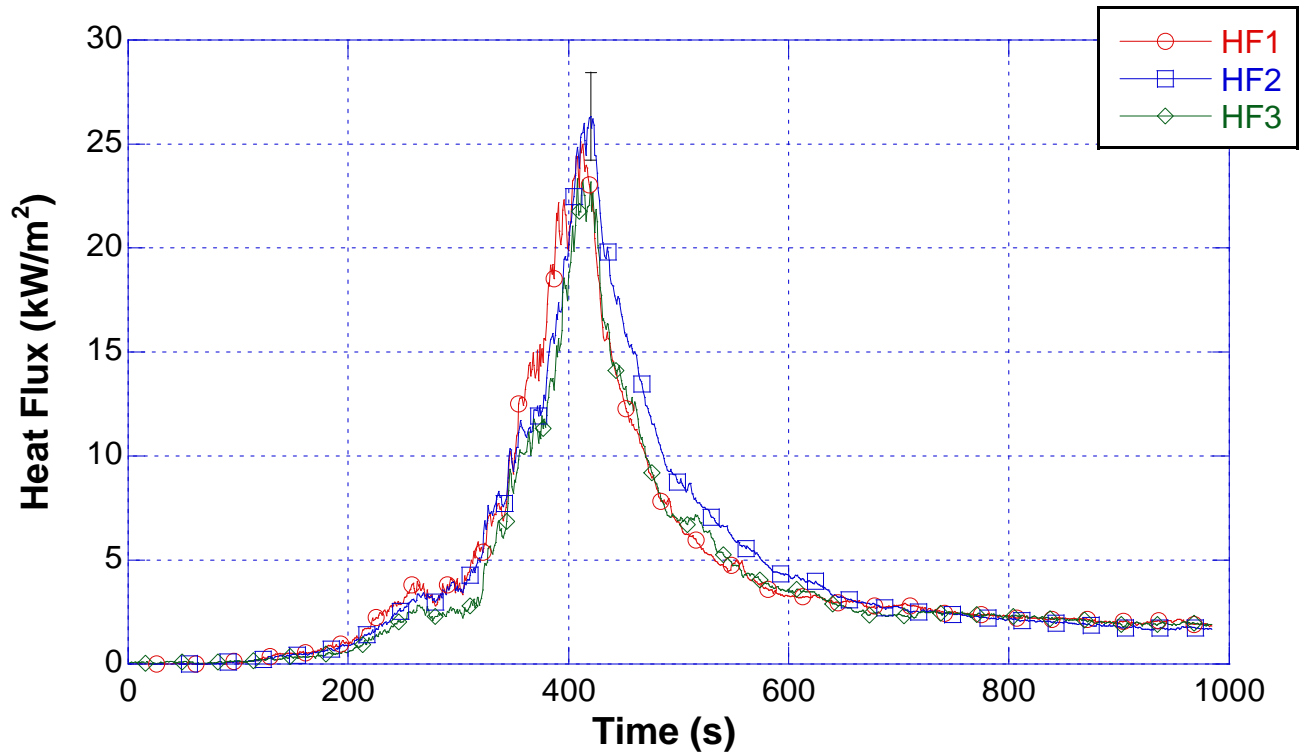


Figure 3.4.1-12. Heat flux versus time for chair 1.

The initial mass of the chair was 23.3 kg (51.4 lbs). The mass loss time history is shown in Figure 3.4.1-13. The total mass loss at 980 s for upholstered chair 1 was 16.5 kg (36.4 lbs). At the end of the test, the wood frame of the chair was completely charred with small flames on various sections as shown in Figure 3.4.1-10. The steel springs in the chair had a mass of 0.7 kg (1.5 lbs). Therefore, about 75 % of the combustible mass was consumed.

The heat of combustion calculations were conducted in the same manner as the trash container fuel packages. The average heat of combustion was 18.4 MJ/kg and the peak heat of combustion was 23.2 MJ/kg, based on the peak heat release rate and a mass loss rate of 0.072 kg/s.

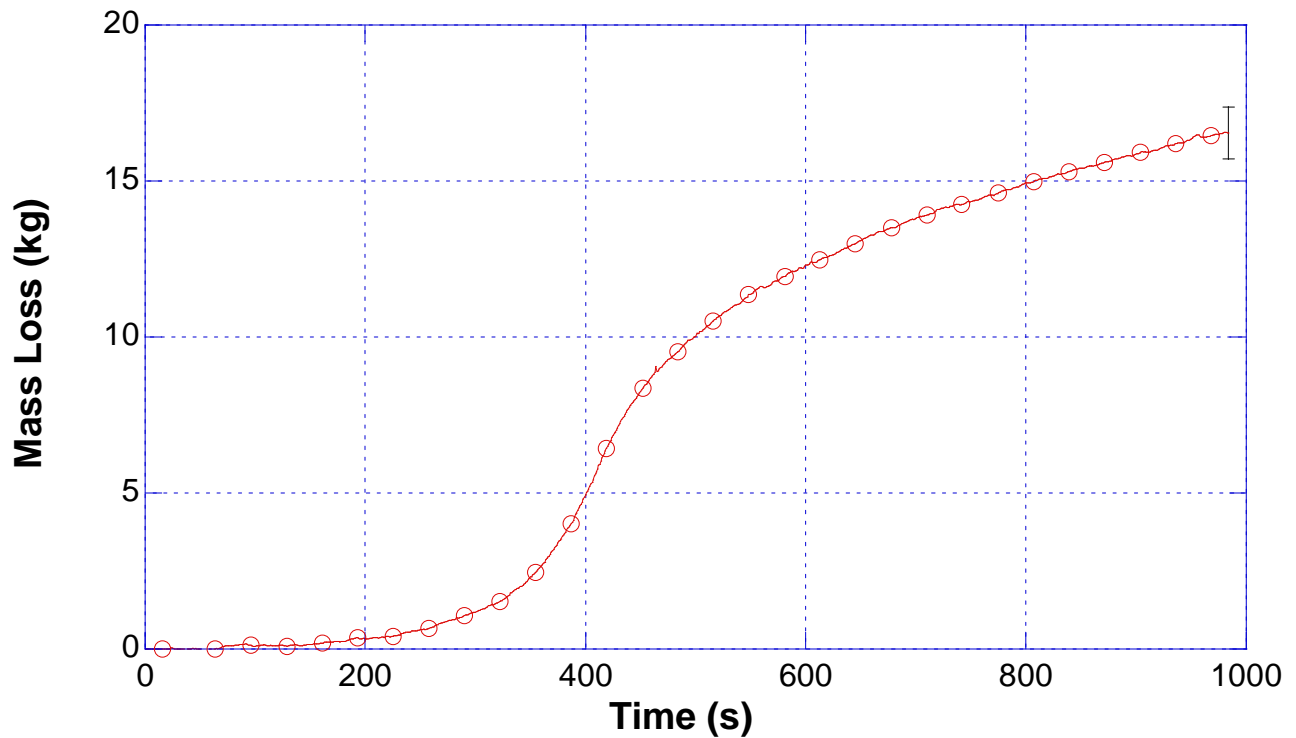


Figure 3.4.1-13. Mass loss versus time for chair 1.

3.4.2 Upholstered Chair 2

Upholstered chair 2 was ignited with a trash container fuel package positioned adjacent to one side of the chair as shown in Figure 3.4.2-1. Figure 3.4.2-1 through Figure 3.4.2-10 each have a photograph taken between 100 s and 800 s after ignition. Most of the photographs are taken at intervals of 100 s with the exception of Figure 3.4.2-6. The image in Figure 3.4.2-6 was recorded at the time of peak heat release rate, 437 s after ignition. Even though upholstered chair 2 had a significantly different ignition source from upholstered chair 1, the images recorded at 400 s after ignition in both cases provide similar levels of fire development within each chair.



Figure 3.4.2-1. Chair 2, ignition



Figure 3.4.2-2. Chair 2, 100 s after ignition



Figure 3.4.2-3. Chair 2, 200 s after ignition



Figure 3.4.2-4. Chair 2, 300 s after ignition



Figure 3.4.2-5. Chair 2, 400 s after ignition



Figure 3.4.2-6. Chair 2, at peak heat release rate, 437 s after ignition



Figure 3.4.2-7. Chair 2, 500 s after ignition



Figure 3.4.2-8. Chair 2, 600 s after ignition



Figure 3.4.2-9. Chair 2, 700 s after ignition



Figure 3.4.2-10. Chair 2, 800 s after ignition

The heat release rate for the chair ignited with the trash container is given in Figure 3.4.2-11. The peak heat release rate of approximately 1.86 MW occurred at 437 s after ignition. Between ignition and 1000 s after ignition, 331.6 MJ of energy was released. This value is approximately 10 % greater than chair 1. A portion of this difference can be accounted for by the energy release of the trash container, which averaged 16.0 MJ.

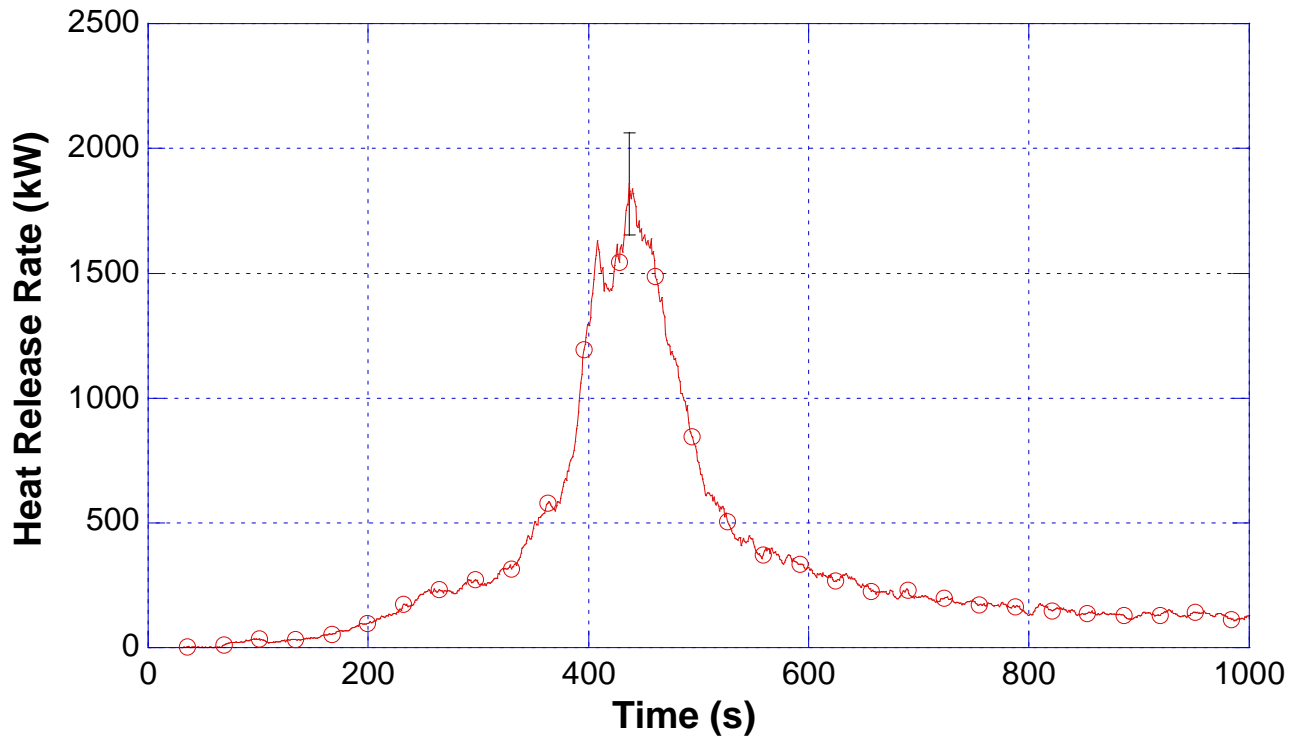


Figure 3.4.2-11. Heat release rate versus time for chair 2.

The heat flux sensor arrangement was similar to the first upholstered chair experiment, with the layout demonstrated in Figure 3.1-1. The heat flux time history of the heat flux is given in Figure 3.4.2-12. Heat flux sensor, HF1 was located on the east side of the chair as was the trash container ignition source. Hence, it shows an increase in heat flux first, followed by HF2 and HF3 as the flames spread across the chair. The peak heat flux was 30 kW/m^2 at approximately 400 s. As the materials filling the wood chair frame burned away, the “view” from each of the sensors equalized during the decay phase.

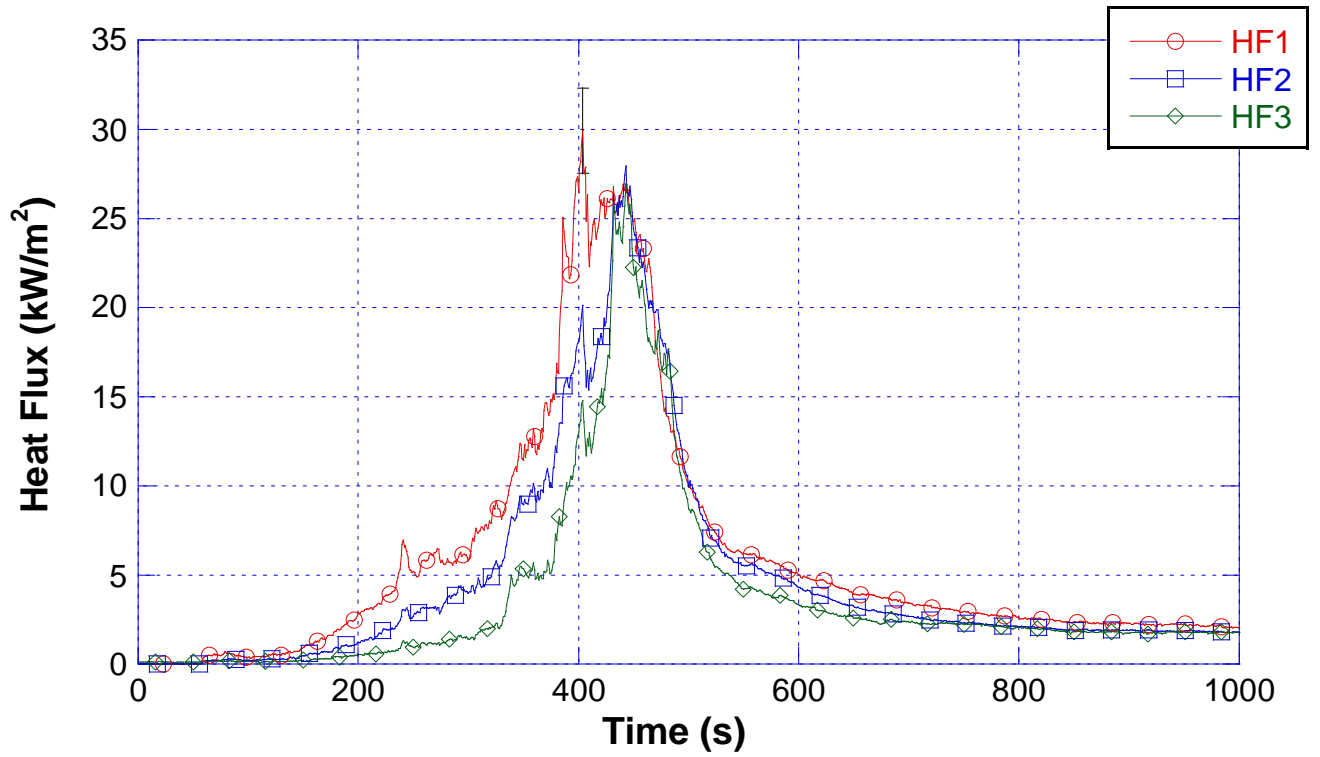


Figure 3.4.2-12. Heat flux versus time for chair 2.

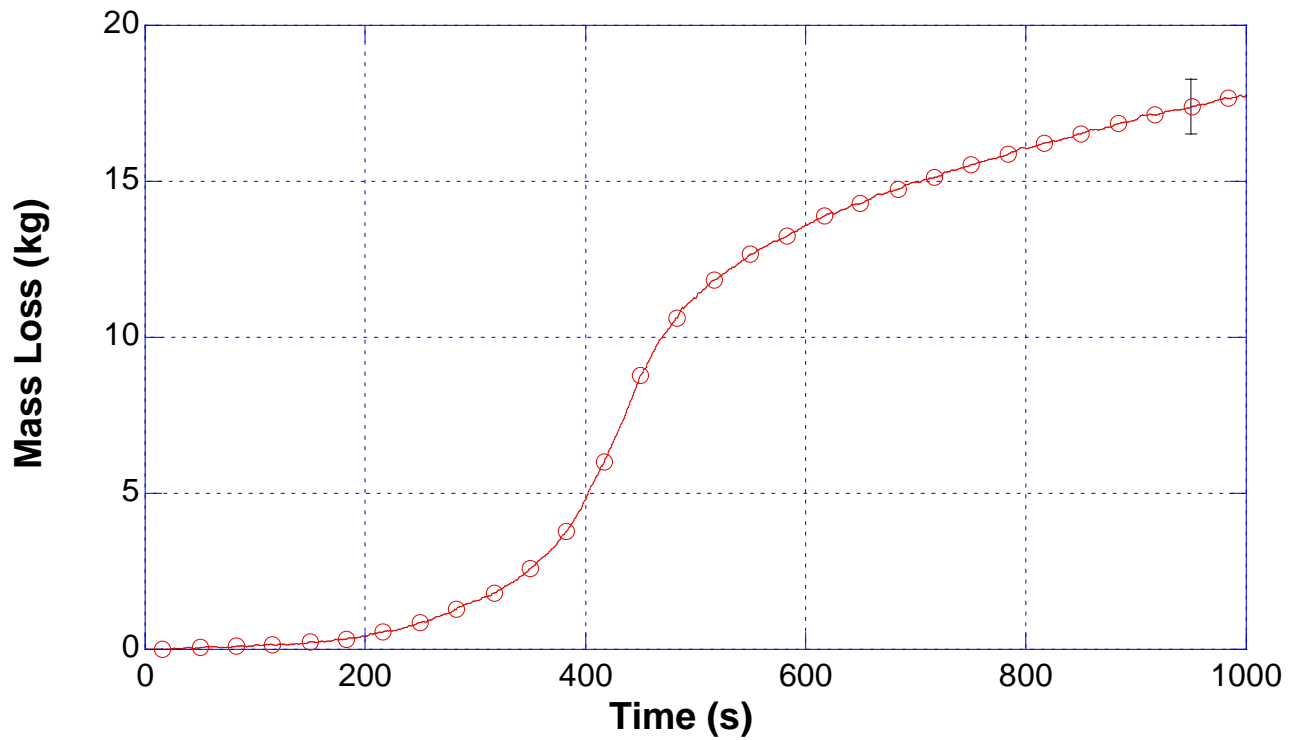


Figure 3.4.2-13. Mass loss versus time for chair 2.

The initial mass of the chair was 23.45 kg (51.6 lbs). In addition, a trash container fuel package with a mass of approximately 0.7 kg (1.5 lbs) was added to load cell and placed on the floor next to the chair bringing the total initial mass to 24.2 kg (53.2 lbs). The chair was allowed to burn for 1000 s, during that time, 17.8 kg (39.2 lbs) of fuel was lost to the combustion process. The mass of the chair's springs and metal connectors left after the fire had a mass of 0.8 kg (1.8 lbs). Again, approximately 75 % of the combustible mass was consumed during the experiment.

The heat of combustion calculations were conducted as for the trash container fuel packages. The average heat of combustion was 18.7 MJ/kg and the peak heat of combustion was 23.0 MJ/kg. These values are within 2 % of the heat of combustion values from upholstered chair 1.

3.5 Sleeper Sofa Fuel Package

The sleeper sofa had dimensions of 1.83 m (6.0 ft) wide, 0.75 m (2.5 ft) deep, and 0.83 m (2.7 ft) in height. Two sofas were measured. The first sofa had a total mass of 82.7 kg (182 lbs) and the second sofa had a total mass of 79.7 kg (175 lbs).

The sofa was composed of a wood frame surrounding a metal foldout sleeper sofa mechanism and foundation. A thin inner spring mattress was folded up in the mechanism and the seat cushions were placed on top of it. The frame was covered with a polyester based fabric. In the areas of the arms of the sofa and the front portion of the sofa thin layers of polyurethane foam and polyester batting padding were attached to the wood frame and covered with the upholstery material. The back cushion area was also part of the fixed wood frame assembly. Polyurethane foam padding was installed over metal spring supports and covered with polyester padding and upholstery material. Measuring the amount of material or dimensions of the materials attached to the frame was not practical full disassembly of the sofa would have been necessary.

Each sofa had a 1.32 m (4.33 ft) wide, 1.83 m (6.0 ft) long and 0.13 m (0.42 ft) thick inner spring mattress. The materials inside the mattress appeared to be polyurethane over a felted material on each side of the spring assembly. Each mattress had a mass of 16.4 kg (36.2 lbs) and 17 kg (37.5 lbs), respectively.

Each sofa had two seat cushions. The cushions had a core of polyurethane foam, which was covered with polyester batting in a polyester fabric cover, similar to the upholstered chair seat cushions. Each cushion measured 0.76 m (2.5 ft) wide, (2.2 ft deep) and 0.13 m (0.42 ft) thick and had a mass of 2.4 kg (5.3 lbs).

Both of the sofa experiments used the same ignition scenario; an electric match located at the intersection of a rear corner of a seat cushion, an arm of the sofa, and a lower corner of a back cushion.



Figure 3.5-1. Sofa 1, ignition



Figure 3.5-2. Sofa 1, 100 s after ignition



Figure 3.5-3. Sofa 1, 200 s after ignition



Figure 3.5-4. Sofa 1, 300 s after ignition



Figure 3.5-5. Sofa 1, 400 s after ignition



Figure 3.5-6. Sofa 1, at peak heat release rate, 455 s after ignition



Figure 3.5-7. Sofa 1, 500 s after ignition



Figure 3.5-8. Sofa 1, 600 s after ignition



Figure 3.5-9. Sofa 1, 700 s after ignition



Figure 3.5-10. Sofa 1, 800 s after ignition



Figure 3.5-11. Sofa 2, ignition



Figure 3.5-12. Sofa 2, 100 s after ignition



Figure 3.5-13. Sofa 2, 200 s after ignition



Figure 3.5-14. Sofa 2, 300 s after ignition



Figure 3.5-15. Sofa 2, at peak heat release rate, 389 s after ignition



Figure 3.5-16. Sofa 2, 400 s after ignition



Figure 3.5-17. Sofa 2, 500 s after ignition



Figure 3.5-18. Sofa 2, 600 s after ignition



Figure 3.5-19. Sofa 2, 700 s after ignition



Figure 3.5-20. Sofa 2, 800 s after ignition

Figure 3.5-1 through Figure 3.5-10 and Figure 3.5-11 through Figure 3.5-20 present images recorded between ignition and 800 s after ignition for both of the sofa experiments. Each set contains images taken every 100 s after ignition during that period. In addition, Figure 3.5-6 for sofa 1 and Figure 3.5-15 for sofa 2 show the fires at the time of peak heat release rate, 455 s and 389 s after ignition respectively. The times to peak heat release rate were more than 60 s apart. The fire spread for both of the sofas was very similar for the first 200 s. During the interval from 200 s to 300 s, sofa 1 had flames moving across the back side of the sofa, while sofa 2 contained the flames to the seat cushion area resulting in flames from one end of the sofa to the other. By 400 s after ignition sofa 1 and sofa 2 had similar levels of flame throughout. At 800 s after ignition, the wood frames of both sofas were still burning along with debris in and below the pullout mattress mechanism.

The heat release rate curves for sofas 1 and 2 are shown in Figure 3.5-21. The peak heat release rate for sofa 1 was 2.4 MW at 455 s after ignition. The peak heat release rate for sofa 2 was 2.6 MW at 389 s after ignition. The trend and general shape of the heat release rates of the sofas were quite similar. The total heat released for each sofa was 864 MJ and 842 MJ, respectively.

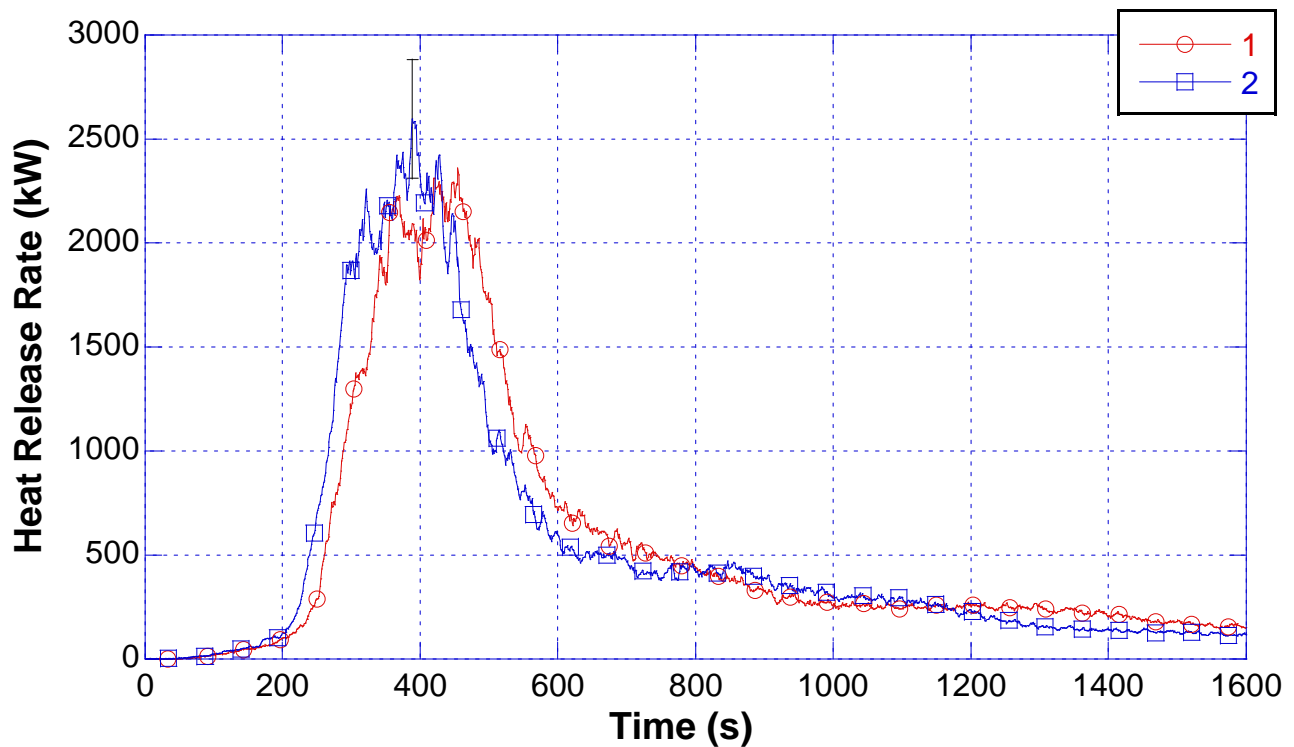


Figure 3.5-21. Heat release rate versus time for sofas 1 and 2.

The heat flux time histories for each are presented on different graphs, Figure 3.5-22 and Figure 3.5-23, for clarity. The heat flux sensors were arranged as in the bed fuel package experiments in section 3.3. The layout is demonstrated in Figure 3.1-1. Heat flux sensor 1 (HF1) on the east side of the sofa (ignition side) was closest to the flames early in the fire and responds accordingly, followed by the sensor to the south (HF2) and then HF3 which is to the west of the sofa. The two heat flux sensors which have a view of the sides of the sofa had a similar peak heat flux, while the heat flux sensor on the south side had the front (width) of the sofa and the broad flame front that goes with it in view, hence the higher peak heat flux. This trend was demonstrated in both of the sofa experiments. The peak heat fluxes were also similar for both experiments.

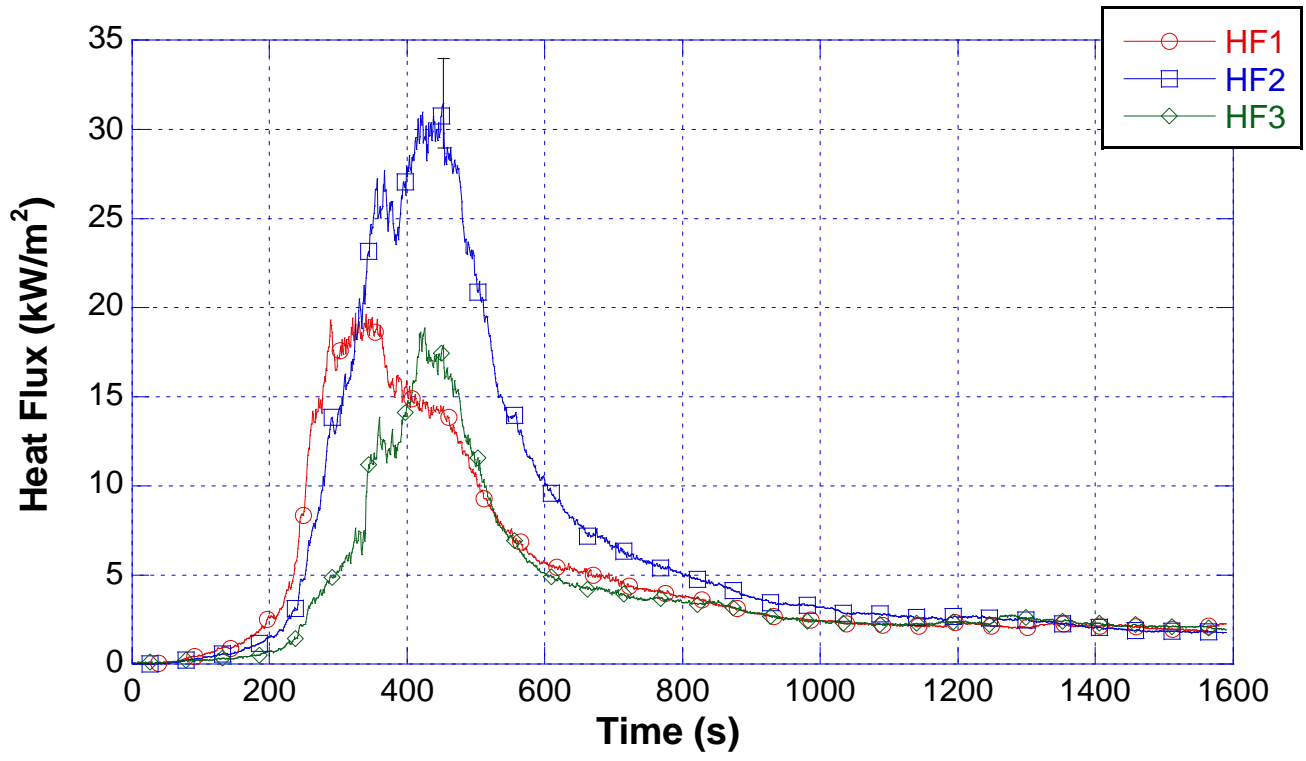


Figure 3.5-22. Heat flux versus time for sofa 1.

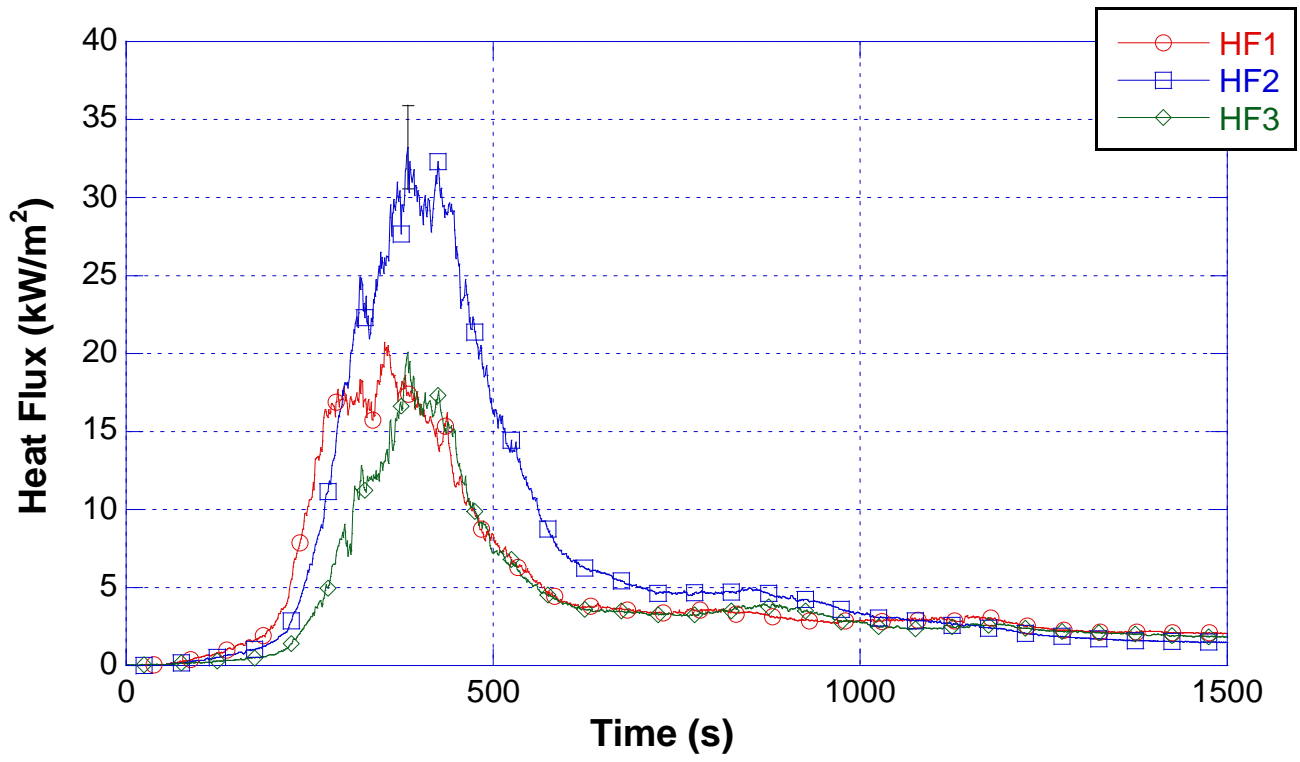


Figure 3.5-23. Heat flux versus time for sofa 2.

The mass loss for the first sofa experiment is shown in Figure 3.5-24. The initial mass of sofa 1 was 82.8 kg (182 lbs). The mass loss after 1590 s was 48.3 kg (106.2 lbs). The metal frame and springs had a post-experiment mass of 29.4 kg (64.57 lbs). There was approximately 5.1 kg (11.2 lbs) of combustible material remaining at the time that the experiment was terminated. Therefore, about 90 % of the combustible material burned within the 1590 s time period.

The mass loss time history for the second sofa is given in Figure 3.5-25. The initial mass of sofa 2 was 79.7 kg (175.3 lbs). The mass loss after 1500 s was 45.4 kg (99.8 lbs). The metal frame and springs had a post-experiment mass of 28.8 kg (63.4 lbs). As a result, there was approximately 5.5 kg (12.1 lbs) of combustible material remaining at the time that the experiment was terminated. This resulted in a similar percentage of combustible material burned as sofa 1.

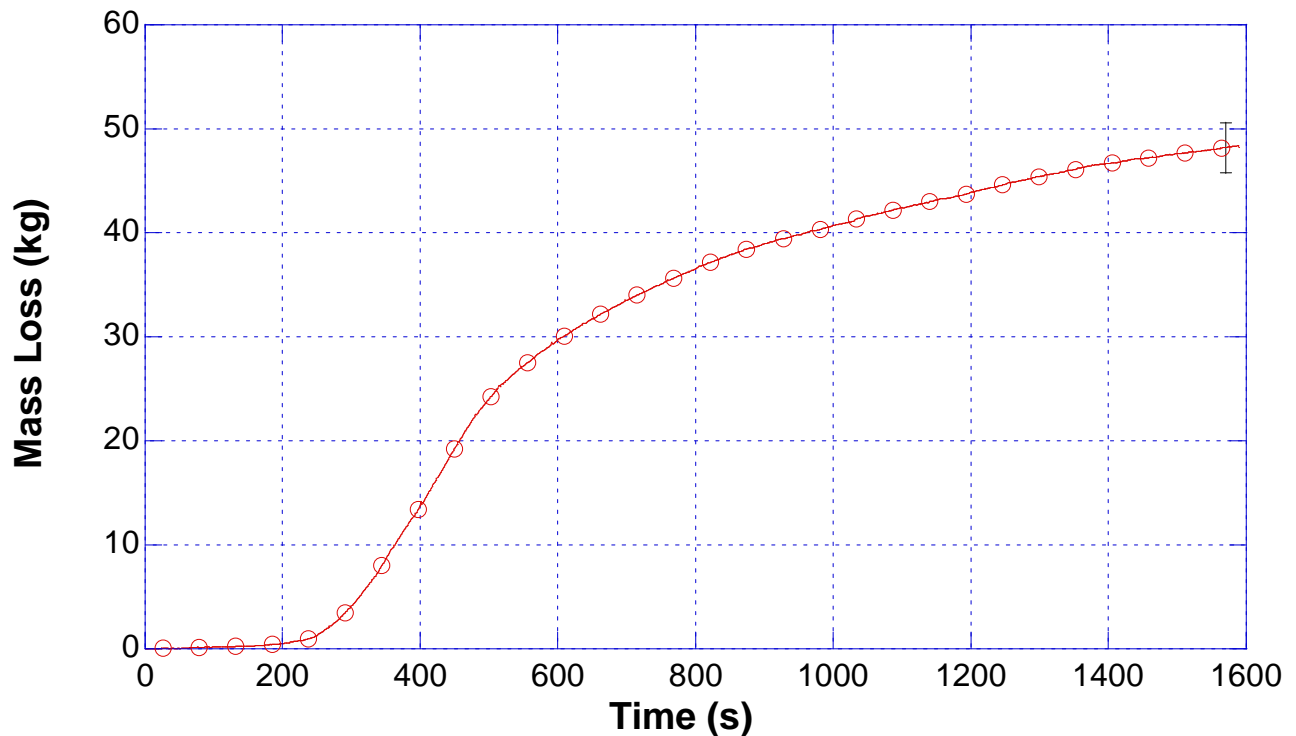


Figure 3.5-24. Mass loss versus time for sofa 1.

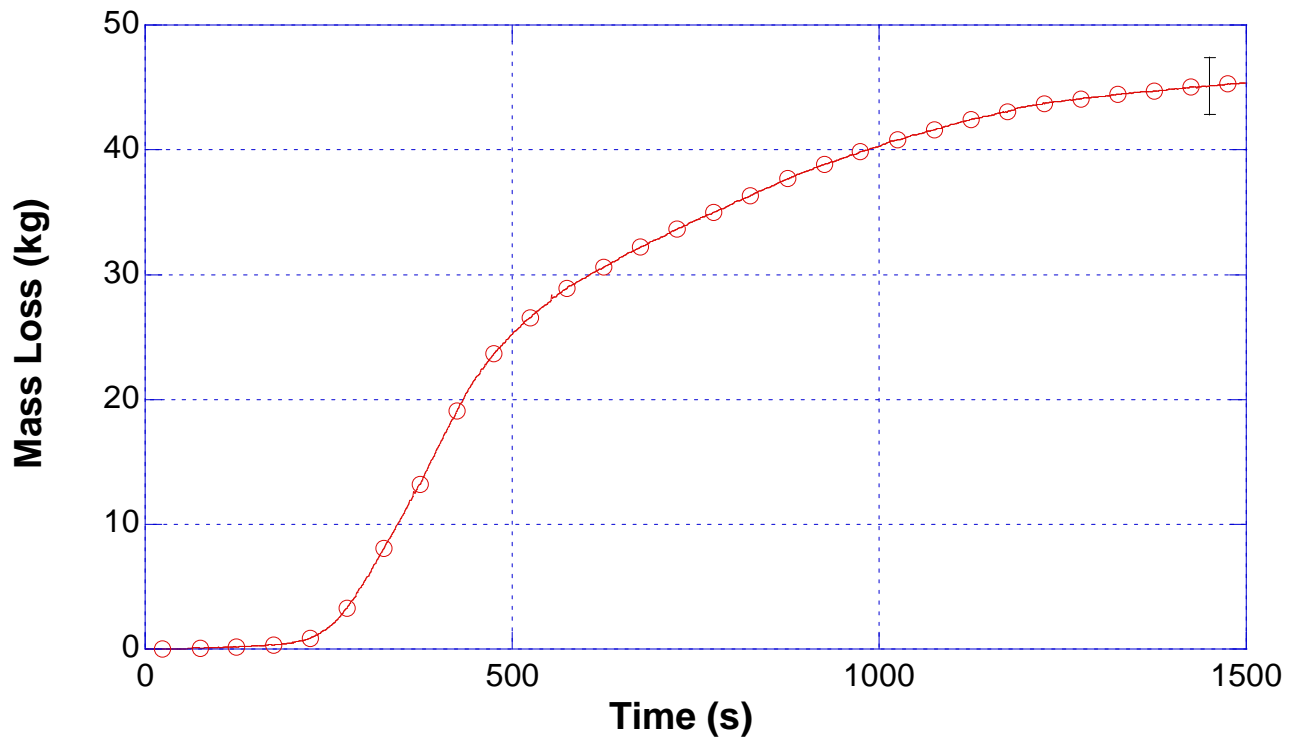


Figure 3.5-25. Mass loss versus time for sofa 2.

3.6 Discussion - Heat Release Rate Experiment Results

Eight heat release rate experiments were conducted to characterize the ignition source and the furniture items with the highest heat release rates. The average peak heat release of the trash container ignition source was 32 kW. The upholstered chairs had an average peak heat release rate of 1.76 MW. The bed fuel packages had an average peak heat release rate of 4.3 MW. The sofas provided an average peak heat release rate of 2.48 MW.

In the structure fire experiments, the bedroom had a bed fuel package as well as two upholstered chairs. These fuels alone have the peak potential for more than 7.8 MW of heat release rate. While this does not account for any interior finish or wood furnishings, it is more than enough energy to flashover a typical residential scale room.

The sofa and three upholstered chairs are the principle furnishings for the living room in the structure fire experiments. Based on the heat release experiments, the potential average peak heat release rate of the four pieces of furniture is also approximately 7.8 MW. Again this does not account for any energy added do to carpeting or carpet padding that will be installed in the bedroom, living room and hallway.

The peak heat release rate for each of the furnishing items occurred between 389 s and 474 s in these free burn experiments. These fuel packages coupled with interior finish fuels and the wood furnishings in the bedroom and living room should have the ability to sustain post-flashover conditions for several minutes, which will provide the time needed to examine the impact of a wind control device and or external water streams.

4 Experimental Arrangement

A multi-room structure was constructed in the NIST Large Fire Research Facility in order to conduct a series of wind driven experiments. After the structure was complete and instrumented a series of “wind only” experiments were conducted to develop an understanding of the pressures and velocities throughout the rooms and passage ways of the structure. Additional wind experiments were conducted to assess the effectiveness of wind control devices based on pressure and velocities within the structure. Water distribution experiments were also conducted in the structure to examine the impact of different means of introducing water in to the fire room from a window. Finally, a series of eight fire experiments were conducted in the furnished structure to measure the temperatures, heat fluxes, gas concentrations, pressures, gas velocities, and heat release rate to develop an understanding of the fire environment caused by the wind driven flows and to examine the ability of the wind control devices and or external water application to mitigate the hazards.

4.1 Facility

The NIST Large Fire Facility is located on the NIST campus in Gaithersburg, MD. The main test area of the building is approximately 36.6 m (120 ft) from East to West and 18.3 m (60 ft) from North to South. The north half of this area has a ceiling height of 10.7 m (35 ft). The structure was built in this area of the building, under the 9 m (30 ft) x 12 m (40 ft) oxygen consumption calorimetry hood. This hood has a maximum exhaust flow of 42,000 l/s (90,000 SCFM). This flow rate will be used for all of the experiments. Approximately 7.9 m (26 ft) to the west of the structure is a 4.9 m (16 ft) wide roll-up door. A large mechanical fan was positioned in this doorway to provide the wind conditions for the experiments. The north wall of the target room was 1 m (3.33 ft) from the north wall of the facility.

4.1.1 Structure

The structure was composed of three rooms; a bed room, a living room and a target room. The bed room, target room and living room were connected by a hallway. A door from the living room leads to a corridor that extends 7.3 m (24 ft) corridor in each direction, when measured along the inside of the exterior wall. The south side of the corridor is closed with no exit. The north side of the corridor had an exit vent on the ceiling, which led to an insulated exhaust chimney that vents into the oxygen consumption calorimetry hood. The only other opening to the facility is the bedroom window, when it vented during the fire experiments. The window served as the wind inlet during the experiments. A schematic plan view of the structure is given in Figure 4.1.1-1.

One layer of 13 mm (0.5 in) thick cement board panels were laid on the concrete floor of the facility to form a protective foundation for the structure. This layer was covered with 13 mm (0.5 in thick) gypsum board. The structure was framed with steel studs and track as shown in Figure 4.1.1-2. The studs were set to 0.40 m (16 in) centers. The ceiling support was composed of wood truss joist I-beams (TJIs) with a 299 mm (11.88 in) depth. The TJI was composed of laminated veneer lumber flanges with a cross section of 38 mm (1.5 in) x 57 mm (2.25 in) and an 11 mm (0.43 in) thick oriented strand board web as shown in Figure 4.1.1-3.

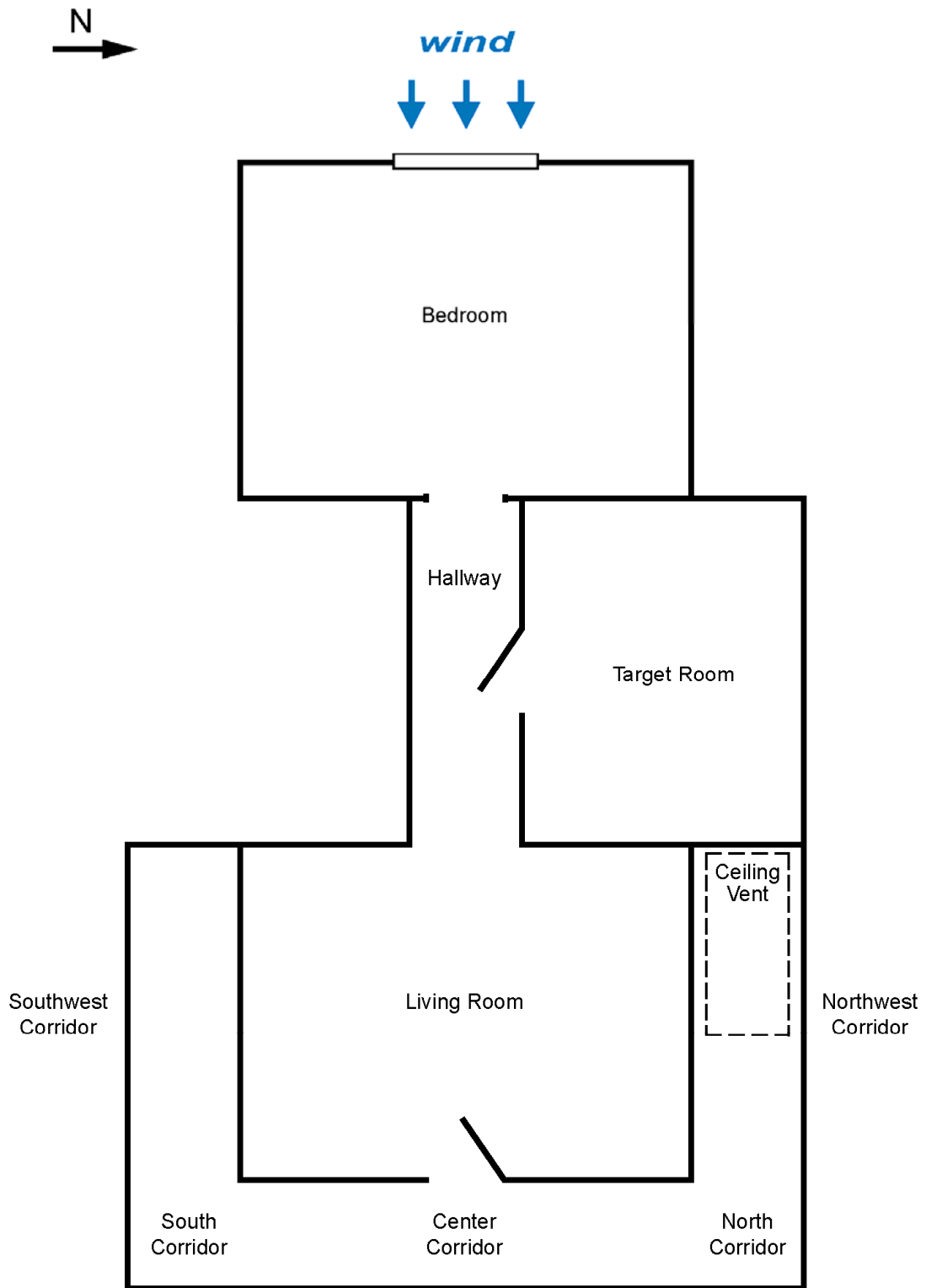


Figure 4.1.1-1. Schematic plan view of the experimental structure.

The walls and the ceiling of the structure were made from three layers of 13 mm (0.5 in) gypsum board. Each layer was taped and spackled. The orientation of the gypsum board panels was rotated 90°, to eliminate potential smoke and heat leakage at wall and ceiling seams. The inner layer of gypsum board was changed after each experiment and the second and third layers were patched as needed. The inner layer of gypsum board was sprayed with two coats of latex paint before each experiment.

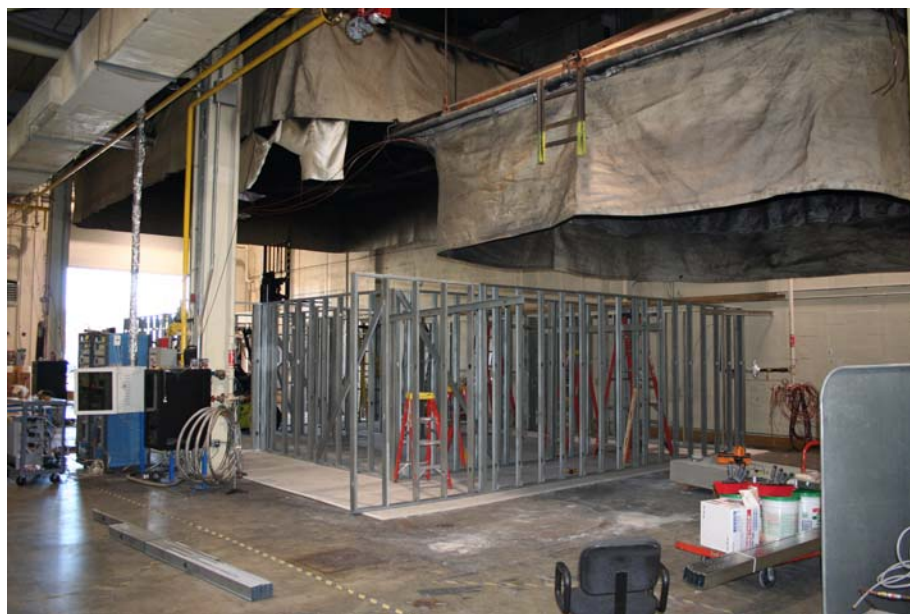


Figure 4.1.1-2. Steel framing for walls of experimental structure inside the NIST Large Fire Facility.

A layer of 11 mm (0.44 in) thick oriented strand board (OSB) was placed on top of the gypsum board/cement board foundation to serve as the sub-floor and the base for the carpet padding and carpet. The structure was designed so that the finished interior dimensions would be based on the size of sheet materials such as gypsum board and OSB in order to facilitate rapid reconstruction between experiments by minimizing the amount of cutting required. The dimensions of the structure are given in the floor plan shown in Figure 4.1.1-4. The ceiling height throughout the structure is 2.44 m (8.0 ft). The structure has three doorways that are used as part of the experiments; 1) between the bedroom and the hallway, 2) between the target room and the hallway, and 3) between the living room and the corridor. Each of these doorways is 1.98 m (6.5 ft) tall and 0.92 m (3.0 ft) wide.

The east wall of the corridor and the interior of the vent stack were lined with a layer of 13 mm (0.5 in) thick calcium silicate board. These areas were subject to severe flame impingement during the experiments. These areas were not painted between tests and were repaired as needed to contain the fire in the corridor and have the flames and combustion products vent into the exhaust hood. Steel access doors were installed in the target room and the south end of the corridor. These doors are not shown on the drawings as they were sealed over during the experiments.



Figure 4.1.1-3. Ceiling supports for experimental structure.

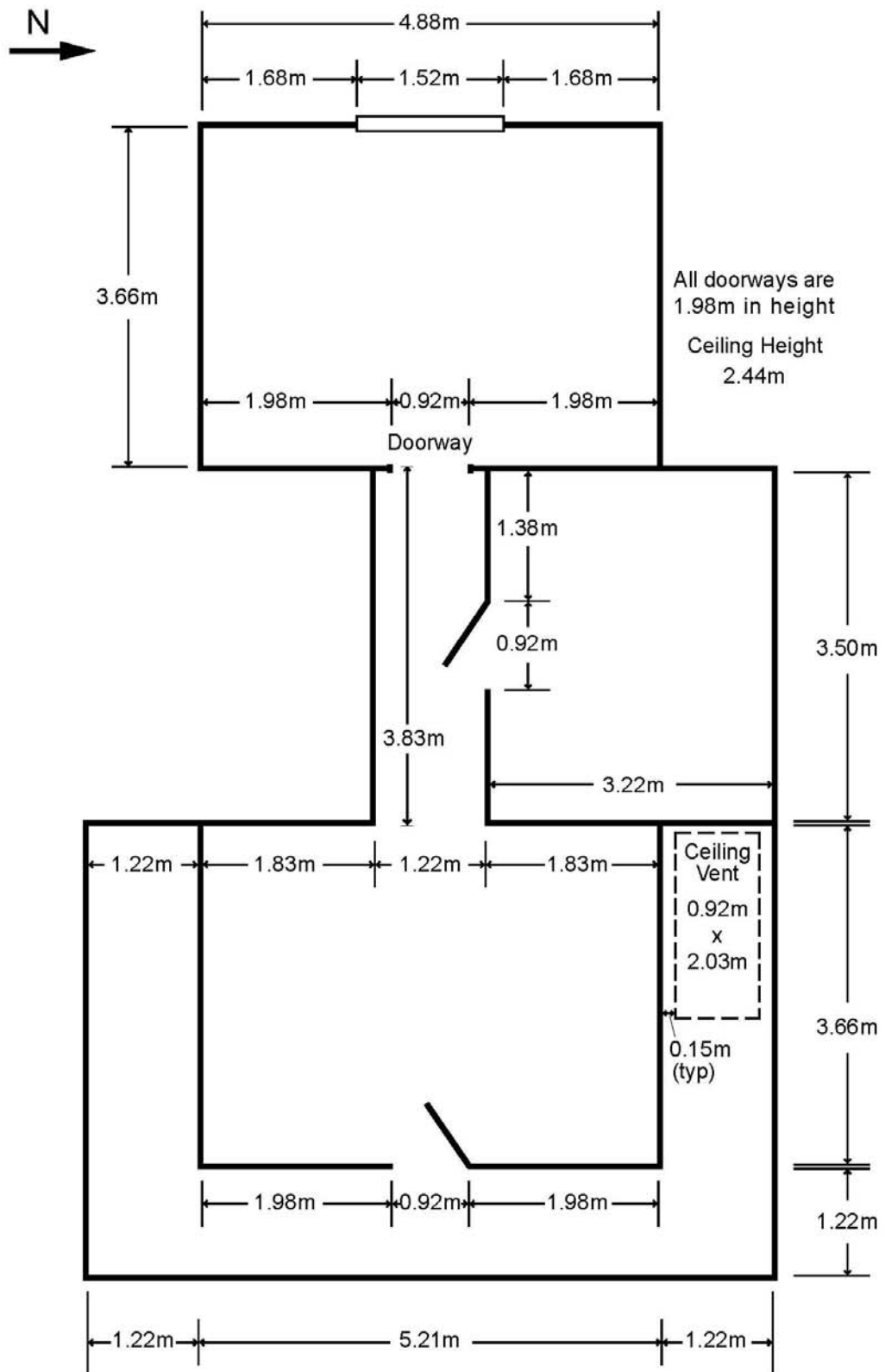


Figure 4.1.1-4. Dimensioned floor plan of experimental structure.

4.1.2 Instrumentation

A schematic plan view of the instrumentation arrangement is shown in Figure 4.1.3-1. There is a discussion of uncertainties for each measurement below in Section 4.1.3. Gas temperatures were measured with bare-bead, Chromel-Alumel (type K) thermocouples, with a 0.5 mm (0.02 in) nominal diameter. Thermocouple arrays were installed in the center of the bedroom, the hallway, the center of the target room, the center of the living room, southwest corner of the living room, and four locations in the corridor. The vertical arrays had thermocouples located 0.025, 0.3, 0.61, 0.91, 1.22, 1.52, 1.83, 2.13 m below the ceiling (BC). Additional single thermocouples were installed in conjunction with other instrument locations; such as the bi-directional probes and the gas sampling points. In addition, thermocouples were used in a few experiments to monitor thermal conditions of the target room door. A photograph of the center thermocouple array in the living room is shown in Figure 4.1.3-5.

Heat flux was measured with Schmidt Boelter total heat flux gauges. The gauges were installed from the outside of the walls of the structure with the sensing faces of the gauges facing the interior of the structure and flush with the interior surface. The gauges were positioned in the center of the south wall of the bedroom and the living room and along the east wall of the corridor. All of the heat flux gauges were installed 1.52 m (5 ft) below the ceiling, a position chosen to be representative of the height of a crawling firefighter's facepiece. Because the face of the gauge is parallel to the wall (vertical), the sensing surface is likely to "see" a lower heat flux than a gauge that was positioned at the same height, with the sensing surface facing the ceiling (horizontal). However the vertical position was chosen to correspond with a crawling firefighter's facepiece.

Differential pressure transducers were located at the positions noted in Figure 4.1.3-1. Each transducer had a 6 mm (0.25 in) diameter copper tube running through the wall of the structure at 1.22 m (4 ft) below the ceiling to measure the pressure difference between the interior and exterior of the structure at the given location. The photograph in Figure 4.1.3-4, shows the installation of a thermocouple, heat flux sensor and a differential pressure sample port on the south wall of the living room, along with RFID tags which were being tested for a project on firefighter tracking and accountability.

Gas velocity was measured utilizing differential pressure transducers connected to bidirectional velocity probes[43]. These probes were located in sets of three outside the bedroom window, in the hall, in two locations in the North-South portion of the corridor and in the entry to the vent stack, 2.44 m (8.0 ft) above the ceiling of the corridor. With exception of the window and vent locations which are detailed in Figure 4.1.3-1, the probes are located 0.3 m (1 ft), 1.22 m (4 ft), and 2.13 m (7 ft) below the ceiling. A single thermocouple is attached to each bi-directional probe. The bi-directional probes installed in the west window are positioned at 0.38 m (1.25 ft), 0.76 m (2.50 ft) and 1.14 m (3.75 ft) below the top of the window opening, centered on north-south axis, as shown in Figure 4.1.3-3. The back face of the probe was 60 mm (0.20 ft) in front of the window glass. The bi-directional probe array installed in the hall can also be seen in the photograph.

Gas concentrations were sampled at four different points in the structure, two in the bedroom and two in the living room. The gas sampling points are located in the center of the south wall of both rooms, 0.91 m (3 ft) north of the south wall and at positions 0.61 m (2 ft) and 1.83 m (6 ft) below the ceiling. The

sampling tubes were connected to a calibrated pump which pulled the gas samples through a sample conditioning system to eliminate moisture in the gas sample. The dry gas sample was then piped to a series of gas analyzers. In all of the experiments, oxygen was measured using paramagnetic analyzers and carbon monoxide and carbon dioxide were measured using non-dispersive infrared (NDIR) analyzers for all four locations. In the latter experiments, total unburned hydrocarbons were measured from the two upper layer positions 0.61 m (2 ft) below the ceiling using flame ionization detectors (FID). Details of this gas sampling and measurement system can be found in [44, 45]. Single thermocouples were also co-located with the gas sample inlet ports. Figure 4.1.3-5 is a photograph of the south wall of the living room, which shows the gas sampling ports.

The heat release rate experiments were conducted in the NIST Large Fire Laboratory utilizing the 9 m by 12 m oxygen depletion calorimeter. The data from the calorimeter and the data from the sensors installed in the structure were recorded at intervals of 1 s on a computer based data acquisition system.

4.1.3 Estimated Measurement Uncertainty

There are different components of uncertainty in the length, temperature, heat flux, gas concentration, differential pressure, gas velocity and heat release rate reported here. Uncertainties are grouped into two categories according to the method used to estimate them. Type A uncertainties are those which are evaluated by statistical methods, and Type B are those which are evaluated by other means [46]. Type B analysis of systematic uncertainties involves estimating the upper (+ a) and lower (- a) limits for the quantity in question such that the probability that the value would be in the interval ($\pm a$) is essentially 100 %. After estimating uncertainties by either Type A or B analysis, the uncertainties are combined in quadrature to yield the combined standard uncertainty. Multiplying the combined standard uncertainty by a coverage factor of two results in the expanded uncertainty which correspond to a 95 % confidence interval (2σ). For some of these components, such as the zero and calibration elements, uncertainties are derived from instrument specifications. For other components, such as differential pressure, past experience with the instruments provided input in the uncertainty determination.

Each length measurement was taken carefully. Length measurements such as the room dimensions, instrumentation array locations and fan placement were made with a hand held laser measurement device which has an accuracy of ± 6.0 mm (0.25) over a range of 0.61 m (2.00 ft) to 15.3 m (50.0 ft) [47]. However, conditions affecting the measurement, such as levelness of the device, yields an estimated uncertainty of ± 0.5 % for measurements in the 2.0 m (6.6 ft) to 10.0 m (32.8 ft) range. Steel measuring tapes with a resolution of ± 0.5 mm (0.02 in) were used to locate individual sensors within a measurement array and to measure and position the furniture. Some issues, such as “soft” edges on the upholstered furniture, result in an estimated total expanded uncertainty of ± 1.0 %.

The standard uncertainty in temperature of the thermocouple wire itself is ± 2.2 °C at 277 °C and increases to ± 9.5 °C at 871 °C as determined by the wire manufacturer [48]. The variation of the temperature in the environment surrounding the thermocouple is known to be much greater than that of the wire uncertainty [49, 50]. Small diameter thermocouples were used to limit the impact of radiative heating and cooling. The estimated total expanded uncertainty for temperature in these experiments is ± 15 %.

In this study, total heat flux measurements were made with water-cooled Schmidt-Bolter gauges. The manufacturer reports a $\pm 3\%$ calibration expanded uncertainty for these devices [51]. Results from an international study on total heat flux gauge calibration and response demonstrated that the uncertainty of a Schmidt-Boelter gauge is typically $\pm 8\%$ [41].

The gas measurement instruments and sampling system used in this series of experiments have been demonstrated an expanded ($k = 2$) relative uncertainty of $\pm 1\%$ when compared with span gas volume fractions [44]. Given the limited set of sampling points in these experiments an estimated uncertainty of $\pm 10\%$ is being applied to the results.

Differential pressure reading uncertainty components were derived from pressure transducer instrument specifications and previous experience with pressure transducers. The transducers were factory calibrated and the zero and span of each was checked in the laboratory prior to the experiments yielding an accuracy of $\pm 1\%$ [52]. The total expanded uncertainty was estimated at 10% .

Bi-directional probes and single thermocouples were used to measure the velocity. The bi-directional probes used similar pressure transducers as those used for the differential pressure measurements discussed above. Bare-bead Type K thermocouple are co-located with the probe. The estimated total expanded uncertainty for velocity in these experiments is $\pm 18\%$.

The NIST Large Fire Facility 9 m x 12 m oxygen consumption calorimetry hood was used for these experiments. The estimated expanded uncertainty of the measurement system is $\pm 11\%$ on the measured heat release rate. Details on the operation and uncertainty in measurements associated with the oxygen depletion calorimeter can be found in [40]. However for the wind driven experiments, there will be a bias for the heat release rate measurement to err on the low side, due to combustion products being blown out of the hood. While the hood was calibrated with a gas-burner prior to testing and shown to be within 11% even with the large roll-up door on the west wall of the facility open, no mechanical wind was being generated. At the higher calibration, nominally 8 MW, the system was measuring 5% to 10% on the high side. The total uncertainty will be presented as $\pm 11\%$, however in some of the wind driven experiments, the heat release rate measurement would tend to under report the peak heat release rate value due to the loss of combustion products.

In the following sections, the measurements will be presented in graphic and tabular form. In the graphs an error bar will represent the estimated uncertainty of the measurement. In the tables the uncertainty will be included in the table of as part of the caption.

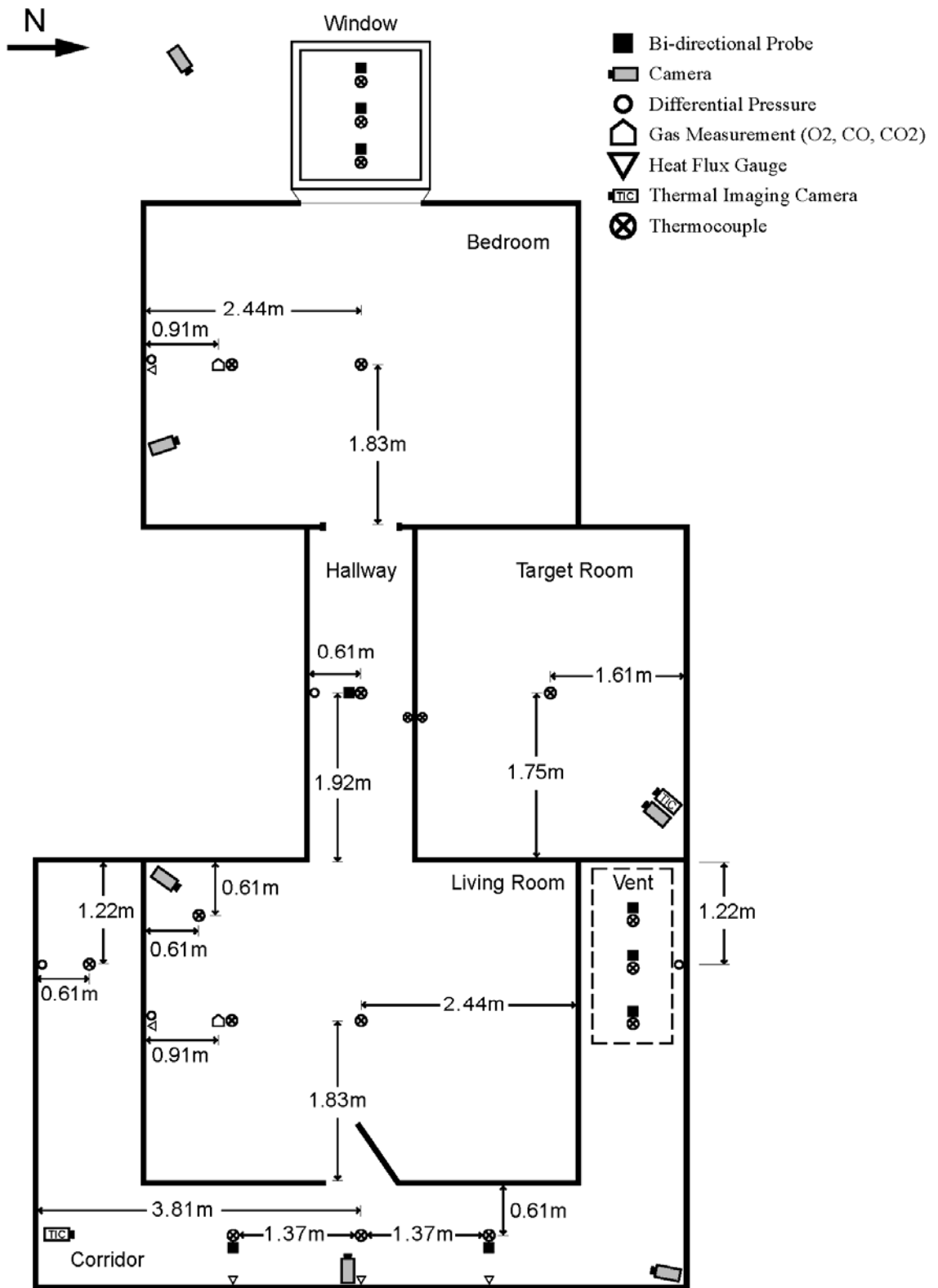


Figure 4.1.3-1. Schematic floor plan of instrumentation types and locations.



Figure 4.1.3-2. Thermocouple arrays along center line of structure looking from east to west.



Figure 4.1.3-3. Bi-directional probe array in west window.



Figure 4.1.3-4. Wall mounted thermocouples, heat flux sensor, and differential pressure sampling port.



Figure 4.1.3-5. Gas sampling probe installation on south wall of living room.

4.2 Fuel Load

Used furnishings were purchased from a hotel liquidator in order to obtain 10 sets of similar furniture to use in the heat release rate experiments and in the wind driven fire experiments in the structures. The furniture was of similar style from the same manufacturer. For example, the upholstered chairs were made by the same manufacturer, had similar mass (range 23.3 kg (51.4 lbs) to 24.0 kg (52.9 lbs)), and similar materials of construction. The furnishings were manufactured in 1998 and 1999.

The bedroom fuel load and its arrangement is shown in Figure 4.2-1 through Figure 4.2-3. Descriptions of the furnishing dimensions, materials, and mass are given in Table 4.2-1. The total mass of the furnishings, carpeting and carpet padding in the bedroom fuel package was 406 kg (894 lbs). Based on metal removed after the experiments, the combustible mass of the bedroom fuel package was 350 kg (769 lbs). Taking those totals and dividing by the floor area of the bedroom yielded total and combustible fuel loadings of 22.8 kg/m² (4.7 lb/ft²) and 19.6 kg/m² (4.0 lb/ft²), respectively. This did not take the subfloor or the painted gypsum board walls and ceilings into account.

The living room fuel load and its arrangement is shown in Figure 4.2-4 through Figure 4.2-6. Descriptions of the furnishing dimensions, materials and mass are given in Table 4.2-2. The mass of fuel load in the living room was less than the bedroom. The total mass of the furnishings, carpeting and carpet padding in the living room was 254 kg (558 lbs). Based on metal removed after the experiments, the approximate combustible mass of the living room fuel package was 218 kg (479 lbs). Taking those totals and dividing by the floor area of the living room yielded total and combustible fuel loadings of 14.2 kg/m² (2.9 lb/ft²) and 12.2 kg/m² (2.5 lb/ft²), respectively. Again, this did not take the subfloor or the painted gypsum board walls and ceilings into account.

Table 4.2-3 documents the fuel load in the hall. In experiments 1 through 3, a hollow core wood door was installed in the doorway between the hall and the target room. In the remainder of the experiments, the wood door was replaced with a steel door, so the only installed fuel load was the carpeting and carpet padding. With the wood door considered, the combustible fuel load in the hall was 4.8 kg/m² (1 lb/ft²). All totaled, the installed combustible fuel load for each structure fire test was approximately 590 kg (1300 lbs).

The principle interior finish of the structure was the gypsum board walls and ceilings. The walls and ceilings were painted with two coats of latex paint. A previous study has shown that gypsum board with two coats of latex paint has a peak heat release rate of approximately 200 kW/m². However it only provides that energy for approximately 10 s based on cone calorimeter results [53]. The only other combustible material in the structure was the oriented strand board (OSB) sub flooring. If the OSB became exposed to high heat flux conditions (>35 kW/m²), based on cone calorimeter experiments, it would generate an average heat release rate in the range of approximately 200 kW/m² to 300 kW/m² [54].

Bedroom

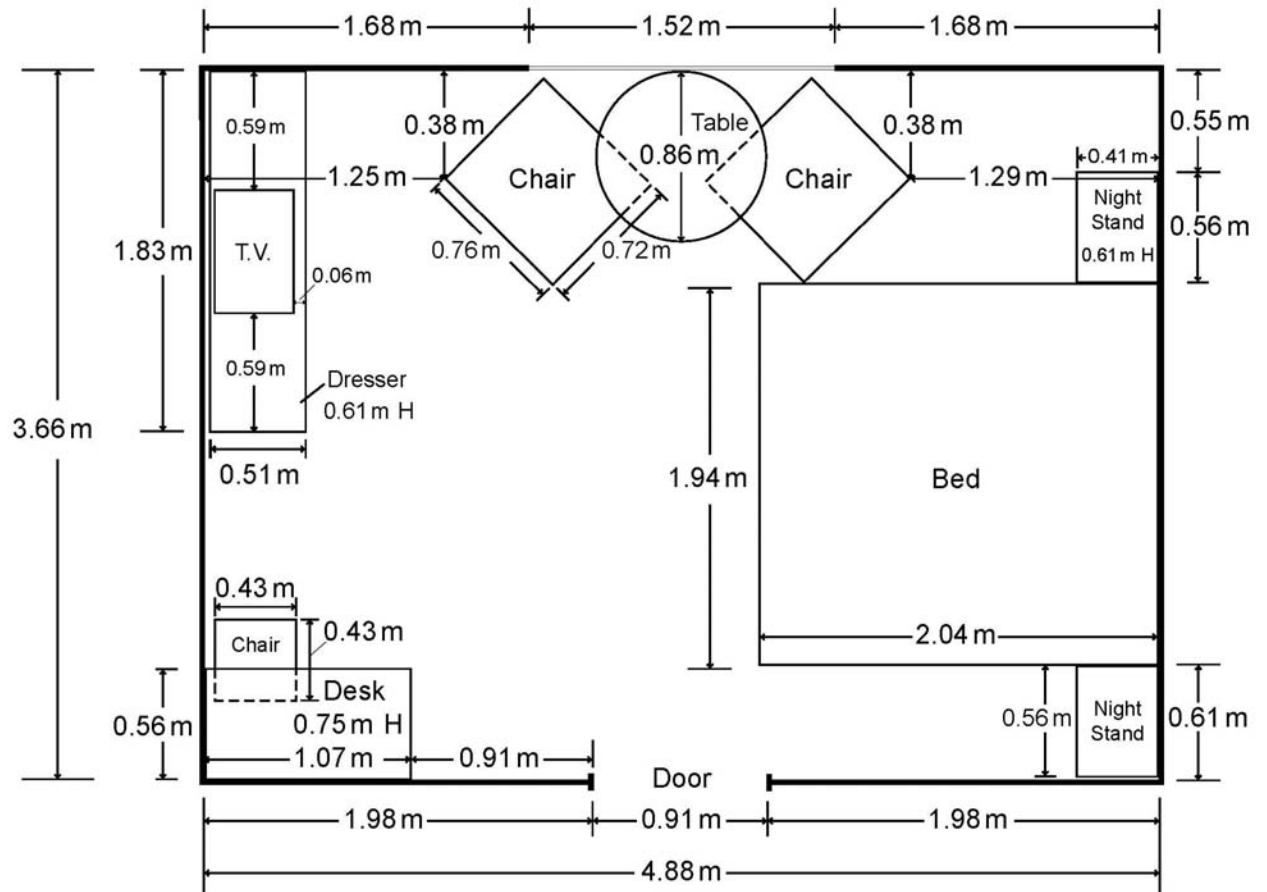


Figure 4.2-1. Schematic floor plan of bedroom with furniture locations.



Figure 4.2-2. Bedroom furnishings, looking north.



Figure 4.2-3. Bedroom furnishings, looking south.

Table 4.2-1. Bedroom fuel load description.

Item	Material Description	Dimensions	Mass (kg)	Approx. Combustible Mass (kg)
Bed Frame	Steel with plastic rollers and supports		14.71	1
Box Spring	Fabric covered metal springs with wooden frame	2.03 m x 0.97 m x 0.19 m thick	17.66	11.5
Box Spring	Fabric covered metal springs with wooden frame	2.03 m x 0.97 m x 0.19 m thick	18.83	12.6
Mattress	Inner Spring Mattress	80 in x 76 in W x 9 in thick	47	22.5
Bedding Set	60 % Cotton, 40 % polyester	King size fitted sheet, flat sheet, comforter, pillow cases & bed skirt	5.93	5.93
Pillows	55 % cotton and 45 % polyester shell, 100 % PE fill	0.66 m x 0.51 m x 0.20 m thick	1.1	1.1
Night Stand	wood and wood composite	0.56 m x 0.41 m x 0.61 m H	19.81	19.1
Night Stand	wood and wood composite	0.56 m x 0.41 m x 0.61 m H	19.8	19.1
Dresser	wood and wood composite	72 in x 20 in x 24 in H	74.57	72
Desk	wood and wood composite	42 in x 22 in x 29.625 in H	26.73	26.7
Desk Chair	wood frame, PE fabric over PU foam cushion	17 in x 17 in x 28.25 in H	7.32	7.3
Wall Mirror	wood frame, mirrored glass	0.64 m x 1.14 m x 25 mm thick	11.8	2
Upholstered Chair	PE fabric over wood frame, seat cushion: 90 % PU, 10 % PE, back cushion: 90 % PE, 10 % PU	0.72 m x 0.76 m x 0.73 m H	24.07	23.2
Upholstered Chair	PE fabric over wood frame, seat cushion: 90 % PU, 10 % PE, back cushion: 90 % PE, 10 % PU	0.72 m x 0.76 m x 0.73 m H	23.65	22.9
TV	Plastic case, CRT, metal base	0.66 m x 0.41 m x 0.43 m H	23.32	22.6
Lamp	metal and plastic with cloth shade and vinyl electric cord	0.83 H, shade max dia. 0.5 m	2.7	1
Lamp	metal and plastic with cloth shade and vinyl electric cord	0.83 H, shade max dia. 0.5 m	2.7	1
Plastic Trash Container	HDPE	0.22 m x 0.20 m x 0.27 m H	0.32	0.32
Paper (trash)	news print paper		0.3	0.3
Round table	wood, wood composite, and plastic	0.86 dia, 25 mm thick top, 0.74 m H	17.81	17.5
Carpet padding	12 mm thick PU padding	3.66 m x 4.88 m	29.1	29.1
Carpet	100 % nylon pile carpeting with polyolefin backing	3.66 m x 4.88 m	31.94	31.94
Total			406.46	349.69

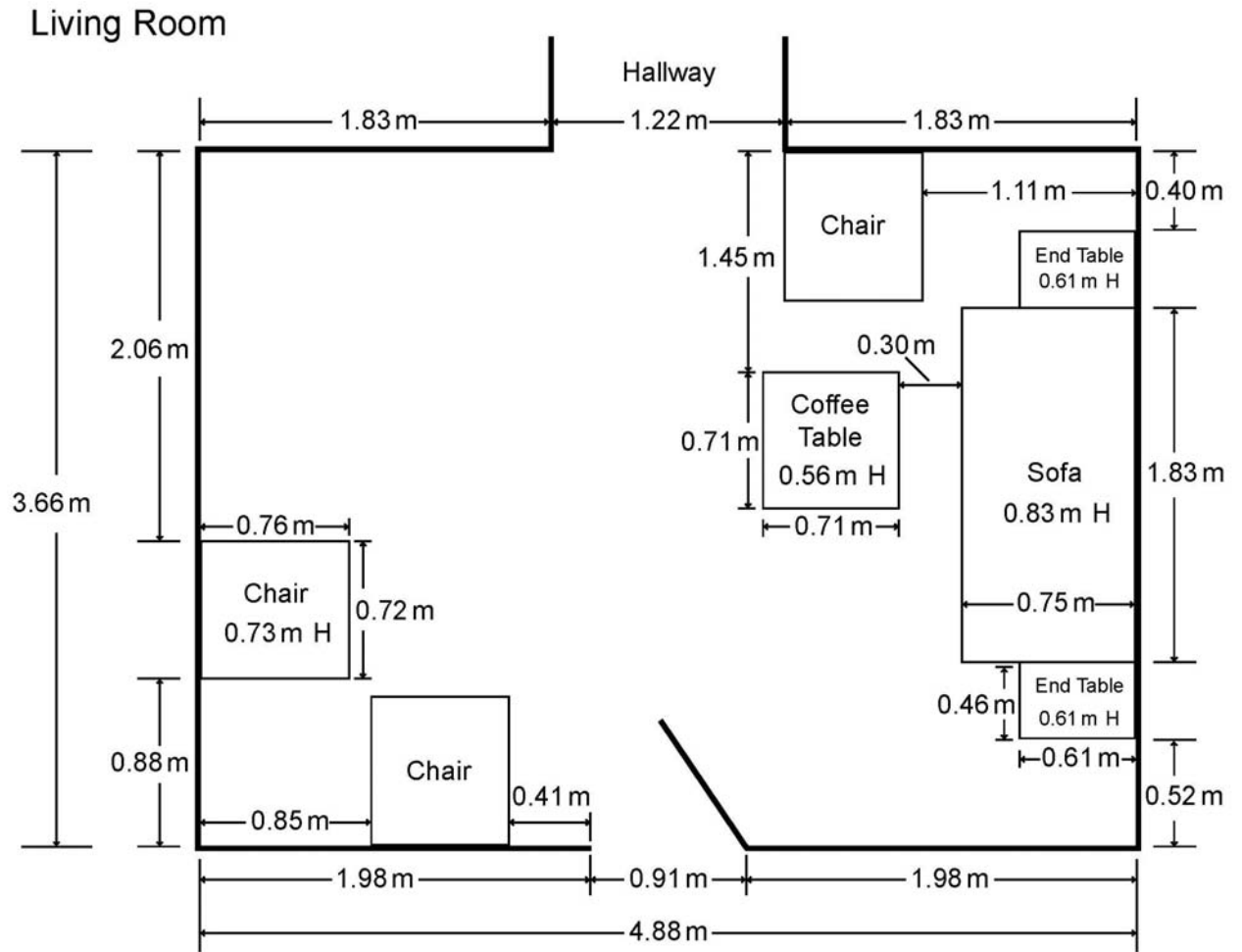


Figure 4.2-4. Schematic floor plan of living room with furniture locations.



Figure 4.2-5. Living room furniture, looking north.



Figure 4.2-6. Living room furnishings, looking east.

Table 4.2-2. Living room fuel load description.

Item	Material Description	Dimensions	Mass (kg)	Approx. Combustible Mass (kg)
Sofa	PE fabric over wood frame with PU foam back. Seat Cushions PE wrapped over PU foam	1.83 m x 0.75 m x 0.83 m	80	50
Upholstered Chair	PE fabric over wood frame, seat cushion: 90 % PU, 10 % PE, back cushion: 90 % PE, 10 % PU	0.72 m x 0.76 m x 0.73 m H	24.35	23.5
Upholstered Chair	PE fabric over wood frame, seat cushion: 90 % PU, 10 % PE, back cushion: 90 % PE, 10 % PU	0.72 m x 0.76 m x 0.73 m H	24	23.2
Upholstered Chair	PE fabric over wood frame, seat cushion: 90 % PU, 10 % PE, back cushion: 90 % PE, 10 % PU	0.72 m x 0.76 m x 0.73 m H	24	23.2
Coffee Table	wood and wood composite	0.71 m x 0.71 m x 0.56 m H	15.56	15.5
End table	wood and wood composite	0.61 m x 0.46 m x 0.61 m H	9.55	9.5
End Table	wood and wood composite	0.61 m x 0.46 m x 0.61 m H	9.63	9.6
Lamp	metal and plastic with cloth shade and vinyl electric cord	0.83 H, shade max dia. 0.5 m	2.7	1
Lamp	metal and plastic with cloth shade and vinyl electric cord	0.83 H, shade max dia. 0.5 m	2.7	1
Carpet padding	12 mm thick PU padding	3.66 m x 4.88 m	29.1	29.1
Carpet	100 % nylon pile carpeting with polyolefin backing	3.66 m x 4.88 m	32	32
Total			253.59	217.6

Table 4.2-3. Hallway fuel load description.

Hall	Material Description	Dimensions	Mass (kg)	Approx. Combustible Mass (kg)
Door	wood and cardboard	2.0 m x 0.9 m x 38 mm thick	10.3	10
Carpet Padding	12 mm thick PU padding	3.66 m x 0.91 m	5.4	5.4
Carpet	100 % nylon pile carpeting with polyolefin backing	3.66 m x 0.91 m	6.1	6.1
Total			21.8	21.5

4.3 Wind Source

A mechanical wind source was chosen for the experiments to accommodate scheduling, repeatability and location. The Montgomery County Fire and Rescue Service/ Cabin John Park Volunteer Fire Department's Yankee Air Boat, was used to provide the "wind" for all of the wind driven experiments. The boat has a 1.98 m (6.5 ft) propeller which is driven by a 5.7 l (350 cu. in) gasoline powered engine. The boat has two steering vanes.

The boat was positioned 9.6 m (31.5 ft) from the west exterior of the structure, The fan was centered on the window and the steering vanes were locked down in the "straight" position as shown in Figure 4.3-1. The roll-up door was raised to create an opening, 4.05 m (13.3 ft) high and 4.88 m (16.0 ft). The boat was leveled so that the centerline of the propeller hub was parallel to the floor of the large fire facility. The centerline of the propeller was 2.13 m (7.0 ft) above ground level. The fan was operated at speeds between 800 rpm and 3000 rpm. Based on hand-held anemometer readings this range provided air speeds of 2.2 m/s (5 mph) to 11.4 m/s (25 mph) at the window opening of the structure.



Figure 4.3-1. Air boat from inside of fire lab looking west.



Figure 4.3-2. Air boat from outside of the fire lab looking east.

4.3.1 Wind Speed and Pressure Experiments

Prior to each fire experiment, the fan was positioned as described above. The bedroom window was removed resulting in a 1.52 m (5.0 ft) by 1.52 m (5.0 ft) opening. The data acquisition system was turned on and background data was collected. The fans for the exhaust control system were turned on and flowing 42,000 l/s (90,000 SCFM). Then the fan was started and allowed to warm-up to achieve a steady idle of 800 rpm. The pressure probes were checked to ensure that all were responding to the increased air flow through the structure. The fan speed was then increased to 1000 rpm and held steady for at least a minute and then the speed was increased to 1500 rpm. This pattern was repeated, increasing the fan speed by 500 rpm increments each time, up to 2500 rpm. Then measurements were taken as the fan speed was decreased in a similar manner until the fan was back to 800 rpm.

Table 4.3-1 is a summary of the wind speed, measured in m/s, averaged over a 30 s interval of the period that the fan speed was steady. The speeds are given for each of the bi-directional probe positions. It can be seen that the speeds through the window, hall and vent positions are higher than the speeds measured in the corridor positions. This is due to recirculation in the corridor flow paths. The measurements from the top bi-directional probe in the hall remained low relative to the two lower hall bi-directional probe positions at fan speeds of 1500 rpm and above. This may be due to a low pressure area near the ceiling caused by the doorway soffit which extends 0.46 m below the ceiling, whereas the probe was 0.3 m below the ceiling. The wind speeds reported here are slightly lower than speeds which may be reported for a given experiment due to differences in outside wind conditions and the flows through the structure caused by the hoods, which were subtracted out of each data set to develop a baseline wind speed from only the fan. The flow through the structure due to the calorimetry/exhaust system is approximately 0.45 m/s (1 mph) with a system flow rate of approximately 42,000 l/s (90,000 SCFM).

Table 4.3-2 is a summary of the differential pressures measured in Pa and averaged during the same time periods as the speeds in Table 4.3-1. The largest increase in pressure was seen in the bedroom and decreased as the distance away from the fan increased. The pressure gradient created by the fan through the structure was consistent with the flow path from the window to the vent opening and the wind speeds in Table 4.3-1. The air in the structure will flow from a higher pressure to a lower pressure and because of the location of the fan the only place the air could flow was to the vent or any gaps or cracks it could find in the structure to the outside. This flow will be emphasized as the pressure created by the fire is added.

Table 4.3-1. Summary of average wind speeds with respect to fan speeds, (m/s \pm 15 %).

Location	Distance below Ceiling (m)	800 rpm	1000 rpm	1500 rpm	2000 rpm	2500 rpm
Window	0.84	0.86	1.87	3.02	4.33	6.21
	1.20	1.04	2.02	3.29	4.37	6.20
	1.60	0.83	1.91	3.31	4.53	5.54
Hall	0.03	0.05	0.09	0.22	0.36	0.69
	1.20	0.42	1.16	2.12	2.95	3.99
	2.10	0.33	1.01	1.79	2.22	3.44
CS	0.03	-0.02	-0.06	-0.13	-0.25	-0.41
	1.20	-0.09	-0.23	-0.59	-1.14	-2.66
	2.10	0.03	0.07	0.10	0.45	0.63
CN	0.03	0.12	0.40	0.64	0.85	1.22
	1.20	0.12	0.29	0.65	0.92	1.29
	2.10	0.23	0.81	1.55	2.37	3.05
Vent	West	0.29	0.83	1.62	2.27	3.28
	Central	0.38	1.02	1.89	2.65	3.89
	East	0.39	0.98	1.88	2.71	3.84

Table 4.3-2. Summary of average baseline differential pressures with respect to fan speed, (Pa \pm 15 %).

Location	800 rpm	1000 rpm	1500 rpm	2000 rpm	2500 rpm
Bedroom	7.18	18.22	42.82	67.69	98.68
Hall	5.40	13.75	32.22	48.33	71.57
Living Room	5.20	12.78	29.93	45.52	66.28
Corridor SW	5.39	13.87	31.63	47.14	66.93
Corridor NW	3.95	9.88	22.61	33.45	46.73

4.3.2 Wind Control Device Experiments

Two wind control devices (WCD) were used during these experiments. The devices function by covering the window opening and blocking or reducing the flow of air into the room. Both of the devices used in these experiments were made from a proprietary high temperature textile material that is flexible, resists abrasion, and can withstand temperatures of approximately 1100 °C (2000 °F).

The main differences between the two devices are size, weight and stiffness. The smaller WCD measured 1.8 m (6.0 ft) by 2.4 m (8.0 ft) and weighed approximately 12.3 kg (27.1 lbs). It was reinforced with metal rods and had a rope fastened at each corner to secure it. This device, given the size and shape, could be deployed by one firefighter from the floor above the fire. Figure 4.3.2-1 shows the small WCD deployed over the 1.52 m (5.00 ft) by 1.52 m (5.00 ft) window opening under approximately 20 mph wind conditions as generated by the fan. The metal rods hold the fabric flush to the face of the structure. The upper corners were tied off to the structure and the lower corners were secured with weights.



Figure 4.3.2-1. Small WCD deployed over window opening.



Figure 4.3.2-2. Large WCD deployed over window opening.

The second WCD measured 2.95 m (9.66 ft) by 3.66 m (12.0 ft) and weighed approximately 20.5 kg (45.2 lbs). This WCD had a chain sewn into the bottom of the curtain to assist with deployment. It also had tether straps attached at each corner. This device would typically require two or more firefighters to deploy and secure in place. Figure 4.3.2-2 shows the large WCD deployed over the same window opening under similar wind conditions as the small WCD. In this case the fabric was blown into the window opening. The upper corners were secured to the structure and the lower edge was secured with weights. The right side of the WCD may have been pushed further into the window opening but it is being held by the three bi-directional probes in the window opening.

Table 4.3-3 and provide a comparison of the speeds and pressure increases in the structure with and without the WCDs as well as the impact of closing the door to the corridor. The wind speed in the hall

was reduced from approximately 4 m/s (9 mph) to near 0 m/s with the WCDs in place over the opening. The table also points out that the WCDs have the same effect as closing the door to the corridor.

Closing one of the apartment openings, either the window opening with a WCD or the door to the corridor, changed the pressure in the structure significantly. When a WCD was used, the pressures in the bedroom, hall, living room and corridor went from values in excess of approximately 30 Pa to less than 1 Pa. When the flow path was interrupted by closing the corridor door the pressure changes were very different from the WCD experiments. With the corridor door closed the pressure inside the bedroom, hall and living room increased and equalized at approximately 45 Pa and 120 Pa for fan speeds of 1500 rpm and 2500 rpm respectively.

Table 4.3-3. Change of wind speed in the hall and vent based on the deployment of a WCD or closing the door to the corridor at two fan speeds, (m/s \pm 15 %).

Flow Condition	Location	1500 rpm	2500 rpm
Open	Hall	2.12	3.99
	Vent	1.89	3.89
Small WCD	Hall	0.01	0.00
	Vent	-0.06	0.00
Large WCD	Hall	-0.02	-0.01
	Vent	0.01	0.02
Corridor Shut	Hall	-0.06	-0.06
	Vent	-0.01	0.05

Table 4.3-4. Change of pressures in the apartment due to the deployment of a WCD or closing a door to the corridor at two fan speeds, (Pa ± 15 %).

Flow Condition	Location	1500 rpm	2500 rpm
Open	Bedroom	42.82	98.68
	Hall	32.22	71.57
	Living Room	29.93	66.28
	Corridor SW	31.63	66.93
	Corridor NW	22.61	46.73
Small WCD	Bedroom	0.74	0.58
	Hall	0.52	0.40
	Living Room	0.27	0.02
	Corridor SW	0.27	0.14
	Corridor NW	2.43	7.69
Large WCD	Bedroom	0.32	0.95
	Hall	0.22	0.94
	Living Room	0.08	0.17
	Corridor SW	0.13	0.45
	Corridor NW	2.32	5.64
Corridor Shut	Bedroom	46.31	121.98
	Hall	45.83	121.54
	Living Room	45.61	121.14
	Corridor SW	1.03	1.09
	Corridor NW	2.62	8.92

4.3.3 Water Spray Distribution Experiments

A series of water distribution tests was conducted to examine the ability of the air flow to push water into the structure. A matrix of interlocking water collection pans were placed on the floor of the living and one row of pans was placed up the hallway. Each pan was 0.5 m (1.6 ft) on a side and 0.3 m (1 ft) high. The center line of pans was centered on the window opening with 4 additional rows of pans added on both sides. The pans were 7 deep from the west wall of the bedroom to the east wall of the bedroom. A row of six pans extended down the center of the hall. With this arrangement of pans, there was a 0.15 m (0.5 ft) gap in the east-west direction and a 0.18 m (0.6 ft) gap between the north wall and the pans and a 0.20 m (0.7 ft) gap between the south wall and the pans. The gap in the east-west direction was adjusted based on the spray configuration.

The experiments were conducted by having the facility hoods operating as they would for a fire test at 42,000 l/s (90,000 SCFM), starting the fan and bringing it up to a constant speed of 2500 rpm, yielding a wind speed of 7 m/s to 9 m/s (15 mph to 20 mph) for these experiments. A hose stream with a pre-set flow rate was discharged for a minute and the water was collected in the pans. The pans were then weighed and the mass of water and the location of the pan was recorded.

Three experiments were conducted. In the first experiment, an adjustable fog nozzle at the narrow setting (approximately 30°), flowing approximately 5.0 l/s (80 gpm), was discharged parallel to the west

wall of the structure in front of the window opening. The second experiment used the same nozzle and flow rate, but discharged the water directly in the window opening. The third experiment used a 24 mm (15/16 in) smooth bore nozzle, flowing 10 l/s (160 gpm) discharged into the window at approximately a 60° angle above the floor and bounced off of the ceiling. A cement board target, 0.61 m (2 ft) x 0.61 m (2 ft) was installed on the ceiling, centered on the window centerline and 0.61 m (2 ft) east of the west wall. The solid stream was aimed to impact the center of the target in order break up the stream. The water distribution data is presented in Figure 4.3.3-5 through Figure 4.3.3-7. The values in the pans represent the number of kg/min. Any pan that is shaded gray did not contain a measurable amount of water.

The fog stream across the window experiment resulted in a total of 149 kg (328 lbs) of water being collected from the pans inside the compartment. Converting to l/s yields approximately 2.49 l/s (39.5 gpm) entering the room. This is about half of the total flow rate. Figure 4.3.3-5 shows some of the “heavy streams” from the fog nozzle, which appear to be composed of larger high velocity water drops are not pushed into the window opening by the wind. It appeared that the smaller, lower velocity, dispersed drops were “pushed” by the wind toward the window opening and the west wall. However, given the pattern of distribution, it appears the momentum from the fog stream is dominant relative to the force from the wind.

The water distribution data from the fog stream discharged into the window opening is given in Figure 4.3.3-6. The total mass of water collected in the pans for a one minute discharge was approximately 217 kg (478 lbs). This is equal to a flow rate of approximately 3.7 l/s (58 gpm), 73 % of the total flow. In this case, most of the water that was unaccounted for appeared to be deposited in the hallway area, on either side of the row of pans and water that ran down the east wall of the bedroom, but did not flow into the pans.



Figure 4.3.3-1. Water spray distribution experiment arrangement.



Figure 4.3.3-2. Fog stream discharged across window opening.



Figure 4.3.3-3. Fog stream discharged into window opening.



Figure 4.3.3-4. Solid stream discharged into window opening.

Figure 4.3.3-7 has the data from the solid water stream experiment. The total mass of water collected was approximately 359 kg (788 lbs). This accounts for a water flow rate of 6.0 l/s (95 gpm) out of 10 l/s (160 gpm). Similar to the narrow fog stream discharged through the window, the water that appeared to be unaccounted for was discharged against the east wall of the bedroom, but did not flow in to the pans against the wall, on either side of the pans in the hallway and beyond. Evidence of water discharge was noted through the living room and stopped just short of the door to the corridor. This is significantly deeper water penetration into the structure than from the other two methods. Also note that the pattern of water discharge in the bedroom for the hose streams discharged directly through the windows were similar. Given that the flow rate of the solid stream is twice that of the fog nozzle, it is not surprising

that the mass of the water collected in the pans in the hallway during this experiment is more than twice the amount.

The objective of these experiments was to get a sense for where the water was going within the bedroom and hallway areas of the structure given different means of discharge. Based on these limited experiments, discharging water through the window opening is much more efficient than discharging water across the window opening, even with a 6.7 m/s to 8.9 m/s (15 mph to 20 mph) wind. The experiments also showed that the solid stream was distributing water through the living room and up to the corridor.

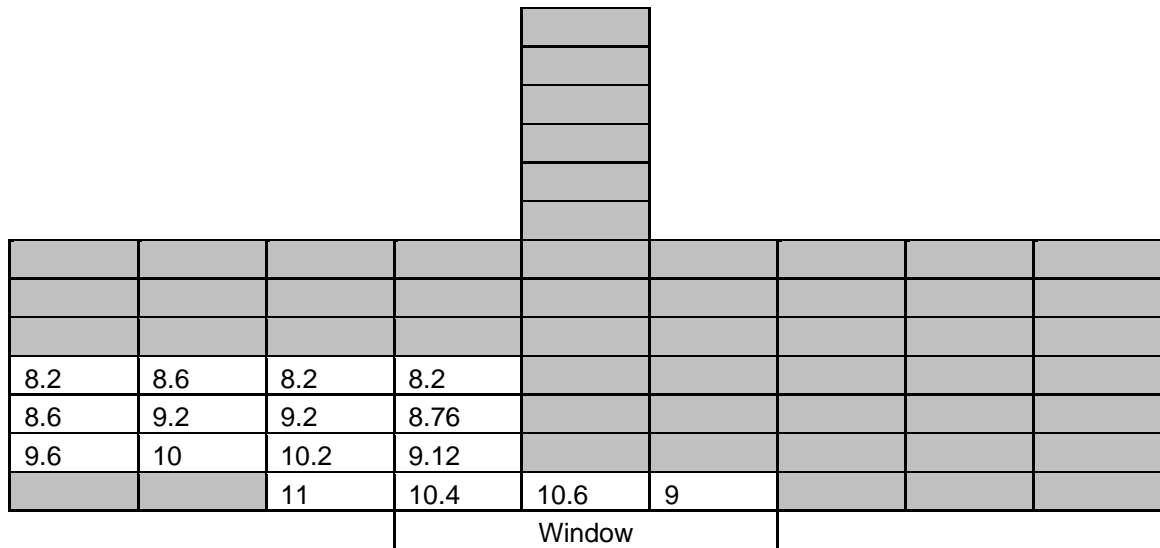


Figure 4.3.3-5. Water distribution results for fog stream discharged across window opening (kg), the gray area does not contain a measurable amount of water.

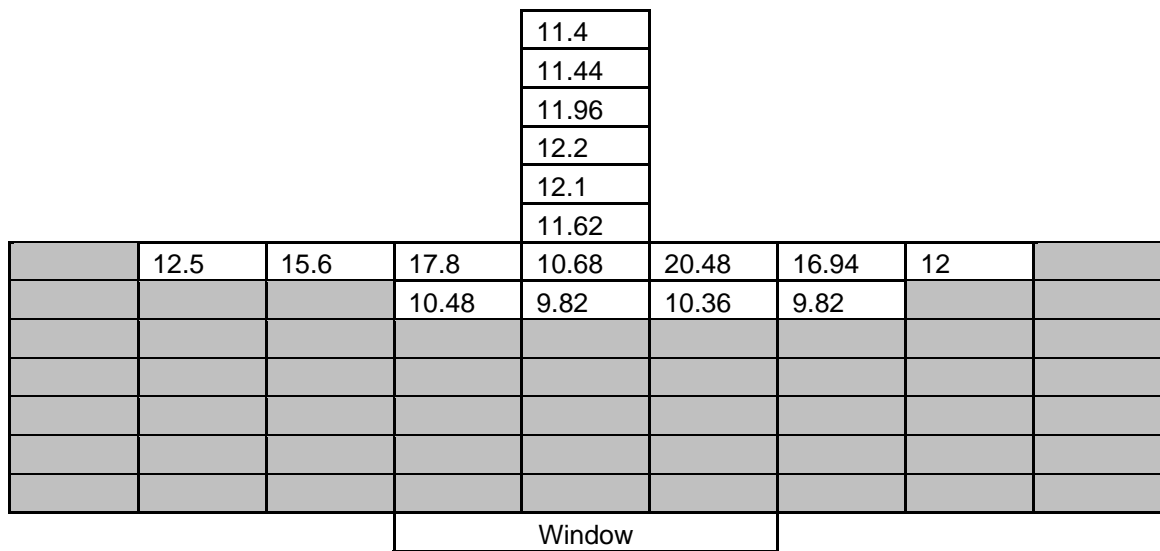


Figure 4.3.3-6. Water distribution results for fog stream discharged into window opening (kg), the gray area does not contain a measurable amount of water.